Characterization of [^{18}F]FPyKYNE-Losartan as a Novel PET Tracer for Imaging AT_1 Receptors

By
Maryam Hachem

uOttawa

This thesis is submitted to the Faculty of Graduate and Postdoctoral Studies as a partial fulfillment of the
M.Sc. program in Cellular and Molecular Medicine.

University of Ottawa, Faculty of Medicine,
Department of Cellular and Molecular Medicine

Submitted May, 2015

Supervisor: Jean N. DaSilva, PhD
National Cardiac PET Centre
University of Ottawa Heart Institute

Abstract

The Angiotensin II Type I Receptor (AT_1R) is the main receptor that produces most of the physiological actions of the Renin Angiotensin System (RAS). Alterations of AT_1R expression in renal and cardiovascular diseases make this receptor an attractive target for developing an imaging agent to monitor its expression in disease states. [^{18}F]FPyKYNE-Losartan has been developed as a derivative of the clinically used AT_1R blocker Losartan. The aim of this work was to characterize this tracer and evaluate its potential as an imaging agent for AT_1Rs, thereby, progressing towards human imaging of the AT_1R. MicroPET imaging in rats and PET imaging in pigs displayed specific AT_1R binding, high kidney-to-blood and image contrast, and slow clearance from kidneys. [^{18}F]FPyKYNE-Losartan was shown to have 2 types of labeled metabolites in rat plasma and kidneys: hydrophilic and hydrophobic, whereas, only hydrophilic metabolite(s) in pig plasma. Plasma protein binding of [^{18}F]FPyKYNE-Losartan was determined, by an in vitro ultrafiltration method, to be 97% which is very similar to that of Losartan (98%). FPyKYNE-Losartan displayed full antagonism of Ang II pressor effect in rats in vivo, with an ED_{50} of 25.5 mg/Kg and 4-times (25%) less potency than Losartan. In vitro binding studies confirmed the binding selectivity of [^{18}F]FPyKYNE-Losartan. B_{max} and K_d parameters were determined to be 348 $\pm$ 112 fmol/mm^2 and 49.4 nM, respectively. Rat dosimetry studies exhibited that the sex averaged effective doses of [^{18}F]FPyKYNE-Losartan according to ICRP 60 and 103 protocols are 2.97E-02 (mSv/MBq) and 3.06E-02 (mSv/MBq), respectively, which are within an acceptable range compared with other F-18 labeled tracers and within the safety limits of the FDA. In conclusion, [^{18}F]FPyKYNE-Losartan has an excellent potential for translation towards human imaging to monitor AT_1R expression and guide therapy.

Table of Contents

List of Tables

List of Figures

List of Abbreviations

%ID	Percentage of total injected dose
%ID/g	Percent of injected dose per gram of tissue
%ID/organ	Percent of injected dose per organ weight
[^{18}F]FDG	[^{18}F]fluorodeoxyglucose
^{11}C	Carbon-11
^{13}N	Nitrogen-13
^{15}O	Oxygen-15
^{18}F	Fluorine-18
AC	Adenylyl cyclase
ACE	Angiotensin converting enzyme
ACEi	Angiotensin Converting Enzyme Inhibitor
Ang I	Angiotensin I
Ang II	Angiotensin II
Ang III	Angiotensin III
Ang IV	Angiotensin IV
ARB	Angiotensin II type 1 receptor blocker
$AT_{1A}R$	Angiotensin II type 1 receptor subtype A
$AT_{1B}R$	Angiotensin II type 1 receptor subtype B
AT_1R	Angiotensin II type 1 receptor
AT_2R	Angiotensin II type 2 receptor
AT_3R	Angiotensin II type 3 receptor
AT_4R	Angiotensin II type 4 receptor
AUC	Area under the curve

BBB	Blood-brain barrier
B_{max}	Maximal binding density
BP	Blood pressure
Bq	Bequerel
BSA	Bovine serum albumin
BW	Body weight
Ci	Curie
CPM	Counts per minute
CTA	Computed tomography angiography
CVV	Clathrin coated vesicle
DAG	Diacyl glycerol
DPM	Disintegration per minute
DV	Distribution volume
ECG	Electrocardiogram
ED	Effective dose
ED_{50}	Half maximal effective dose
EDE	Effective dose equivalent
EDTA	Ethylenediaminetetraacetic acid
EtOH	Ethanol
FDA	Food and drug administration
FDG	2-deoxy-2-(^{18}F)fluoro-D-glucose
FOV	Field of view
FPyKYNE	2-[F-18]fluoro-3-pent-4-yn-1-yloxypyridine
GI_{50}	Concentration for 50% of maximal inhibition

GIT	Gastrointestinal tract
GPCR	G protein-coupled receptor
GPK	G protein-coupled receptor kinase
$G_{\alpha i}$	Inhibitory G-alpha subunit
$G_{\alpha q}$	G protein αq subunit
HF	Heart failure
HPLC	High performance liquid chromatography
I.p.	Intra-peritoneal
I.v.	Intra-venous
IC_{50}	Half maximal inhibitory concentration
ICRP	International commission on radiological protection
ID_{50}	Half maximal inhibitory dose
IP_3	Inositol 1,4,5-triphosphate
IRW	Inveon Research Workplace
IVC	Inferior vena cava
JAK	Janus kinase
K_a	Association constant
K_d	Dissociation constant
K_i	Inhibitory constant
LD_{50}	Half maximal lethal dose
LK	Left kidney
LLI	Lower large intestine
MAPK	Mitogen-activated protein kinase
MeCN	Acetonitrile/ methyl cyanide

MI	Myocardial infarction
Na_3PO_4	Trisodium phosphate
NaCl	Sodium chloride
$NaHCO_3$	Sodium bicarbonate
NSB	Nonspecific binding
PET	Positron emission tomography
PIP_2	Phosphatidylinositol 4,5-bisphosphate
PKA	Protein kinase A
PKC	Protein kinase C
PLC	Phospholipase C
$PLC_{\beta 1}$	Phospholipase-Cβ1
PVC	Partial volume correction
RA	Right atrium
RAS	Renin-angiotensin system
RK	Right kidney
ROI	Region of interest
RPM	Revolutions per minute
Rt	Retention time
SA	Specific activity
SAR	Structure-activity relationship
SB	Specific binding
SD	Standard deviation
SI	Small intestine
SPECT	Single photon emission computed tomography

STAT	Signal transducer and activator of transcription
SUV	Standardized uptake value
TAC	Time activity curve
TB	Total binding
TLC	Thin layer chromatography
TRV	Test-retest variability
UB	Urinary bladder
ULI	Upper large intestine
ULI	Upper large intestine
UV	Ultra-violet
V_B	Vascular Fraction

Acknowledgements

First and foremost, I want to praise and thank God, Allah (SWT) the Almighty, who has granted me countless blessings and the ability to accomplish this thesis.

My efforts towards the completion of this thesis would never have been enough if it weren't for the instrumental help and cooperative efforts of a wide team of individuals at the University of Ottawa Heart Institute, National Cardiac PET Centre, to whom I sincerely express my greatest gratitude.

To start with, I owe a debt of gratefulness to my supervisor, Dr. Jean N. DaSilva, whose guidance and knowledge have been invaluable. I knew later that he had a good impression about me since the first day we met. I hope I did not let you down! Thank you for giving me the opportunity to be part of your team for the past two years. It has been a tough yet outstanding part of my life, and I owe a huge part of what I've learned to you. Many thanks also go to the members of my thesis advisory committee, Dr. Rob deKemp and Dr. Chris Kennedy, for their remarkable comments and suggestions. Their input into the project was influential. I would also like to extend my thanks to Dr. Rob Beanlands for his endless support throughout this project.

My deepest thanks to the PET Physics Group, specifically Dr. deKemp and Chad Hunter for working very closely with me on PET image analysis, tracer kinetics and dosimetry studies. Their contribution to our studies has been essential. Also, many thanks to Dr. Mario Tiberi not only for his valuable input and critique of our work, but his highly appreciated assistance with pharmacological analyses.

I wish to acknowledge the radiochemistry staff personnel, Tayebeh Hadizad and Yanick Lee, for the formulation and synthesis of our tracer, and the Animal Care and Veterinary Service team including Dan de vette, Claire Wolf, Chantal Braiden and Caroline St. Denis for the daily handling and caring of all animals used in this work. I am also very grateful to Richard Seymour for performing rat surgeries so perfectly, and Marika Kolajova and Julia Petryk for their technical assistance with the studies. None of the studies would have been possible without you. I must also thank present and past members of our PET bio-testing lab for their help in data collection, including Stephanie Thorn, Basma Ismail, Jonas Vaskas, Ehsen Tayyabi, James Haley, Kasia Drozd, and Julie Ting.

I would like to further thank the granting agencies which provided funding for this work: the Canadian Institutes of Health Research grant MOP-126079, and the Ontario Preclinical Imaging Consortium grant MRI ORF #RE03-51 (Ontario Research Foundation).

SPECIAL THANKS

I dedicate a special thank you to my beloved family. I thank them for all their love, care and encouragement. Words cannot express how grateful I am to my parents for raising me with a love of seeking knowledge, their support in all my pursuits and the sacrifices they've made on my behalf. Dad- thanks for being an exceptional father, and for giving me my analytical mind and committed personality that got me here. I aim to follow through your footsteps and make you proud. Mom- you are my guardian angel, thanks for your truly unconditional love and the strength you've planted in me. Your prayers for me were what sustained me thus far. I also could not have completed this work without the compassion

and support of my siblings, Fatima, Khawla, Muhammad and Omar. I love you all and I dedicate this thesis to you.

I would also like to thank my friends, Abed, Mohammad and Maysaa, who enriched me continuously with spiritual support and were my incentives to strive towards my goal. You inspire me to reach new heights, and I genuinely thank you for your unconditional friendship.

Finally, I'd like to express my love and appreciation to my fiancé Khaled who spent all the stages of this thesis with me, and was very patient even at the most stressful times. Your faith in me gave me the strength and perseverance to make it to the end. I cannot thank you enough for being by my side, for your unwavering emotional support, and mostly for being the loyal and loving person you are. I love you and dedicate this thesis to you.

Maryam Hachem
University of Ottawa
May 2015

1. Introduction

1.1. The Renin-Angiotensin System (RAS)

The renin angiotensin system (RAS) plays key roles in the regulation of many physiological processes of the cardiovascular, renal and central nervous system. These processes include vasoconstriction, promoting sodium and water reabsorption, stimulating autonomic nervous system activity and cardiovascular function (Brewster et al., 2004; Paul et al., 2006) (Figure 1). Alterations in the RAS result in cardiac, renal and vascular diseases (Givertz, 2001). Thus, studying this system is critical to guide and better understand the therapy with angiotensin converting enzyme inhibitors (ACEi) and angiotensin receptor blockers (ARBs) to reduce morbidity and mortality.

1.2. RAS Pathways

The RAS pathways are either systemic or local. The systemic pathway, which is the regulator of blood volume, electrolyte balance and blood pressure, is triggered by a physiological stimulus such as a decrease in blood pressure (Weir et al., 1999). This would lead to the release of the α-glycoprotein angiotensinogen from the liver and its cleavage into the decapeptide angiotensin I (Ang I) by the enzyme renin from the kidneys. Ang I is then converted into the octapeptide angiotensin II (Ang II) by a membrane bound metallopeptidase, angiotensin converting enzyme (ACE) (Figure 2). The majority of ACE is bound to cell membranes of several organs including the lung, kidney, intestine, cerebrum, heart, adrenal gland and the vasculature. However, it has been shown that most of the conversion of Ang I to Ang I occurs in the lung (Niu et al., 2002). Ang II is the active regulatory effector peptide responsible for much of the RAS actions through Ang II receptors (Inagami, 1994; Weber, 2001; Zaman et al, 2002) (Figure 3). It is further metabolized into Ang III by the deletion of the Asp residue.

In addition to the systemic RAS, there is a local angiotensin-generating system in several tissues referred to as tissue RAS (Leung and Carlsson, 2001). The local pathway is involved in growth, proliferation, protein synthesis, regional hemodynamic regulation and organ function. In the heart, Ang II directly modulates cardiac function as evidenced by effects on myocardial contractility and metabolism, and hypertrophic growth (Baker et al., 1992; Dostal et al., 1999). RAS components are also present in the brain and control responses to Ang II, such as increased sympathetic activity, water intake and release of vasopressin (Obermuller et al., 1991).

It is important to note that recent findings about the RAS system have shown that it is not a classical proteolysis linear cascade, but a cascade that involves multiple mediators, receptors, and multifunctional enzymes, thus, making it a more complicated pathway than it seems (Ribeiro-Oliveria et al., 2008).

1.3. Angiotensin II and its Physiological Effects

Ang II is the central effector molecule of the renin-angiotensin system. It is a critical hormone that was first demonstrated to be a vasoactive agonist directly inducing contraction of blood vessels and plays a chief role in cardiovascular homeostasis (Taubman, 2003). However, over the years Ang II has been shown to play other very important roles such as stimulating aldosterone secretion, sodium reabsorption, catecholamine release, increasing sympathetic nervous system activity, renin release, cellular growth, and thirst appetite (Kobori et al., 2007). In addition, Ang II has roles in mediating hypertension, heart failure, diabetes, and cardiac remodeling, and is implicated in endothelial dysfunction, atherosclerosis, and congestive heart failure (Mehta et al., 2007). It also acts as a growth factor that regulates cell proliferation, apoptosis, fibrosis, and a proinflammatory mediator that participates in inflammatory responses (Taubman, 2003; Ruiz-Ortega et al., 2001; Mehta et al., 2007).

The main goal of Ang II is to maintain blood pressure and regulate blood flow to vital organs, which explains why Ang II acts as a focal point that integrates all these complex processes (Mehta et al., 2007).

1.4. Angiotensin II Receptors: Types, Localization and Function

1.4.1. Two Main Ang II Receptors: AT_1 and AT_2 Receptors

Ang II elicits its multiple actions through stimulating specific targets on the surface of cells (Timmermans et al., 1992). Two primary receptors for Ang II have been identified in mammals: Ang II type 1 and Ang II type 2 receptors (AT_1R and AT_2R, respectively) (Bottari et al., 1993). Definitive evidence for this heterogeneity was obtained from the introduction of nonpeptide Ang II receptor antagonists DuP753 (Losartan) and PD123117. Sites having high affinity for DuP753 were designated AT_1R and those of high affinity for PD123177 were designated AT_2R (Timmermans et al., 1992).

AT_1 and AT_2 receptors are G-protein-coupled receptors (GPCRs) and have the features of seven transmembrane domains (Figure 4). The AT_1R has a molecular weight of 40 kDa and is composed of 359 amino acids (Griendling et al., 1996), while the AT_2R has a molecular weight of 41 kDa with 363 amino acids (Dasgupta and Zhang, 2011). They share a very limited sequence homology constituting of ~ 34% amino acid sequence (Rockman et al., 2002; Inagami et al., 1992). In the kidney, the highest density of AT_1Rs is localized in the renal medullary interstitial cells (Kakinuma et al., 1993). In the heart, the highest density of AT_1Rs is along the conduction system and vagal ganglia, and in the central nervous system it is in the regions above the blood brain barrier (Wharton et al., 1998; Lenkei et al., 1995). As for AT_2Rs, they are mainly distributed in the adrenal gland, heart and brain (Allen et al., 1999).

Most species, including humans, pigs, dogs, bovine and rabbits, express a single autosomal AT_1R gene; but others as rodents, express 2 AT_1R genes: AT_{1A} and AT_{1B} which have 94-96% protein sequence homology (de Gasparo et al., 2000; Elton et al., 1992; Chiu et al., 1993). AT_{1A} receptor is expressed in kidney, liver, adrenal gland, ovary, brain, testes, lung, heart, adipose tissue and placenta of adult mice. AT_{1B} receptor is only found in brain, testes and adrenal gland (Burson et al., 1994). However, ligand binding to the AT_1R in humans and in rats are essentially the same (based on ligand affinity and potency), meaning

that the two receptor subtypes in rats are pharmacologically identical to each other and to the human AT_1R (Chiu et al., 1993).

Ang II mediates most of its effects via the AT_1R, and this receptor-ligand axis is responsible for most of the effects associated to the RAS. Activation of the AT_2R has been shown to have opposing effects to those of the AT_1R. It has been suggested that the AT_2R may act as a regulatory mechanism to prevent overactivation of the RAS. It may play roles in cellular differentiation, vasodilation, apoptosis and anti-proliferation (Dinh et al., 2001) (Figure 5). Moreover, the pathophysiological roles and signaling mechanisms of AT_2 are less clear than AT_1 receptors.

1.4.2. Other Ang II Receptors: AT_3 and AT_4 Receptors

Other Ang II receptors in the system have also been identified: AT_3Rs and AT_4Rs. The AT_3R is still not well defined. Although it is named AT_3, it showed low binding to angiotensin III, so researchers suggest that it should be called a non-AT_1 and non-AT_2 binding site as it is insensitive to both Losartan and PD123319, respectively (Barra et al. 2008). However, its function is poorly understood. The AT_4R on the other hand, has low affinity for angiotensin II but high affinity for the hexapeptide Ang II (3–8), a fragment of angiotensin II, now referred to as Ang IV (Guimaraes and Pinheiro, 2005). This receptor site is prominent among brain structures concerned with cognitive processing, motor and sensory functions and has roles in learning and memory (de Gasparo et al., 2000).

1.5. AT_1R

1.5.1. Signaling Pathway

Most actions of the multifunctional hormone Ang II on its target cells are virtually mediated via AT_1Rs (de Gasparo et al., 2000). Activation of the AT_1R takes place when Ang II binds to it and induces a conformational change. This change enables its interaction with the G-protein further initiating signal

transduction via membrane effector systems. $G_{\alpha q}$, which is the main G-protein associated with the AT_1R, will activate phospholipase-Cβ1 ($PLC_{\beta 1}$) following the activation of the AT_1R (de Gasparo et al., 2000; Sadoshima J, 1998). This causes the cleavage of phosphatidylinositol 4,5-bisphospate (PIP_2) into inositol triphosphate (IP_3) and diacylglycerol (DAG). IP_3 leads to the increase in intracellular Ca^{2+} levels and DAG causes the activation of PKC (protein kinase C), which in turn, phosphorylates cascades downstream of AT_1R that produce Ang II actions (de Gasparo et al., 2000; Bernstein et al., 1996). Simultaneously, the other G-protein component Gαi would be inhibiting AC (adenylyl cyclase). AT_1Rs could also activate other G protein-dependent pathways such as MAPK and JAK/STAT mechanisms. Such mechanisms are dependent on PLC action and promote cell growth and differentiation (Mehta et al., 2007) (Figure 6). While the activation of $G_{\alpha q}$ and IP_3 occurs within seconds, MAP kinase and JAK/STAT activation occurs within minutes to hours (Marrero et al., 2004; Schmitz et al., 1998). In addition to the G protein-dependent pathways, research has identified existing G protein-independent pathways that are associated with β-arrestins. However, the number of transcripts stimulated by these pathways are less important than those stimulated by G protein-dependent pathways (Tilley, 2011). Moreover, the AT_1R like other GPCRs, could be modulated by "biased agonists" that exhibit intrinsic "functional selectivity", thereby specifically activating G protein-independent pathways while simultaneously blocking G protein activity. An example on a biased agonist to AT_1Rs is the modified peptide [Sar^1I-le^4-Ile^8]-Ang II (Christensen et al., 2010; Godin et al., 2012).

1.5.2. AT_1R Binding Sites

The amino acid sequences and residues involved in the process of ligand binding to the AT_1R have been identified through extensive studies and mutational analyses (de Gasparo et al., 2000). These studies established that Ang II binds by primarily interacting with the extracellular region of the receptor, specifically with its N-terminus and the first and third extracellular loops. Ang II also interacts with the hydrophobic intracellular region of the receptor at the level of several residues like Lys^{102} at the top of

transmembrane helix III and Lys^{199} near the top of transmembrane helix V. In addition, Ser^{105} and Lys^{102} residues in the outer region of transmembrane helix III participate in Ang II binding by forming the intramembrane binding pocket. Other essential amino acids include 4 cysteine residues that form disulfide bonds. These bonds have been implicated not only in Ang II binding, but in stabilizing the receptor as well. On the other hand, the binding site of nonpeptide antagonists is distinct from that of Ang II. It has been defined by amino acids located within the hydrophobic transmembrane region of the receptor. However, there is little overlap between both binding sites, specifically at the level of the regions located between helices I, V, VI and VII, and the binding pocket formed by the transmembrane helices of the AT_1R (de Gasparo et al., 2000).

1.5.3. Regulation

The AT_1R, like most GPCRs, undergoes the cyclic process of signaling, desensitization, internalization, resensitization and recycling to the plasma membrane (de Gasparo et al., 2000). Prolonged agonist stimulation induces GPCR kinases (GPKs) to phosphorylate the receptor. Cytosolic β-arrestins then interact with the phosphorylated receptor and uncouple it from the G protein complex prior to enclosing it in a clathrin- coated vesicle (CCV). Dissociation of β-arrestin is followed by dephosphorylation of the receptor by phosphatases and its recycling to the plasma membrane for another round of stimulation (van Koppen et al., 2004). Within 10 min after activation, AT_1Rs are endocytosed, 25% of them are recycled to plasma membrane and the remainder is degraded in lysosomes (Griendling et al., 1987). In addition to phosphorylation, internalization and degradation, the AT_1R is up- and down-regulated through controlled gene transcription (i.e. AT_1R mRNA production). Other processes have been highlighted as well, including receptor dimerization and cross-regulation by other receptor systems (Thomas, 1999).

1.5.4. AT_1R in Disease

The normal expression of AT_1Rs is modified in pathogenic conditions. Diseases that involve modifications in AT_1Rs are: cardiac hypertrophy, ischemic and idiopathic cardiomyopathy, ventricular remodeling, heart failure (HF), myocardial infarction (MI), hypertension, atherosclerosis, renal disease and diabetes.

For instance, an increase in Ang II will lead to an increase in AT_1R activation, but chronic exposure to Ang II will cause down-regulation of the AT_1R (Griendling et al., 1987). It has also been shown in rat models of reduced renal mass hypertension, that AT_1Rs were up-regulated in the heart by 4-folds (Wang et al., 1997). In pig models of renal artery stenosis, overexpression of AT_1Rs was shown to be associated with renovascular hypertension (Xia et al., 2008). Moreover, a marked increase in AT_1Rs was observed in myocardium, brain, and renal glomeruli in rat models of myocardial infarction (Meggs et al., 1993; Reiss et al., 1993; Tan et al., 2004; Mento et al., 1998), as well as increases in Ang II in humans post-MI (McAlpine et al., 1988; Unger, 2002). In rats with induced diabetes, a decrease in renal AT_1R expression was identified primarily in proximal tubule cells (Cheng et al., 1994). Furthermore, AT_1Rs were up-regulated in the atherosclerotic plaque (Yang et al., 2012). It is in these cases where the importance of anti-RAS treatments arises.

1.6. Anti-RAS Treatments

To treat diseases such as heart failure, renal failure, hypertension, atherosclerosis, stroke and diabetes, therapeutic agents as angiotensin converting enzyme inhibitors (ACEis) and angiotensin receptor blockers (ARBs) are used. Numerous evidence has revealed that ACEis and ARBs have inhibitory effects on cardiac remodeling. They can subsequently treat heart failure and improve survival rates (Pfeffer et al., 1988). In renal diseases, blockade of RAS by anti-RAS treatments not only results in lowering blood pressure and reducing loss rate of renal function, but also delays the progression of renal failure (Vogt et al., 2004).

1.6.1. ACEi

ACEis work directly by inhibiting the synthesis of Ang II, thus leading to decreased Ang II levels in plasma and kidneys (Cohn, 2000; Amiri et al., 1997). However, for HF, ACEis were partially effective, explaining why additional treatments were needed. This was when ARBs started to be used, as they have shown promising benefits for HF patients (Cohn, 2000).

1.6.2. ARBs

ARBs can either be surmountable (i.e. Losartan) or insurmountable (i.e. Candesartan and EXP3174). Compounds termed "surmountable" or competitive antagonists physically block the active site of the receptor, while "insurmountable" or non-competitive antagonists bind to allosteric sites and induce conformational changes to the receptor that prevent agonist binding (Vanderheyden et al., 1999). Surmountable antagonists do not impair the maximum response of Ang II. In contrast, insurmountable antagonists not only cause a rightward shift in the Ang II dose-response curve but also reduce the maximal response to agonist stimulation. Another difference is related to the dissociation time of each type of antagonists. Surmountable antagonists dissociate rapidly from the receptor while insurmountable antagonists bind tightly and dissociate so slowly as to cause functional loss of the receptors (de Gasparo et al., 2000). These distinct antagonist-receptor interactions could be due to differences in the acid-base groups. While insurmountable antagonists have di-acidic groups, surmountable antagonists contain only one acidic group (Takezako et al., 2004).

1.7. Nuclear Imaging

Nuclear imaging is a medical specialty that involves the application and detection of decaying radioisotopes to help in the diagnosis and treatment of disease. In most cases, the radioisotope is

combined with a biologically active compound to form a radiolabelled probe capable of imaging a specific biochemical pathway or event in vivo.

Two nuclear imaging modalities exist which detect the radiation emitted upon radionuclide decay of the radioisotope: positron emission tomography (PET) and single photon emission computed tomography (SPECT). PET and SPECT have been used extensively for non-invasive imaging of metabolic pathways connected with the pathophysiology of a disease, enabling early detection and diagnosis (Hutchins et al., 2008).

The importance of imaging AT_1R density arises from the fact that prognosis of cardiac/renal diseases in patients would become possible, hence, better understanding of disease state and guiding therapy following use of anti-RAS treatments, monitoring their effects, and ultimately decreasing morbidity and mortality rates.

1.7.1. Single Photon Emission Tomography (SPECT)

SPECT is a type of nuclear medicine tomographic imaging technique that detects gamma rays to provide 3D information. The radioisotopes used, such as technetium-99, iodine-123 and indium-111 (which have long half-lives), decay through the emission of single gamma rays, which are then detected by gamma cameras.

One advantage of SPECT over PET is the ability to image multiple tracers simultaneously. They could be distinguished by the unique energy range of their emitted gamma rays (Rahmim and Zaidi, 2008). However, both SPECT and PET provide quantitative functional and metabolic information, such as blood perfusion, protein concentrations and ligand binding (Hutchins et al., 2008).

1.7.2. Positron Emission Tomography (PET)

Positron emission tomography (PET) is a nuclear non-invasive, highly sensitive imaging technology. By injecting radiolabeled tracers, 3D images are obtained and reconstructed by a computer software to show concentration and location(s) of the tracer of interest (Gambhir, 2002). Molecules are labeled with a positron emitting radionucleotide (such as ^{11}C, ^{13}N, $^{15}0$ and ^{18}F) detected by PET cameras to provide a spatial and temporal distribution (Cherry and Gambhir, 2001).

In PET, the radioactive tracer's nucleus undergoes β+ decay and emits a positron: an electron's anti-particle. When the positron interacts with an electron, the two particles destroy each other via a process called annihilation (van der Veldt et al., 2013) (Figure 7). This reaction liberates two gamma photons with specific energies (511 KeV) traveling in opposite directions (180^o) which PET detectors will capture simultaneously and convert into an electrical signal. The signal is recorded over a long period of time and reconstructed to provide 3D image which could then be analyzed (Berger, 2003) (Figure 8).

Among the most commonly used PET radiotracer is [^{18}F]FDG and ^{82}Rb. ^{18}F-FDG or FDG (chemically: 2-deoxy-2-(^{18}F)fluoro-D-glucose), is a glucose analog with the fluorine-18 (half-life= 109.7 min) positron-emitting radioactive isotope substituting the normal hydroxyl group at the 2' position in the glucose molecule. After injecting FDG into the patient, the distribution of FDG within the body is observed using a PET scanner. FDG's uptake is a marker for glucose uptake in the tissues, which in turn is closely correlated with tissue metabolism. FDG is now the standard radiotracer used for PET cancer patient management and neuroimaging (Kelloff et al., 2005; Almuhaideb et al., 2011). Rubidium-82 (physical half-life= 75 seconds) is an analog to potassium that is rapidly taken up by heart muscle. Rubidium-82 is rapidly extracted from the blood and is taken up by the myocardium in relation to blood flow. Thus, areas of the heart with adequate blood flow would have more ^{82}Rb activity compared to areas with less blood flow. PET scan images are very helpful in identifying the location and extent of reduced blood flow to the heart muscle, a case referred to as ischemia (Carli et al., 2007; Yoshinaga et al., 2010).

Initially, PET was essentially used on humans and larger research animals, but now with the development of microPET scanners, these studies could be done on small animals as rats and mice. A single imaging study in a single animal could provide the entire whole-body biodistribution kinetics (Cherry and Gambhir, 2001).

1.7.2.1. Quantification and Kinetic Modeling

PET image data can be quantified in numerous ways and several methods have been developed to analyze the behavior of radiotracers in animals and humans. PET scanners typically provide images in terms of radioactivity concentration, that is the amount of Becquerel (Bq) or Curie (Ci) per ml, where 1 Bq = 1 disintegration per second (dps) or 2.7×10^{-11} Ci (i.e. 1 mCi= 37 MBq). The changing activity concentration in the Region of Interest (ROI) over time is then used to generate time-activity curves (TAC), presented as %ID (injected dose)/ml. Subsequently, standard uptake values (SUV, g/ml) or an SUV curve can be used to display regional tracer uptake normalized to the administered dose of tracer and to body weight (assuming 1 ml roughly equals 1 g). SUV values allow comparison between different animals or humans (Kinahan and Fletcher, 2010).

SUV = Activity concentration (MBq/ml) / Injected dose (MBq)/Weight (g)

Using [N-^{11}Cmethyl]-(–)-Cocaine PET studies in humans, Logan et al. (1990) described a graphical method of quantifying the PET time-activity data which represents the ratio of radiotracer in tissue relative to plasma at equilibrium provided it binds to its receptor reversibly and that its kinetics follows a one- or two-compartment model. This graphical analysis can be used to estimate distribution volume (DV), a ratio of tissue ligand concentration versus plasma ligand concentration. In essence, $\int_0^T C_{PET}(t)dt/C_{PET}(T)$ (min) is plotted against $\int_0^T C_P(t)dt/C_P(T)$ (min·cm^3/ml); where C_{PET} (t) is the concentration of tracer in the tissue and C_P (t) is the concentration of tracer in plasma, and a straight line is fitted to the linear part of the data. If the ligand binds reversibly, the plot will become linear after an

initial transitional phase. The slope of this linear regression provides an estimate of the DV (in ml/cm^3) of the tracer in the predefined region. DV is an index of receptor density (B_{max}) and ligand affinity (K_d) for the receptor. The higher is the protein expression or binding affinity ($1/K_d$), the higher is the DV. From a kinetic point of view, for a simple two-compartmental model DV is expressed as follows:

$$DV= (K_1/k_2) (1 + k_3/k_4) ;$$

K_1, k_2, k_3 and k_4 are the rate constants. K_1 represents the transportation rate of a ligand from capillary to tissues [ml/min/g], and k_2 is the clearance rate back to the venous system [1/min]. k_3 and k_4 are the association and disassociation rates of the ligand to and from the specific binding sites [1/min]. The ratio k_3/k_4 represents B_{max}/K_d (Logan J, 2000; Kimura et al., 2007).

From a physiological point of view, the DV of a given tracer is an indicator of that tracer's concentration in a given tissue. If the tracer binds to a specific target, its concentration can be an indicator of binding potential to a given molecular target. Binding Potential (BP) is a crucial measure in the use of PET to measure the density of "available" receptors. Thus, the DV can be used as an indirect indicator of protein expression and/or binding potential for reversibly binding ligands, i.e. a higher protein expression or binding affinity will result in a higher DV value; where affinity is defined as the tightness of fit between the drug and the receptor ($1/K_d$).

The effects of plasma protein binding and nonspecific binding are implicit to the DV calculation. That is, free ligand in the blood is not distinguished from plasma-bound ligand, and contributions from nonspecific binding in addition to free ligand and specifically bound ligand are included in the DV estimate. The DV can also be modulated by the plasma input function; which is an indicator of tracer concentration in the plasma available for tissue uptake. Thus, the DV is defined as the concentration of radiotracer in tissue over plasma at equilibrium (steady-state) and provides a quantifiable parameter for repeated measurements and assessment of repeatability and reliability (Logan et al. 1990). A DV of 1 indicates no contrast between the tracer in the target tissue and tracer in the blood; there is no specific binding.

1.7.2.2. Partial Volume Effect Correction (PVC)

PET images are inherently affected by the partial-volume effect, which is one of the limitations of PET scanners. Partial volume effects are complex. They depend on tracer activity distribution, object geometry, and on scanner resolution which may vary across the imaging field-of-view (Rousset et al., 1998; Soret et al., 2007). This means that the measured tracer activity concentration is not accurate due to the relatively low image resolution and the limited tissue sampling. The low spatial resolution of the PET system causes blurring of the image, so that high activities of hot lesions are spread to the surrounding, which is called spill-out. This specially occurs when the object or area imaged is too small, like in the case of microPET imaging for small animals. The same effect also causes a spill-in of the background into the volume of interest. Hence, hot lesions tend to appear less aggressive (reduced maximum) but bigger (more spreading) than they actually are (Hammers et al., 2003; Gousias et al., 2008). Therefore, although it can only be approximate, PVC should be done to obtain more accurate results.

1.7.2.3. Why PET?

An advantage PET has over other types of imaging such as MRI or computed tomography (CT), is that it reveals functional changes of an organ or tissue on a cellular level, whereas MRI and CT scans measure structural changes rather than functional. If the radioactive element is incorporated into a pharmacological compound, the localization of radioactivity can be attributed to the distribution and retention of that compound due to binding specific cellular targets such as cell-surface receptors (Wahl, 2002). Thus, PET scans can diagnose certain diseases earlier than MRI or CT scans, given that many diseases involve functional changes in cells and not structural at their early stages.

Another advantage is that it uses isotopes, as carbon-11, nitrogen-13, oxygen-15 and fluorine-18, which do not alter the nature of organs nor the properties of the endogenous molecules or pharmacological compounds used such as drugs (Wahl, 2002).

PET scans can also detect small areas of disease that other imaging techniques wouldn't be able to show. For example, PET could be useful in determining whether an unknown mass left over after treatment is scar tissue or an active tumor.

1.7.2.4. Disadvantages of PET

One downside of PET is that it is not ideal in means of providing anatomical information, such as size, shape and structure of tumors. In addition, measuring metabolic changes in cells could give false results due to differences in the body. For instance, a diabetic patient could have a different rate of processing glucose than a normal patient, which could slightly skew the results.

There are physical barriers to PET including limited anatomic resolution and the need for even higher sensitivity. PET scanners are also in limited supply because they are very expensive. Even more expensive are the cyclotrons and radiochemistry operations that produce the radioactive atoms and radiotracers for PET imaging, which is another drawback of resorting to PET.

1.8. Desirable Properties of Radiotracers

For a radiotracer to be useful as an imaging probe, a number of key general properties are desirable: it should have low nonspecific binding, minimal peripheral metabolism (in blood) but rapid clearance from plasma and nonspecific regions to reduce background in the target tissue. High membrane permeability and intracellular trapping are preferable as well, besides having high target specificity and affinity for molecular targets (Laurelle et al., 2003; Pike, 2009; Victor W, 2009; Fumita et al., 2002).

Having high specific activity is essential to prevent saturation of the specific binding sites, especially when they are expressed in low amounts. Specific activity (SA) is the measure of labeled to unlabeled component in the total mass of an injected tracer, thus, it has an influence on detectable receptor signals. In cases where low specific activity is combined with a low receptor density, receptors could easily become

saturated by unlabeled ligand and hence wouldn't be imaged properly as the signal (activity associated with the receptor) may be too low to detect (Hume and Gunn, 1998).

Furthermore, tissue distribution, localization, and target binding should enable simple kinetic modeling to estimate quantitative data, and radiation dosimetry must allow for multiple diagnostic imaging studies (if necessary).

The radiochemistry of the tracer is important too. Its synthesis ought to be rapid and suitable for automated modules, and the label must be incorporated strategically in order to preserve the overall chemical and pharmacological properties of the parent molecule.

If the radiotracer is a neuroimaging probe, in addition to previous characteristics it should be a nontoxic lipophilic molecule of low molecular weight (<450) to cross the BBB. Generally, binding affinity and lipophilicity are the most crucial properties for in vivo radioligands (Villemagne et al., 2012).

1.9. PET AT_1R Radioligands

1.9.1. Previous Tracers

In our laboratory, a number of PET tracers have been developed for in vivo AT_1R measurement. The O-[^{11}C]methyl-Candesartan and [^{11}C]methyl-Losartan are both derived from ARBs. Both tracers exhibited binding specificity and selectivity for AT_1Rs over AT_2Rs (Hadizad et al., 2009a; Hadizad et al., 2009b). However, [^{11}C]methyl-Candesartan displayed favorable metabolism compared to [^{11}C]methyl-Losartan. The [^{11}C]methylated derivative of EXP3174, the active metabolite of Losartan, displayed good signal to noise ratio and in vivo binding stability in rats (Hadizad et al., 2010) (Figure 9). Other AT_1R PET tracers were also developed by different groups and experimental studies were performed on them.

The John Hopkins group, for instance, has synthesized several ^{11}C-labeled AT_1R radioligands, including: MK-996, L-159,884, and most recently KR31173. [^{11}C]KR31173 was shown to be the most successful of their previous tracers. Ex vivo studies and in vivo PET studies displayed tracer retention that

correlated with the biodistribution of the AT_1R (i.e. adrenal glands > kidneys > lung > heart), and binding selectivity for AT_1R over AT_2R. Specific binding to renal AT_1Rs was reported in several species including mice, dogs, and baboons, while cardiac AT_1R specific binding was observed in rats, pigs and humans. [^{11}C]KR31173 thus exhibited suitable PET imaging of the AT_1R in multiple species (Zober et al., 2006; Higuchi et al., 2010; Fukushima et al., 2012).

1.9.2. Structure-Activity Studies that Led to the Selection of [^{18}F]FPyKYNE-Losartan

Structure-activity relationship (SAR) studies performed on the lead compound Losartan showed that the 2-butyl and acidic tetrazole groups were important requirements for high affinity as a potent non-peptide AT_1R antagonist used orally to treat hypertension (Timmermans et al., 1991; Bernhart et al., 1993; Almansa et al., 1997; Carini et al., 1991). Carini et al. reported that “hydrogen bounding groups” (eg. OH, COOH, CH2OCH3, COOCH3) at the 5-position are the most effective for good binding to AT_1Rs. Methylation at the 5-hydroxy moiety produced a derivative with similar binding affinity (Losartan and methyl Losartan: IC_{50}= 19-32 nM) and in vivo activity (blood pressure lowering) in comparison to Losartan (Carini et al., 1991). Similarly, esterification of the 5-carboxyl group of structurally similar derivatives of EXP3174 (active metabolite of Losartan) with methyl or ethyl-ester groups also produced potent antagonists that bind with high affinity to AT_1Rs (Almansa et al., 1997; Carini et al., 1991; Okazaki et al., 1998) (Figure 10).

Furthermore, SAR studies have established that the modification of the 7-carboxylic acid of Candesartan to the corresponding methyl-ester led to minimal changes both in affinity and antagonistic effect (Kubo et al., 1993; Yoshimura et al., 1994). Using structurally similar Candesartan derivatives (butyl instead of ethoxy group), Yoshimura et al. (1994) reported that the methylated derivative was scarcely hydrolyzed in rat plasma and showed enhanced lipophilicity for increased BBB penetration and low

metabolism of 7-methyl-ester derivatives. [^{11}C]methyl-Candesartan displayed favorable metabolism compared to [^{11}C]methyl-Losartan.

Based on these SAR studies and in vivo studies, our laboratory developed the C-11 labeled methylated derivatives of the clinically used Losartan and Candesartan, and the [^{11}C]methyl-ester derivative of EXP3174. However, to date, no AT_1R PET tracer was able to demonstrate BBB penetration, proper kinetics and appropriate metabolism and stability. Moreover, the C-11 half-life is too short for large scale use in humans. So for all these reasons collectively, a new tracer was needed.

1.9.3. [^{18}F]FPyKYNE-Losartan

F-18 labeled tracers are more promising agents to study AT_1Rs than C-11 tracers. They possess multiple advantages over C-11 tracers, namely: a longer half-life (109.8 min vs. 20.4 min of C-11), allowing multiple injections per one formulation, shipment to sites without the need of a cyclotron and radiochemistry, and providing higher image resolution due to lower positron energy (0.63 MeV; distance in water= 2.4 mm).

These are the factors that led to the development of the most recent tracer in our laboratory: 2-[F-18]fluoro-3-pent-4-yn-1-yloxypyridine-Losartan, referred to as [^{18}F]FPyKYNE-Losartan. It is synthesized via click chemistry, in 5-10% yield with a specific activity of 400-1500 mCi/μmol, and high chemical (>95%) and radiochemical (>97%) purities using the TRACERLab® FX N Pro (G E Healthcare) automated dual reactor module (Arksey et al., 2014) (Figure 11). Moreover, preliminary evaluation of [^{18}F]FPyKYNE-Losartan with PET in rats displayed high uptake in the kidneys with good contrast to surrounding tissue. Co-administration with Candesartan (2.5, 5 and 10 mg/Kg), produced a dose-dependent reduction in tracer uptake by the kidney (47-65%), while no difference was found following the injection of the AT_2R blocker PD123319, indicating binding selectivity for AT_1R over AT_2R. Blocking AT_1Rs with Candesartan (5 and 10 mg/Kg) caused a reduction in the proportion of authentic tracer in rat kidney samples at 10 min

compared to controls, further confirming AT_1R specificity. While labeled metabolites were shown to have minimal binding to AT_1Rs (Figure 12).

Thus, [^{18}F]FPyKYNE-Losartan exhibits imaging potential and in vivo stability (Arksey et al., 2014) (Figure 13; Figure 14). It is now being assessed in different disease models.

1.10. Clinical Significance

Non-invasive molecular imaging is a tool that aids in disease diagnosis and guiding therapy for patients at risk of cardiovascular diseases including HF, hypertension, diabetes, vascular and renal failure. Using PET to image AT_1Rs will allow the identification of receptor abnormal expression, relate it to disease progression, and guide therapy accordingly. Predicting the efficacy of anti-RAS treatments (ARBs and ACEi's) is also very important and would become possible. [^{18}F]FPyKYNE-Losartan has the potential to be the imaging agent for this purpose. The fact that it is a derivative of the clinically used drug Losartan will facilitate translational work in humans, as their pharmacological profiles are expected to be similar. Also, keeping in mind the advantages it has over C-11 tracers, our tracer is expected to be more suitable for imaging AT_1Rs than previous tracers.

1.11. Figures

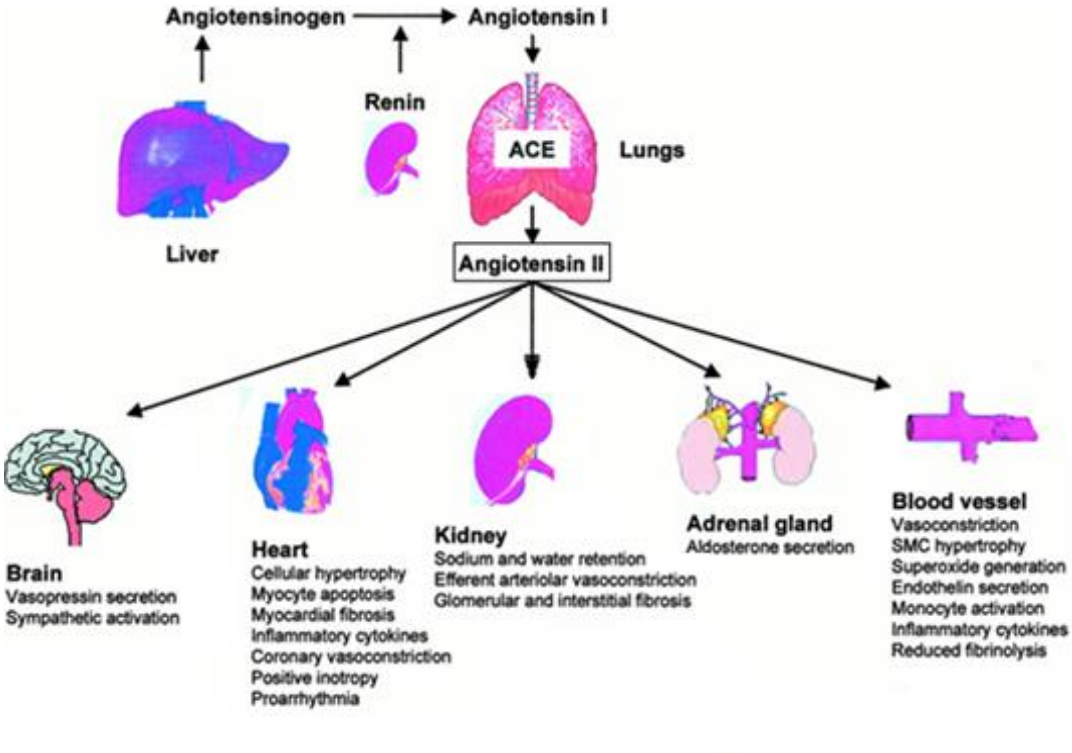

FIGURE 1- PATHOPHYSIOLOGY OF THE RAS. SMC INDICATES SMOOTH MUSCLE CELL. THE MAJORITY OF ANG I TO ANG II CONVERSION OCCURS IN THE LUNGS. ADAPTED FROM GIVERTZ, 2001.

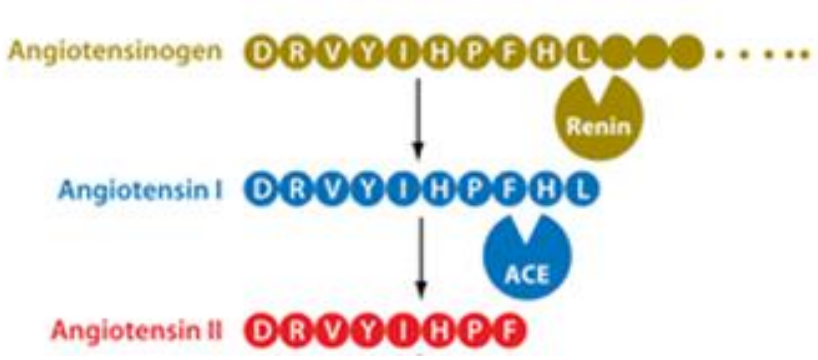

FIGURE 2- ANGIOTENSIN II SYNTHESIS PATHWAY. ACE: ANGIOTENSIN CONVERTING ENZYME. ADAPTED FROM BADER, 2010.

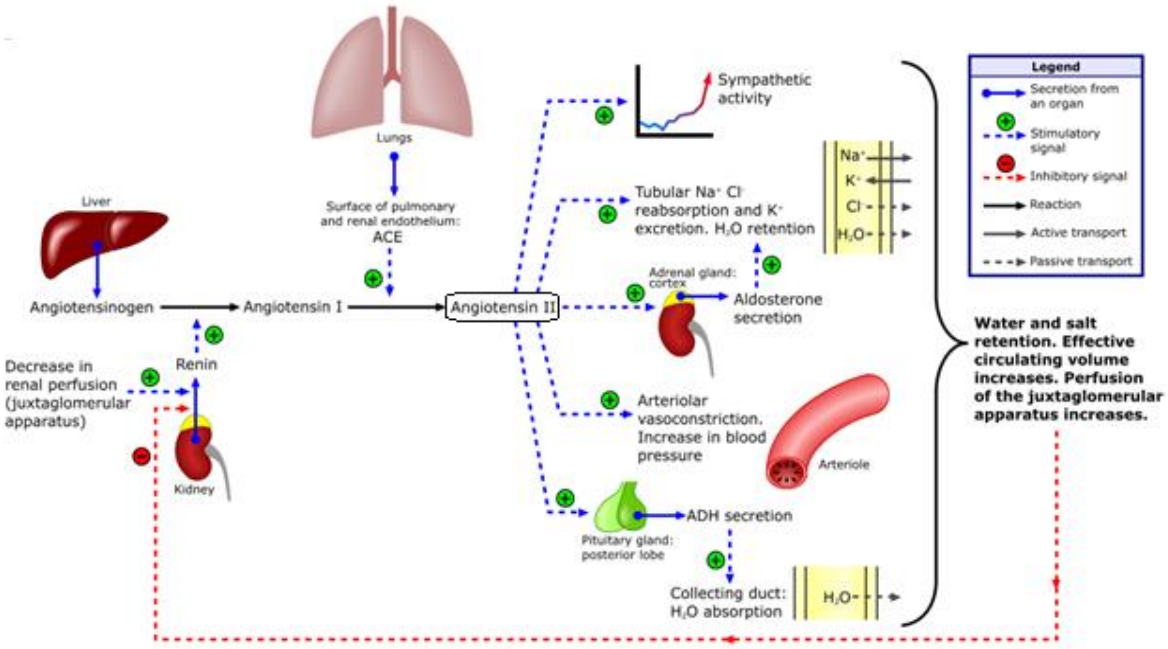

FIGURE 3- RENIN-ANGIOTENSIN-ALDOSTERONE SYSTEM PATHWAY AND EFFECTS. ANGIOTENSINOGEN IS RELEASED FROM THE LIVER AND CLEAVED INTO ANG I BY RENIN RELEASED FROM KIDNEY. ANG I IS ACTIVATED INTO ANG II BY ACE FOUND PREDOMINANTLY IN THE LUNGS. PHYSIOLOGICAL ACTIONS OF ANG II INCLUDE EXCITATION OF SYMPATHETIC NERVOUS SYSTEM, SODIUM REABSORPTION, WATER RETENTION, VASOCONSTRICTION AND STIMULATION OF ALDOSTERONE AND ADH SECRETION (ADAPTED FROM RAD A, 2006).

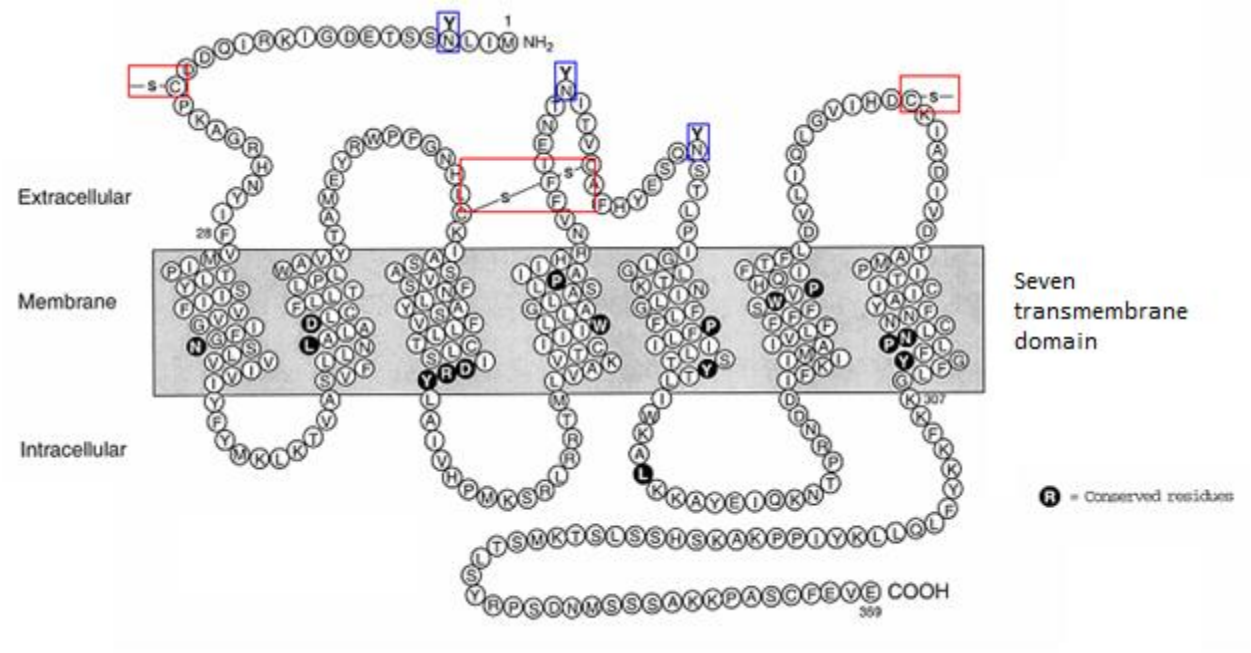

FIGURE 4- AMINO ACID STRUCTURE AND CONFIGURATION OF MAMMALIAN AT_1R. AT_1R IS A SEVEN TRANSMEMBRANE GPCR PROTEIN COMPOSED OF 359 AMINO ACIDS. RED RECTANGLES OUTLINE THE LOCATION OF DISULFIDE BONDS; BLUE RECTANGLES HIGHLIGHT SUBSTRATES FOR N-GLYCOSYLATION. THE AMINO ACID RESIDUES THAT ARE HIGHLY CONSERVED AMONG G PROTEIN-COUPLED RECEPTORS ARE INDICATED BY BOLD LETTERS. ADAPTED FROM DE GASPARO ET AL. 2000.

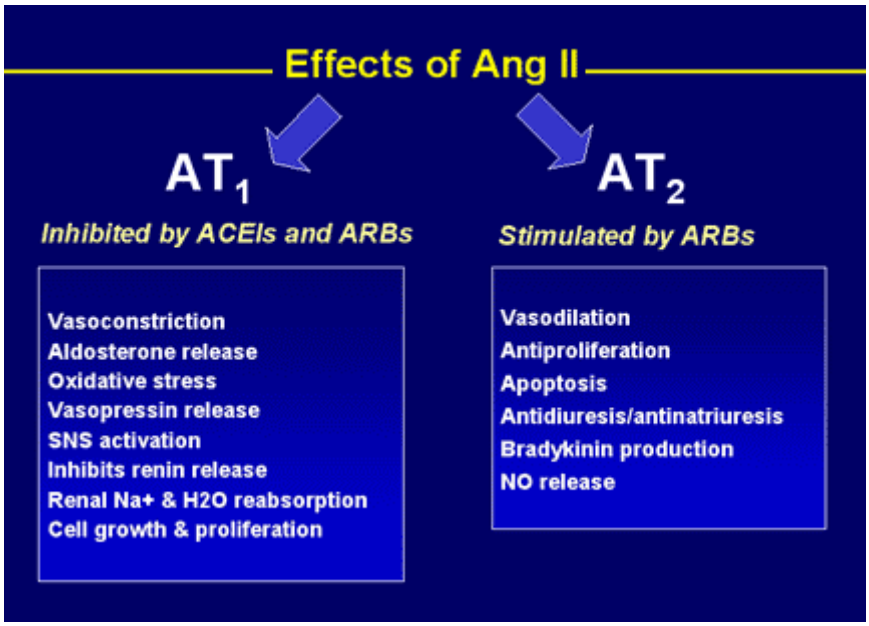

FIGURE 5- ANGIOTENSIN II EFFECTS AT AT_1 RECEPTORS AND AT_2 RECEPTORS. ADAPTED FROM SIRAGY, 1999.

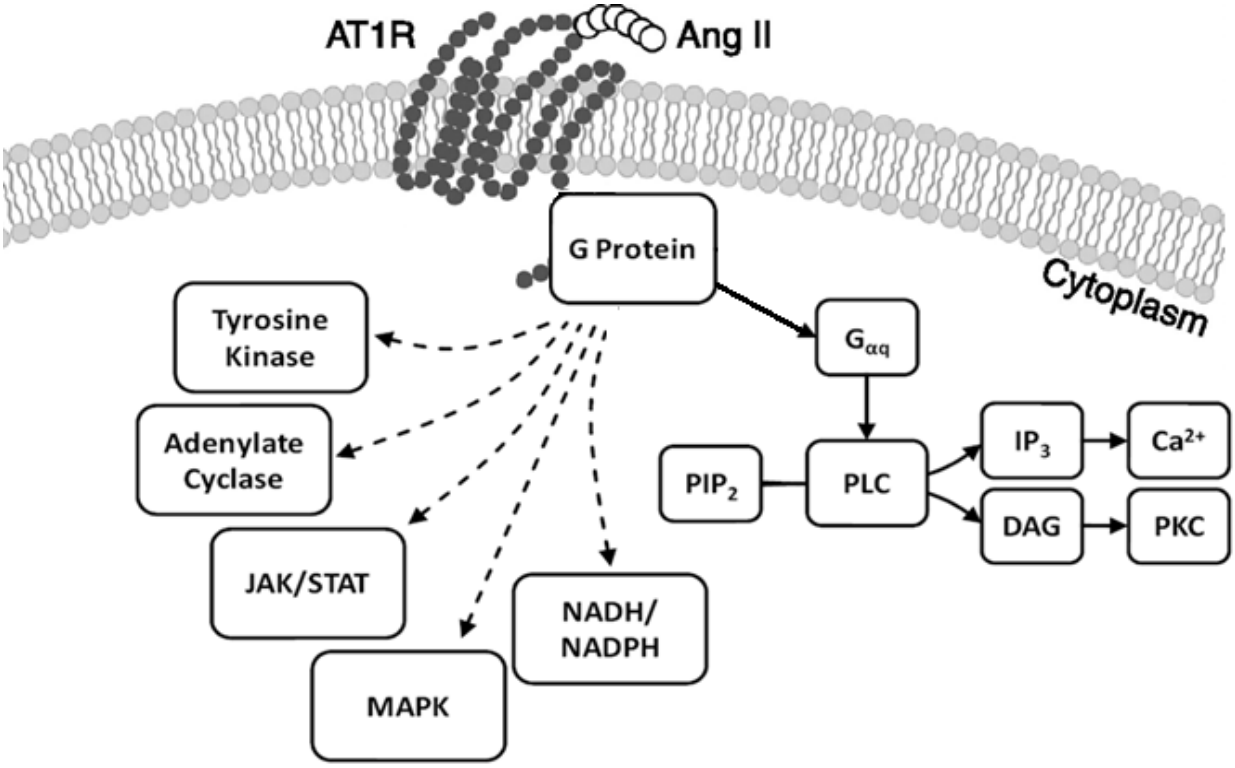

FIGURE 6- SCHEMATIC OF AT_1R SIGNAL TRANSDUCTION PATHWAYS. GAQ: G PROTEIN A SUBUNIT, PIP_2: PHOSPHATIDYLINOSITOL BIPHOSPHATE, PLC: PHOSPHOLIPASE C, IP_3: INOSITOL TRIPHOSPHATE, DAG: DIACYL GLYCEROL, PKC: PROTEIN KINASE C. ADAPTED FROM NOGUEIRA ET AL., 2009.

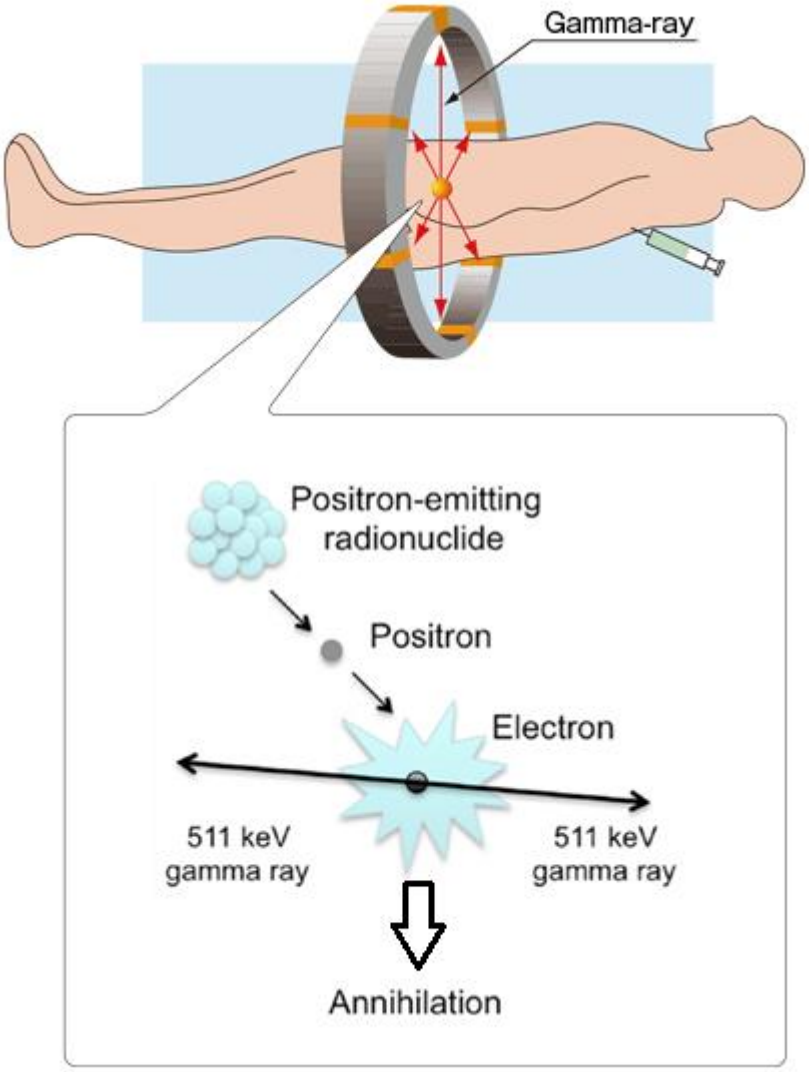

FIGURE 7- SCHEMATIC ILLUSTRATION OF PET SCANNING AND RADIOACTIVE POSITRON DECAY. DETECTION OF POSITRONS OCCURS FOLLOWING ANNIHILATION OF THE POSITRON FOR UNSTABLE ISOTOPE NUCLEUS. ADAPTED FROM VAN DER VELDT ET AL., 2013.

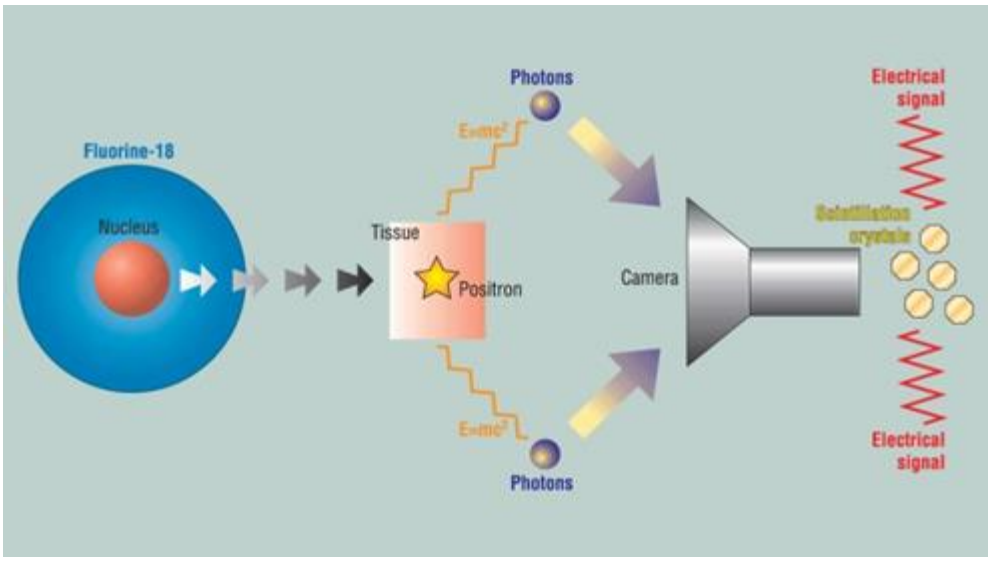

FIGURE 8- THE PROCESS OF PET IMAGING. THE BASIC PRINCIPLES BEHIND PET INVOLVE THE DETECTION OF A RADIOACTIVE ATOM USING A SPECIALIZED SCINTILLATION CRYSTAL DETECTION SYSTEM IN THE PET CAMERA. UPON DECAY OF THE RADIONUCLIDE, A POSITRON (E+) IS EMITTED WHICH COLLIDES WITH AN ELECTRON (E-) IN THE TISSUE, THE ANNIHILATION OF BOTH PARTICLES OCCURS AND CONVERTS MASS TO ENERGY ($E=MC^2$) IN THE FORM OF TWO GAMMA PHOTONS (Γ) WHICH MOVE IN OPPOSITE DIRECTION AT APPROXIMATELY 180^o FROM EACH OTHER. THE PET CAMERA USES SCINTILLATION CRYSTALS PAIRED TO PHOTOMULTIPLIER TUBES POSITIONED IN A CYLINDRICAL ARRANGEMENT AROUND THE SUBJECT TO DETECT THESE PHOTONS. THE CRYSTALS SIMULTANEOUSLY DETECT THE TWO PHOTONS IN COINCIDENCE, AND THEN RECORD THEM OVER A LARGE PERIOD OF TIME. RECONSTRUCTION OF THE ISOTOPE DISTRIBUTION IS POSSIBLE, AND ALLOWS LOCALIZATION OF THE RADIOACTIVE SOURCE. ADAPTED FROM BERGER, 2003.

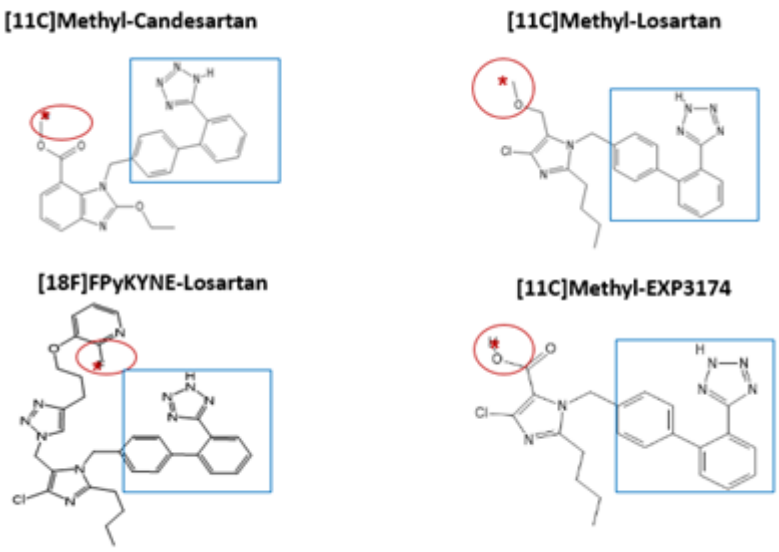

FIGURE 9- AT_1 RECEPTOR RADIOLIGANDS. THE BOXED CHEMICAL STRUCTURE REFERS TO BIPHENYL TETRAZOLE (CH_2N_4) (HADIZAD ET AL., 2009; HADIZAD ET AL., 2010).

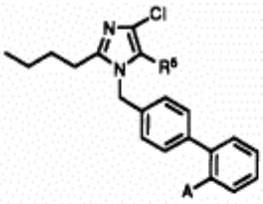

compd no.	R^5	A	IC_{50}[a] (μM)	in vivo activity iv (po)[b]
2	CH_2OH	COOH	0.23	3 (ED_{30} = 11)
5	CH_2OCH_3	COOH	0.099	10 (100)
Losartan → 17	CH_2OH	CN_4H	0.019	ED_{30} = 0.80 (ED_{30} = 0.59)
Methyl-Losartan → 18	CH_2OCH_3	CN_4H	0.032	1 (3)
59	$CH_2NHCOOCH_3$	CN_4H	0.06	1 (>10)
60	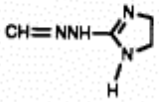	CN_4H	0.29	3 (30)
61	$CH{=}NNHSO_2Ph$	CN_4H	0.66	3 (30)
62	CH(OH)Ph	CN_4H	0.41	3 (>30)

FIGURE 10- SAR AT IMIDAZOLE 5-POSITION. THE TABLE SHOWS THE CORRESPONDING LABELED-ALKYLATED LOSARTAN DERIVATIVES OBTAINED AFTER THE ADDITION OF DIFFERENT PROSTHETIC GROUPS THAT ARE ADDED AT THE 5-POSITION OF IMIDAZOLE. COMPOUND NUMBER 17 IS LOSARTAN AND COMPOUND NUMBER 18 IS METHYL-LOSARTAN. BOTH HAVE SIMILAR IC_{50}'S (ADAPTED FROM CARINI AND DUNCIA ET AL., 1991).

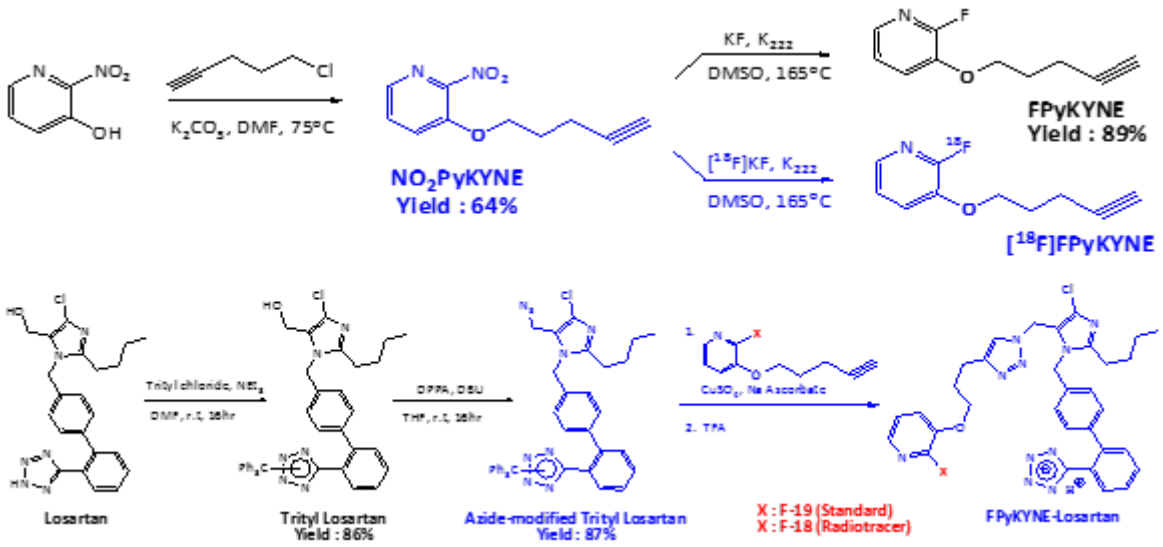

FIGURE 11- RADIOSYNTHESIS OF [^{18}F]FPYKYNE-LOSARTAN. [^{18}F]FPYKYNE ADAPTED FROM THE ORSAY'S METHOD (KUHNAST ET AL.) AND TRIUMF, THROUGH THE AUTOMATED TRACERLAB FX N PRO DUAL REACTOR MODULE. IT IS PURIFIED VIA A CONVENIENT METHOD USING 3 SILICA GEL CARTRIDGES IN SERIES BETWEEN REACTOR-1 AND REACTOR-2, SAVING TIME WITHOUT HPLC (VALDIVIA ET AL., 2012; ARKSEY ET AL., 2014).

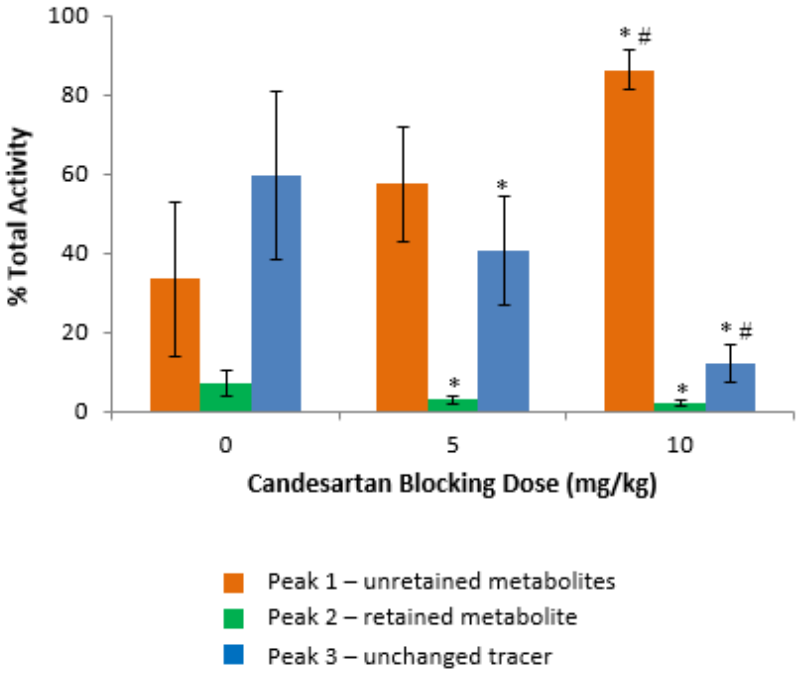

FIGURE 12- KIDNEY METABOLITE PROFILE OF [^{18}F]FPYKYNE-LOSARTAN IN RATS. RATS WERE CO-INJECTED WITH 5 MG/KG (N=4) OR 10 MG/KG (N=5) CANDESARTAN AND 0.5-1.0 MCI [^{18}F]FPYKYNE-LOSARTAN. RESULTS SHOW DECREASED TRACER AND LABELED HYDROPHOBIC METABOLITE PROPORTIONS UPON BLOCKING COMPARED TO CONTROLS (0 MG/KG CANDESARTAN), WHILE LABELED HYDROPHILIC METABOLITES ARE INCREASED. $P < 0.05$ * COMPARED TO BASELINE; # COMPARED TO PREVIOUS DOSE (ARKSEY, 2012).

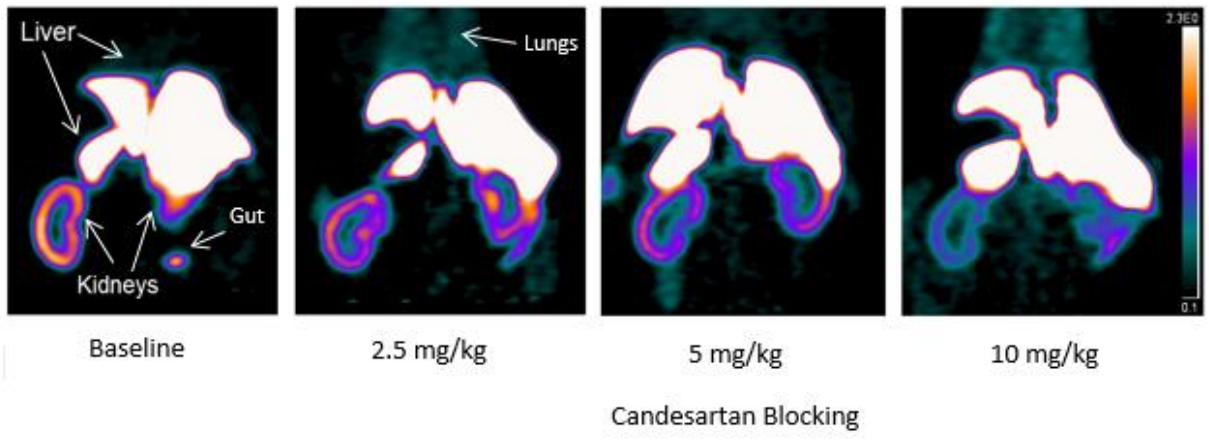

FIGURE 13- MICROPET IMAGING OF [^{18}F]FPYKYNE-LOSARTAN IN RATS. [^{18}F]FPYKYNE-LOSARTAN ALONE (BASELINE) AND IN THE PRESENCE OF CANDESARTAN AT DOSES OF 2.5 MG/KG, 5 MG/KG AND 10 MG/KG. FULL BLOCKAGE OF AT_1Rs IS OBTAINED WITH 10 MG/KG AND NO UPTAKE IS OBSERVED BY KIDNEYS COMPARED TO BASELINE (ADAPTED FROM ARKSEY ET AL., 2014).

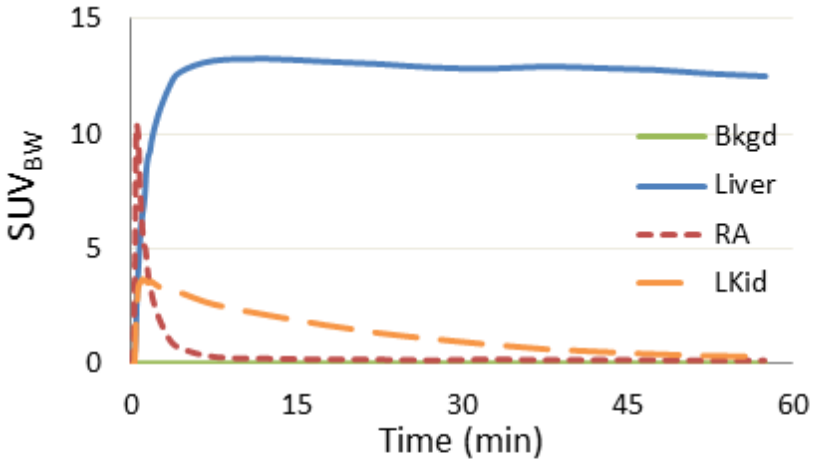

(A)

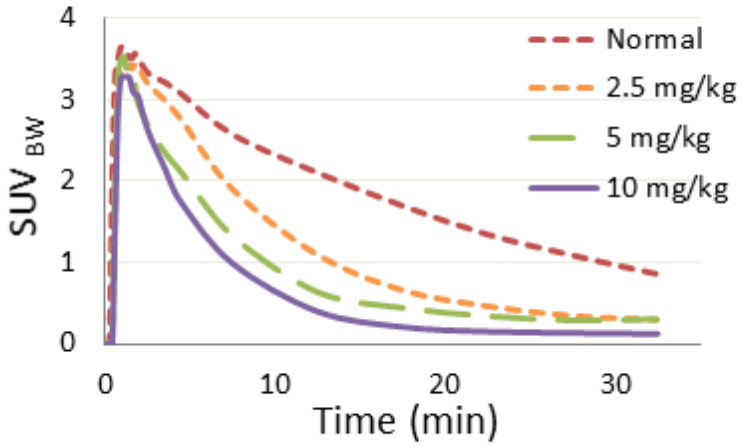

(B)

FIGURE 14- PRELIMINARY MICROPET IMAGING OF [^{18}F]FPYKYNE-LOSARTAN IN RATS. **(A):** TAC (SUV) CURVES OF LIVER, RIGHT ATRIUM (RA), AND LEFT KIDNEY (LK) OBTAINED BY MICROPET IMAGING OF [^{18}F]FPYKYNE-LOSARTAN IN RATS (BASELINE). **(B):** DOSE-RESPONSE EFFECT OF CANDESARTAN ON [^{18}F]FPYKYNE-LOSARTAN UPTAKE BY KIDNEYS. THE GRAPH SHOWS STANDARD UPTAKE VALUE (SUV) CURVES NORMALIZED TO BODY WEIGHT (BW) IN KIDNEY IN NORMAL CONDITION (ONLY [^{18}F]FPYKYNE-LOSARTAN INJECTED) AND IN THE PRESENCE OF CANDESARTAN BLOCKING AT DOSES OF 2.5 MG/KG, 5 MG/KG AND 10 MG/KG. THE DOSE-DEPENDENT DECREASE IN THE SUV PROVIDES EVIDENCE FOR THE SPECIFICITY OF [^{18}F]FPYKYNE-LOSARTAN TO AT_1RS (ARKSEY ET AL., 2014).

2. Thesis Overview

2.1. Hypotheses

- In vitro studies will further confirm that [^{18}F]FPyKYNE-Losartan binds with high affinity and selectivity to AT_1R over AT_2R in kidney tissues, thus, validating PET findings.
- FPyKYNE-Losartan will have an antagonistic effect upon binding to AT_1Rs.
- [^{18}F]FPyKYNE-Losartan will exhibit favorable uptake kinetics in rat and pig kidneys to allow evaluation of AT_1R binding potential via PET.
- Plasma protein binding of [^{18}F]FPyKYNE-Losartan will be similar to that of Losartan.
- The metabolism of [^{18}F]FPyKYNE-Losartan in rat plasma and kidney and in pig plasma will indicate minimal interference of ^{18}F- labeled metabolites to AT_1Rs.
- Dosimetry studies will show that [^{18}F]FPyKYNE-Losartan is safe for progression to humans.

2.2. Research Aims

2.2.1. General Objective

To fully characterize our novel radiotracer [^{18}F]FPyKYNE-Losartan and evaluate its potential as an imaging agent for renal AT_1Rs.

2.2.2. Specific Objectives

1. To validate PET findings using in vitro binding studies and calculate K_d and B_{max} of [^{18}F]FPyKYNE-Losartan.
2. To assess antagonistic activity of FPyKYNE-Losartan in rats through an invasive blood pressure measurement technique following carotid artery cannulation.
3. To characterize the pharmokinetics and time course of [^{18}F]FPyKYNE-Losartan in rat and pig kidneys using PET imaging, and validate reproducibility by test-retest studies.

4. To measure proportions of free and plasma protein bound [^{18}F]FPyKYNE-Losartan in rat plasma by an ultrafiltration method.
5. To evaluate proportions of metabolites along time by ex vivo HPLC metabolism studies: in rat plasma and kidney, and pig plasma during normal and blocked studies.
6. To calculate human dose equivalents of [^{18}F]FPyKYNE-Losartan and residence times for selected organ targets per unit of administered activity.

3. Materials and Methods

The following procedures include some work done by lab colleagues or collaborators, and are specifically confined to: syntheses and radiosyntheses of both unlabeled FPyKYNE-Losartan and [^{18}F]FPyKYNE-Losartan (Dr. Tayebeh Hadizad and Yanick Lee; OHI), determining K_d, B_{max}, and ED_{50} values of our compound using GraphPad Prism® (Dr. Mario Tiberi; OttawaU), performing rat surgeries for antagonistic studies (Richard Seymour; OHI), rat microPET imaging and data analysis (Natasha Arksey; OHI), assisting in pig PET imaging and pig plasma gamma counting (Julie Ting; OHI), pig PET imaging and data analysis of 1 blocking scan performed prior to this thesis (Basma Ismail, Dr. Rob deKemp; OHI), and calculation of rat and human residence times and effective doses using OLINDA/EXM, in addition to fitting equations used for arterial input function corrections (Chad Hunter; OHI). Excluding what has been stated, subsequent methods were personally performed in the course of this thesis.

3.1. General Procedures

3.1.1. Animals

All animal procedures were performed according to the guidelines of the University of Ottawa Animal Care Committee and the Canadian Council on Animal Care for the Use and Care of Laboratory Animals.

Rats used were normal male Sprague-Dawley rats (body weight 200-350 g) (Charles River, Canada). Female Sprague-Dawley rats (200-350 g) (Charles River, Canada) were also used for the dosimetry studies. Rats were housed in pairs on a 12-hour light-dark cycle and were provided with standard rat chow and water ad libitum. They were allowed a minimum of 5 days of acclimatization upon arrival before any experiments are performed. Radioligand injections were administered directly through the lateral tail

vein or via a catheter inserted to the lateral tail vein. Catheters, when used, were flushed with 0.2 ml of heparinized saline to reduce residual activity in the catheter.

Female Yorkshire pigs (body weight 30-35 Kg) (Panmure Farms, Canada) were utilized for PET scanning and HPLC metabolism studies. They were kept for one week upon arrival before performing any studies.

3.1.2. Drugs

Losartan was purchased from Merck & Co. Inc., Candesartan was purchased from Toronto Research Chemicals Inc., and PD123319 from Sigma-Aldrich Co.

3.1.3. Radiochemical Synthesis

Radiosynthesis of [^{18}F]FPyKYNE-Losartan is done using the automated TRACERLab FX N Pro dual reactor module (Figure 15). Briefly, [^{18}F]FPyKYNE is first prepared then purified via a convenient method using 3 silica gel cartridges in series between Reactor-1 and Reactor-2, saving time without HPLC (Valdivia et al., 2012). [^{18}F]FPyKYNE-Losartan is synthesized from the addition of [^{18}F]FPyKYNE to azido-trityl-Losartan via “click chemistry” in chemical and radiochemical purities >97% within 2 hours (Arksey et al., 2014).

The first step in the production of [^{18}F]FPyKYNE-Losartan, is radiofluorination of the nitro precursor. This step occurs in the first reaction vessel using [^{18}F]KF/K222/K2CO3 in anhydrous DMSO at 120^{o}C for 10 min. Purified [^{18}F]FPyKYNE is delivered to the second reaction vessel in a 15-20% yield (decay-corrected) by passing the reaction mixture through a series of three silica cartridges with an eluent of 50:50 ether/pentane (Valdivia et al., 2012). Following evaporation of the solvent, the labeled prosthetic group is then conjugated to the azide-modified tetrazole-protected Losartan precursor for 30 min at 95^{o}C in DMSO (Figure 11). The reaction mixture is then cooled, treated with TFA, and heated to 80^{o}C for 2 min

prior to loading onto HPLC. The fraction containing [^{18}F]FPyKYNE-Losartan is collected and loaded onto a preconditioned C18 cartridge (SPE) to remove the HPLC solvents. Pure [^{18}F]FPyKYNE-Losartan is eluted with minimal EtOH and diluted in saline to provide the final product in 44-70% yield (decay-corrected from [^{18}F]FPyKYNE), or an overall yield of 7-14% (decay-corrected from end-of-beam (EOB)). The yield is much lower than that of the non-radioactive synthesis likely due to shorter reaction times, the amount of F-18 fluoride available for radiofluorination compared to the stoichiometric quantities used for the synthesis of the standard, and product loss in the components of the module (i.e. reaction vessels, tubing, cartridges).

The identity of the product is confirmed by a single peak on analytical HPLC following a co-injection of the formulated product with cold standard.

3.2. In Vitro Binding Studies

In vitro binding assay were performed to confirm PET findings of [^{18}F]FPyKYNE-Losartan's binding potential to the AT_1R. Methods were adapted from previous work (Roth BL; Johnström et al., 2012; Davenport and Russell, 1996; Higuchi et al., 2001; Leenen et al., 2003; Tan et al., 2004). Briefly, naïve rats were sacrificed by decapitation. Kidneys were quickly removed, immersed in isopentane for no more than 5 seconds, frozen on dry ice and stored at -80^{0}C until sectioning. Kidney slices (20 µm, 18^{0}C) were cut by cryostat and thaw mounted on VWR Micro Slides (Superfrost® Plus) three sections per slide. These slides were stored at -80^{0}C until the day of experiment. The buffer used for this study (incubation and washing buffer) was: 150 mM NaCl, 1 mM EDTA, 50 mM Na_3PO_4, 0.1% BSA and 0.1 mM bacitracin (Sigma) at a pH of 7.2. Slides were exposed to an Imaging Screen K (phosphor screen) and imaged with the Molecular Imager® FX. Binding densities were quantified using a computer-assisted image analysis system (QuantityOne Software).

3.2.1. Screen Testing

In the process of optimizing our protocol and ensuring accuracy of our results, our phosphor screens were tested and standard curves with FDG were made using these screens to confirm linearity and reliability of our findings. Likewise, during the actual experiments a standard of [^{18}F]FPyKYNE-Losartan was prepared alongside the slides in every exposure.

3.2.2. Determining Ideal Exposure Time and Image Resolution

Although previous work has specified the appropriate length of exposure time to be 3-4 hours for F-18 tracers to yield good images (Johnström et al., 2012), a 3 hour exposure with our experiments resulted in highly dense images and saturation of the high activities. In this case, standard curves were no longer linear. Therefore, we decided to test the screens with FDG, NaF or any F-18 labeled ligand and produce standard curves after exposing for 30 min, 1 hour, 2 hours and 3 hours, then compare the results and choose the time yielding the best results. Ideal image resolution had to be identified as well. Previous colleagues have used 100 μm resolution for reading the images. However, to confirm whether this was the best resolution at which our images are to be analyzed (among 50, 100, 200 and 800 μm), screens were tested with FDG by creating a standard curve and comparing linearity at each of the specified resolutions**.**

3.2.3. Binding Affinity Study

In vitro binding studies were done to determine affinity of [^{18}F]FPyKYNE-Losartan to AT_1Rs. Specific binding corresponds to the subtraction of total binding (TB) and nonspecific binding (NSB). From the saturation binding curve the parameters K_d and B_{max} were determined representing respectively: the equilibrium dissociation constant, which corresponds to the reciprocal of the equilibrium affinity constant (K_a); and the maximum binding capacity of the ligand, which corresponds to the total amount of receptors (AT_1Rs in our case, binding to the radioligand [^{18}F]FPyKYNE-Losartan). For these experiments, two sets of

slides were needed: one set of 10 slides representing total binding and another set of 10 slides representing nonspecific binding (Figure 16).

3.2.3.1. Total Binding

For the total binding (TB) group, 10 Eppendorf tubes of 2 ml were needed to prepare 10 concentrations of [^{18}F]FPyKYNE-Losartan by serial dilution, ranging from 1 to 500 nM. A volume of 1.5 ml incubation buffer was added to tube 1, whereas 750 µl buffer was added to each of the other 9 tubes.

[^{18}F]FPyKYNE-Losartan solution in tube 1 was prepared by diluting with incubation buffer. The volume of [^{18}F]FPyKYNE-Losartan to remove from the stock into tube 1 was calculated by multiplying the activity needed in tube 1 (determined using specific activity (SA)) with 1.5 ml, then multiplying the result with [volume (ml)/ activity (mCi)] of the stock.

Afterwards, serial dilution was initialized by removing 750 µl from tube 1 into tube 2, vortexing tube 2, then from tube 2 to tube 3, and vortexing tube 3 and so on. These steps were repeated for the rest of the tubes respectively.

PD123319 was present in all the tubes to block AT_2Rs. A stock of PD123319 of concentration 1 x 10^{-3} M was prepared. To obtain a final concentration of 10^{-5} M of PD123319, 15 µl were removed from the stock into tube 10 having a final volume of 1.5 ml and 7.5 µl into all other tubes. Tubes were then vortexed (VWR Vortex).

3.2.3.2. Nonspecific Binding

The binding to all the sites other than the AT_1R is considered nonspecific binding (NSB). To assess NSB, cold Ang II was added in a concentration of at least 1000 times more into all tubes, and that is to flood both AT_1Rs and AT_2Rs with Ang II and block their receptor sites. Similarly to total binding, 10 slides with 3 kidney sections per slide were prepared. Another set of Eppendorf tubes (2 ml) were prepared as

well, having the same volumes and concentrations of [^{18}F]FPyKYNE-Losartan as in total binding and following the same serial dilution procedure. The only difference was that instead of adding PD123319 to the tubes, Ang II was added. The stock of Ang II made was of concentration 1 x 10^{-3} M, then 15 µl were removed from this stock into tube 10 and 7.5 µl into every other tube of this set, to get a final concentration of 10 µM of Ang II in each tube.

3.2.3.3. Standard Curve

To ensure that our serial dilutions were properly done, and that our results are reliable such that increasing activity corresponds to increasing density of activity, a standard curve of [^{18}F]FPyKYNE-Losartan was done alongside the slides in every assay. Five µl were removed out of each tube of either TB or NSB and added to a TLC plate previously marked for the 10 concentrations of tracer.

3.2.3.4. Incubation and Preparation for Exposure

The slides were pre-incubated with buffer for 1 hour at RT while shaking (at 50 rpm), then were incubated with 750 µl of each respective radioligand concentrations without shaking, that is, 250 µl for each slice. The slides were covered with lids to maintain humidity. Incubation was stopped by transferring the slides to racks and washing them while shaking in 250 ml baths of buffer, distilled water, then buffer again for 15 min each. Then slides were dried with a stream of warm air using the heat gun, taped with the TLC plate on a cardboard, and placed in a Ziploc bag prior to exposure to a phosphor screen. The phosphor screen was formerly exposed to white light for 1 hour with the light box to ensure the phosphor crystals were at ground state. The phosphor screen was then placed against the radioactive samples in an exposure cassette (X-ray cassette) to avoid adjusting the position of the screen after contact with the samples in order to prevent blurred images.

3.2.3.5. Image Acquisition and Analysis

The slides were imaged using the BioRad Molecular Imager FX and quantified by QuantityOne software. Images were acquired at 200 µm resolution. For quantification, a rectangular shaped region was drawn by the "volume rectangle tool" around the whole kidney area and total counts were recorded for that area. The same area of each section, and the same rectangular shape was used to quantify all sections for one given dataset (Figure 17). The same approach was applied for the standard. A volume analysis report of the results was exported to an excel sheet. TB and NSB results were plotted on the same graph, and separately the standard curve, showing increasing intensities as a function of increasing radioligand concentration.

A specific binding (SB) curve is obtained by subtracting total binding and nonspecific binding intensities at each concentration of radioligand. K_d describing the binding affinity is determined as the concentration of tracer required to occupy 50% of available receptors, while B_{max} is determined as the maximum number of receptors bound to the tracer.

A Scatchard analysis usually gives more accurate values of these parameters (Davenport and Russell, 1996; Tan et al., 2003). In a Scatchard plot, the slope is equal to the negative reciprocal of the K_d (nM), and the intercept of the line with the abscissa axis is an estimate of B_{max} that could be expressed in a unit of fmol/mg protein, fmol/tissue weight, or fmol/mm^2. These values would then be used as initial estimates in the computer program LIGAND that uses nonlinear curve fitting to calculate the final binding parameters (K_d and B_{max}). Another possible interpretation method is GraphPad Prism®. This software was used for our results. Best-fitted values of K_d and B_{max} were obtained by global nonlinear regression either using the best-fitted graphs of TB and NSB, or the best-fitted graph of SB obtained by subtracting TB and NSB. K_d was acquired in nM and B_{max} in fmol/mm^2. SA (mCi/µmol) of each assay was taken into account to calculate B_{max}, by converting the obtained DPM/mm^2 to mCi using the conversion factor 1 DPM= 450 fCi, then dividing this activity with the SA in mCi/fmol to get a unit of fmol/mm^2. For example, if the SA is 500 mCi/µmol, then that is equivalent to 500 x 10^{-9} mCi/fmol (A). Having a B_{max} of 350000 DPM/mm^2, for

instance, would correspond to 1.6 x 10^{-4} mCi (B) (based on the conversion factor: 1 DPM= 450 fCi), thus, dividing the result of (B) with that of (A) would give a B_{max} of 315 fmol/mm^2. Other factors that should be taken into consideration are the area of tissue and slice thickness (Shuttleworth et al., 2001; Farkas et al., 2012), but since kidney slices are sliced consecutively with equal thickness (20 µm), these factors could be neglected in the calculation.

To show reproducibility and repeatability of our findings, five binding affinity assays were performed with different [^{18}F]FPyKYNE-Losartan formulations/productions. The final binding parameters of our tracer were calculated from the mean of the five assays ± SE (standard error).

3.3. In Vivo Studies

3.3.1. Antagonistic Studies

This study is done to assess arterial blood pressure variations in correspondence to administering AT_1R blockers (ARBs) and the cold compound of our tracer, F-19 FPyKYNE-Losartan standard, further verifying binding specificity and determining the EC_{50} (the concentration required for obtaining 50% of the maximum effect of Ang II in vivo) of FPyKYNE-Losartan.

Male rats (250-350 g) were used for this study. Carotid artery cannulations were performed by a technician (Richard Seymour; OHI) on anaesthetized control rats (60 mg/Kg sodium pentobarbital, i.p.). Although sodium pentobarbital was known to have a variable response rate and likely affect blood pressure, previous research had published the use of this anesthetic for this type of study (Almansa et al., 1996; Champion et al., 1998; Parasuraman et al., 2012). Blood pressure was measured invasively by an optic fiber probe (SAII, SA Instruments, Inc.) (Parasuraman et al., 2012). A catheter was placed in the tail vein through which drugs were injected during the experiment. Once the carotid artery was cannulated, the PE tubing (mouse PE10 tubing) inserted into the artery while doing the surgery was attached to a saline filled bleedback control valve (COPILOT) from one side, and the fiber optic blood pressure probe

fixed through the other side of the valve. The other end of the probe was connected to the PC-SAM extension of the PC-SAM box. ECG leads and body temperature probe were attached to the animal, and PC-SAM software was used to read blood pressure. Animals were kept warm at 37^{o}C by means of thermostat-controlled heating boards. ECG, mean arterial blood pressure, systolic and diastolic blood pressures, and respiratory rate were monitored (Figure 18). Before beginning with the injections, animals were left 15 min for their readings to stabilize. At the end of the experiments, rats were euthanized by an overdose of sodium pentobarbital (90 mg/Kg, i.v.) (Parasuraman et al., 2012).

FPyKYNE-Losartan doses were prepared by dissolving in saline and sodium bicarbonate ($NaHCO_3$), in ratios of 2/3 and 1/3 of total volume, respectively, while heating. However, this vehicle didn't seem to dissolve our lipophilic compound properly at higher doses. Therefore, another vehicle was used. Since ethanol and propylene glycol are known to help dissolve lipophilic compounds- but are allowed in small proportions in rats- we decided to test a vehicle consisting of 5% EtOH, 20% propylene glycol, 50% saline and 25% $NaHCO_3$. Its effect on arterial blood pressure increase upon injecting Ang II in untreated rats was compared to the effect of our initial vehicle (designated vehicle 1). In the ideal case, the new vehicle (designated vehicle 2) should cause no differential outcome in the controls, so that it could be used for the higher doses of FPyKYNE-Losartan. Only then could the corresponding results be merged and compared to those obtained using the initial vehicle.

Final doses were injected in a 0.2-0.4 ml volume, followed by flushing with 0.2 ml of saline.

3.3.1.1. Angiotensin II Dose-Response Effect

To conduct the dose-response curve for Ang II, anesthetized rats (n=4) were injected with Ang II i.v. in a volume of 0.2 ml and the catheter was flushed with 0.2 ml saline.

The doses injected of Ang II were 0.03, 0.1, 0.3, 1, 3, 10, 30 and 100 µg/Kg. For the lower doses, which elicited a rise in diastolic blood pressure of less than 20 mmHg, full recovery from the response was

permitted. For the higher doses, Ang II was injected cumulatively with each successive injection given immediately after the maximal effect of the preceding dose (usually 10-20 sec) (Wong et al., 1990). After plotting the dose-response curve, the submaximal dose was graphically determined as the dose producing the effect just before the maximum effect, in other words the dose causing the submaximal increase in blood pressure.

3.3.1.2. Group I: No Treatment

For the sake of comparison and calculating the inhibition (%) of the effect induced by Ang II for each test compound, submaximal dose effect was assessed in a group of untreated rats (control group) (n=3). For this group, 15 min before injection of Ang II submaximal dose, the animal was pretreated with saline vehicle (0.2 ml) (Almansa et al., 1996; Almansa et al., 1997).

3.3.1.3. Group II: Treatment

3.3.1.3.1. ARBs

The effect of AT_1R blockers Losartan and Candesartan was examined at different doses until obtaining full blockage of AT_1Rs. This study was done to optimize and validate our procedure. Doses were injected i.v. 15 min prior to injecting Ang II at its submaximal dose, then dose-response curves for each blocker were plotted. The inhibition (%) of the effect induced by Ang II (submaximal dose, i.v.) was calculated for each test compound in relation to the one obtained in untreated animals, based on the following equation:

Blocking %= [(normal Ang II increase - blocked Ang II increase) / normal Ang II increase] x 100

OR: 100 – [(blocking effect/ normal effect) x 100]

These equations directly calculate the percentage of AT_1R blocking; the remaining proportion would represent the effect of Ang II bound to AT_1Rs (available receptors).

3.3.1.3.2. Losartan

Losartan powder was dissolved in saline with no heat, then the volume to be removed from the stock and prepare the desired dose (mg/Kg) was calculated. Doses of Losartan tested were: 1 mg/Kg (n=1), 2.5 mg/Kg (n=1), 5 mg/Kg (n=1), 10 mg/Kg (n=1), 20 mg/Kg (n=1) and 30 mg/Kg (n=3).

3.3.1.3.3. Candesartan

Candesartan was prepared by dissolving the powder in a volume of 2/3 saline and 1/3 $NaHCO_3$ while heating. The volume of candesartan solution to be removed was calculated to obtain the following doses: 1 mg/Kg (n=1), 2.5 mg/Kg (n=1), 5 mg/Kg (n=1), 7.5 mg/Kg (n=1) and 10 mg/Kg (n=3).

3.3.1.3.4. FPyKYNE-Losartan

Finally, FPyKYNE-Losartan was injected i.v. 15 min before Ang II submaximal dose injection in increasing doses: 3 mg/Kg (n=1), 10 mg/Kg (n=3), 15 mg/Kg (n=3), 25 mg/Kg (n=1), 30 mg/Kg (n=1) and 50 mg/Kg (n=1) to obtain a dose-response curve. Dose-response curves were fit to a four parameter logistic equation (top and bottom asymptotes, ED_{50} and slope or Hill factor) using GraphPad Prism® (Dr. Tiberi; OttawaU). The ED_{50} (effective dose 50; dose producing 50% of the desired effect in vivo) of the blockers was determined. The blocking effect of our compound was compared to that of Losartan and Candesartan, which are full antagonists, and to untreated rats, in means of inhibiting Ang II's effect on blood pressure.

3.3.2. PET/MicroPET Imaging and Analysis

Two types of PET scanners were used. The human PET scanner (GE Discovery PET/CT (64 Slice) D690) was used for pigs (Figure 19), and a dedicated small animal PET scan (Siemens Inveon TM) for rats (Figure 20).

3.3.2.1. Rat Studies

3.3.2.1.1. MicroPET Imaging

MicoPET imaging was previously done and analyzed by a first user (Natasha Arksey), then reanalyzed in the course of this thesis by a different user (Maryam Hachem) to determine inter-user variability. The method followed for small animal PET was the following: rats (n=7) were anaesthetized with isoflurane (2-2.5%), weighed, and positioned supine on the scanner bed, and body temperature maintained at 37^{o}C. Then, rats were injected with 0.4-1.0 mCi of [^{18}F]FPyKYNE-Losartan in a 1 ml bolus via a 26 gauge catheter into the lateral tail vein. Anesthesia was maintained throughout the scanning process by a continuous flow of isoflurane (1-2%) through a nose cone. Heart and kidneys were maintained in the field of view (FOV). Body temperature, heart and respiratory rates were monitored throughout the scans. Dynamic scans were for 60 minutes.

3.3.2.1.2. Image and Data Analysis

When analyzing rat images, data was reconstructed using Siemens Inveon Acquisition Workplace software (IRW 4.0). Dynamic histograms were created with the following frame composition: 12 x 10 seconds, 3 x 60 seconds, and 11 x 300 seconds. Corrections were done for scatter to compensate for photon deflection, and attenuation to compensate for photon loss caused by tissue density. Regions of interest (ROIs) were placed on the left arterial (LA) cavity (blood pool), liver, and left kidney to obtain time activity curves (TACs), and regional tracer uptake was estimated using the Logan graphical method to generate Distribution Volumes (DVs) for the selected ROIs; as an indirect indication of AT_1R binding.

3.3.2.2. Pig Studies

3.3.2.2.1. PET Imaging

In the course of this thesis, PET imaging was performed with 3 pigs (this part of the studies was done with the help of a medical summer student at our lab, Julie Ting). Pigs were anesthetized by the Animal Care and Veterinary Services staff using a drug called Telazol (0.044 mg/Kg), which is a combination of tiletamine and zolazepam. Xylazine was added to reconstitute the compound. The pigs were also given glycopyrrolate at a dose of 0.01 mg/kg. Once properly sedated, they were masked with isoflurane until unconscious, and finally intubated. The pigs were placed in supine position. First, a CT scout scan was performed (with 40 ml of an iodine based contrast agent), then a low-dose CT for attenuation correction followed by a 10 min 82-Rubidium scan (10 MBq/Kg) to ensure that both kidneys are in the FOV, and finally a 90 min PET scan in the GE Discovery D690 PET-VCT scanner with [^{18}F]FPyKYNE-Losartan (5 MBq/Kg) injected into pig ear vein. Test, retest and blocking studies were carried out for each pig in consecutive weeks. Blocking studies were performed with 10 mg/Kg Candesartan i.v. 10-15 min prior to [^{18}F]FPyKYNE-Losartan injection, to ensure full blockage of AT_1Rs.

3.3.2.2.2. Image and Data Analysis

The IRW software was also used to analyze reconstructed dynamic images of pig scans. Dynamic PET scans were aligned with the corresponding Computed Tomography Angiography (CTA), to ensure accurate creation of regions of interest. A CTA is a computed tomography technique used to visualize arterial and venous vessels throughout the body. Since the organ of interest is the kidney, renal CTA's were performed to image vessels of the kidney. ROIs were placed on the abdominal aorta to account for blood uptake (at frame 4), and on right and left kidneys (RK, LK) (at frame 17).

Using the aorta to derive the input function is more accurate than using the inferior vena cava (IVC) as the model's input function is represented by the radioactivity concentration in arterial plasma (Schain et al., 2013), although there is a slight time difference of around 10 sec separating blood entering the kidneys (through aorta) and blood leaving (through IVC).

Time-activity curves (TACs) were generated for the arterial blood input function (derived from aorta) and kidney uptake, displaying standardized uptake values (SUVs) (Beaulieu et al., 2003; Fabiilli et al., 2013). [^{18}F]FPyKYNE-Losartan renal activity was calculated as SUV (g/mL) at 10-15 min (12.5 min) post-injection (frame 20).

Logan analysis was used to quantify the tracer DV, which is the expected ratio of radiotracer in tissue relative to plasma at equilibrium for receptor ligands binding reversibly (Logan et al., 1996). Basically, it is a function of free receptor, and provides an index of in vivo binding potential which represents receptor density (B_{max}) and ligand affinity ($1/K_d$) for the receptor. Logan slope or tracer DV (mL/cm^3) for every scan was derived graphically from the [^{18}F]FPyKYNE-Losartan curve at 10-90 min (frame 20-35) after injection.

A blocking scan performed previously for preliminary pig data (Basma Ismail, 2012; OHI) was reanalyzed and added to those of the other 3 pigs (for the sake of obtaining more deductive results), and will be designated as blocking scan 4 (see section: 4.3.2.).

3.3.2.2.3. Arterial Input Function Corrections

The radioactivity of unchanged parent tracer in plasma is the only component available for extraction to tissue, and thus is the only factor quantified for the arterial input function. In essence, the input function represents the proportion of total circulating radioactivity available for specific binding. It could be affected by several components, namely: activity in blood cells, labeled plasma metabolites and plasma protein bound tracer, which act to dilute the activity available for targeted tissue uptake. To avoid underestimating the true tissue uptake and retention of the radiotracer, and to achieve meaningful quantification, these sources of activity should be ideally discerned from the unchanged parent radiotracer in plasma (Lammertsma, 2002; Gunn et al., 2001).

To obtain accurate quantitative analysis of PET imaging with [^{18}F]FPyKYNE-Losartan in pigs, input function should be corrected. However, since plasma protein binding in pig plasma was not assessed, two corrections were merely attempted: a whole-blood correction for radioactivity in plasma over time, and a metabolite correction for unaltered parent tracer in plasma. The first correction is done by multiplying with the plasma-to-whole-blood activity ratio (determined from blood and plasma sampling: Section 3.5.). Correction for ^{18}F-labeled metabolites in plasma is applied by multiplying the input function with the fraction of unchanged/unmetabolized tracer at each time point (determined by HPLC metabolite analysis: Section 3.7.). Corrected numbers would then be imported into the IRW software and taken as the reference for Logan's graphical method to export the new DV values.

3.3.2.2.4. Partial Volume Effect Correction

Partial volume effect corrections were also applied. Essentially, kidneys in larger animals as pigs (imaged by the PET/CT scanner) are big enough and are minimally affected by partial volume as opposed to small animals (imaged by μPET), however, the aorta, which is taken as reference for blood, is very small compared to the resolution of PET. So, applying PVC here is an asset. The ROI is accurately drawn around the aorta using the renal CTA. Exact dimensions of the aorta ROI (vertical and horizontal lengths) are then obtained using the ruler tool available in the Siemen's Inveon Workstation (IRW 4.0) software. After fitting an equation relating the recovery coefficient factor to the aorta diameter (mm), a correction factor is determined for the average aorta diameter of all subjects and used for PVC.

3.3.2.3. Reproducibility and Repeatability

Reproducibility is the ability of an entire experiment or study to be reproduced reliably, either by the researcher or by someone else using the same procedure (test-retest). Reproducibility is one component of the precision of a measurement or test method, the other component is repeatability,

which is the degree of agreement of tests or measurements on replicate specimens by the same observer in the same laboratory. It is referred to as “intra-user variability” if the second analysis is done by the same person, or “inter-user variability” when the comparison is between two different users. Both repeatability and reproducibility are usually reported as a standard deviation (ASTM F1469 and ASTM E177; Thackeray et al., 2013; Thorn et al., 2013).

3.3.2.4. Test-Retest and Inter-User Variability

For pigs, test-retest scans were performed to determine reproducibility of the SUV/DV calculation, and to verify reliability of results. Animals were scanned a second time in a different session and using a new [^{18}F]FPyKYNE-Losartan formulation. Results from the test and retest scans of each animal were compared; a 95% confidence interval was generated for the mean difference between both scans and used to determine whether or not this difference is significantly different from zero. A Bland-Altman analysis was also performed to assess the agreement and reliability of the whole procedure (Bland and Altman 1986).

For rat scans, inter-user variability was calculated. Two users analysed the same [^{18}F]FPyKYNE-Losartan images to compare DV values (first user: Natasha Arksey; second user: Maryam Hachem). A Bland Altman plot was created to show variability between the two users and compare repeatability of the results (Bland and Altman, 1986). The following equation comparing DV values of the 2 users was used to calculate test-retest variability (TRV):

$$|\text{User1} - \text{User2}| \,/\, [(\text{User1} + \text{User2}) / 2]$$

3.4. Blood and Plasma Sampling

In the course of carrying out PET scanning and HPLC metabolism studies for pigs, and HPLC for rats, whole trunk blood samples were being collected from the animals to perform blood and plasma counting.

This study is done because when calculating tissue DVs and obtaining TACs, it is important to account for tracer concentration in the plasma relative to whole blood. Any tracer bound to red blood cells (in whole blood) won't cross the capillaries into the tissue, whereas, tracer in plasma would be available for the tissue. Neglecting this aspect would result in inaccurate DVs, more specifically DVs would be overestimated as they would represent a ratio of tissue to blood rather than tissue-to-plasma (where: blood activity < plasma activity).

When a blood input function is not readily available and/or usable from image data, intra-venous (i.v.) blood sampling is used to determine the time-activity of tracer in the plasma (Logan, 1990). In our studies, blood activity data is available from the images analyses (ROIs drawn around the left atrial cavity (in rats)/ aorta or inferior vena cava (in pigs)). However, this gives no information about the relative proportion of [^{18}F]FPyKYNE-Losartan in the plasma compartment relative to whole blood. Thus, blood and plasma sampling was performed to obtain a plasma-to-whole blood ratio, then an adjusted plasma time-activity curve.

Briefly, blood samples were collected into heparinized vacutainers tubes out of which 100 µl of whole blood was taken at the specific time points, transferred to pre-weighed gamma counter tubes (VWR), then tubes were post-weighed and counted for radioactivity in the gamma counter (Packard, Cobra II) (Figure 21). Afterwards, blood was centrifuged at 3000 g (4000 rpm) for 5 min (Figure 22) to obtain plasma, and another 100 µl was removed from the supernatant, transferred to pre-weighed gamma counter tubes, weighed again, and counted for radioactivity. The time points at which blood was collected for the pig studies were 0 (blank), 0.5, 1 , 2, 5, 10, 20, 40, 60 and 90 min.

Decay-corrected counts were normalized to sample weight (net weight) and expressed as plasma-to-whole blood ratio over time. Plasma is considered to represent 55% of whole blood.

3.5. Plasma Protein Binding

Plasma protein binding was assessed using the Centrifree® Ultrafiltration Device (Figure 23) (Lortie et al., 2013). Whole trunk blood samples were collected into heparinized tubes from male Sprague-Dawley rats sacrificed by decapitation without anaesthesia. Blood was centrifuged at 4000 rpm for 5 min, then 1.0 ml of obtained plasma was transferred into a glass culture tube to which 100 µl of authentic [^{18}F]FPyKYNE-Losartan was added. The aliquot of plasma and tracer was added to the upper chamber of the ultrafiltration device following the manufacturer's specifications, while 100 µl were left aside as unfiltered plasma. The device was then centrifuged at 2000 g (4090 rpm) for 30 min. Free tracer in plasma would pass to the bottom chamber through the membrane separating the two chambers (MW cutoff of Mb= 30,000 Da). Then, 100 µl of each of the filtrate (in the bottom chamber) and the plasma protein bound tracer (in the upper chamber) were transferred to pre-weighed gamma tubes and counted in the gamma counter, as well as the 100 µl aliquot of unfiltered plasma and tracer to act as a measure of total plasma activity. To determine net weight of samples, gamma tubes were post-weighed. This study was completed in quintuplicate.

The proportion of free tracer in plasma was calculated based on the following equation:

$$[\ (\text{Activity} / \text{mass})_{\text{filtrate}} / (\text{Total activity} / \text{mass})_{\text{plasma}}\ ] \times 100 \quad (\%)$$

The remaining proportion was made up of the plasma protein-bound radioligand. The final percentage of plasma protein bound [^{18}F]FPyKYNE-Losartan was calculated as the average of the 5 assays.

3.6. Metabolite Analysis

To determine ^{18}F-labeled metabolites that could adversely affect both microPET imaging and kinetic modeling, High Performance Liquid Chromatography (HPLC) metabolite analyses were performed. Analyzing the data made it possible to determine the proportion of detected radioactivity present in metabolites and unchanged tracer in plasma and tissue at selected time points. This study was completed in rats (plasma and kidney) and pigs (plasma only).

The HPLC column-switch method developed by (Hilton et al., 2000; Kenk et al., 2008) was commonly used by our group in previous studies (Figure 24). Mobile phases, columns and procedure conditions were optimized for the use with [^{18}F]FPyKYNE-Losartan (Arksey et al., 2014). Briefly, the HPLC apparatus consisted of 2 pumps (Waters): one eluting solvent A (1:99 MeCN/water [v/v]) at 1.5 mL/min across the capture cartridge (Alltech Direct-Connect refillable guard column, 20 mm) packed with sorbent (HLB VAC RC, Waters Oasis) and fitted with 2.5 lm frits (Alltech, 2- mm filter elements); and the other eluting solvent B (35:65 MeCN/ 0.1 M ammonium formate [v/v]) at 3 mL/min across the analytical column (Luna 10u C18 (2) 100A, 250 x 4.6 mm, 10 μm; Phenomenex). Eluents of both columns were analyzed in series by two detectors: the ultraviolet (UV) absorbance detector at 254 nm (Waters 486), and coincidence radiation detector (Bioscan). Signals were integrated using the PeakSimple Six-Port Chromatography Data System (Chromatographic Specialities), and expressed as the percentage of total noise- and decay-corrected radioactivity signal. Prepared samples (2 mL) were injected onto the capture column, then after elution of proteins, macromolecules and hydrophilic metabolites (6-7 min), column flow was switched delivering solvent B across the capture cartridge, eluting retained compounds onto the analytical column for analysis.

Data was corrected for noise, radioactive decay, and unretained peak of control sample. Equations for correction were the following:

- Noise correction: area of peak-(width of peak x noise AUC); where AUC: area under curve

- Radioactive decay correction: $A_t = A_o / e^{\lambda \, x \, t}$; where:

- A_t = sample radioactivity at the measurement time t
- A_o = radioactivity at the injection time
- $\lambda = \ln 2 / T_{1/2}$
- $T_{1/2}$: half-life of ^{18}F (= 109.77 min)

- Unretained control peak correction: peak 1 % of sample – ((unretained control % x tracer sample %) / tracer control %)

3.6.1. Rat Metabolism Studies

3.6.1.1. Plasma Samples

Restrained rats were injected with 2-4 mCi (74-148 MBq) [^{18}F]FPyKYNE-Losartan via the lateral tail vein, and sacrificed by decapitation at 5, 10, 20, and 30 min post-injection (n=3 rats per time point). Rats serving as controls were not injected and were decapitated first. Collected trunk blood samples were centrifuged at 4000 g for 5 min, then plasma samples were prepared by mixing with 1 g urea to break binding with macromolecules, filtered with a 0.2 μm syringe filter (Nylon Membrane, Acrodisc®(R)), and injected onto the HPLC system. Control plasma samples were prepared by spiking filtered plasma with ~ 10 μCi [^{18}F]FPyKYNE-Losartan right before injection through the injection port of HPLC. The relative proportions of unchanged tracer and labeled metabolites in plasma and kidney were estimated.

3.6.1.2. Tissue Samples

Following decapitation, rats were dissected. Kidneys were collected and kept on ice until use. Kidney tissue was homogenized using the Polytron (PT 1200) on full speed (setting 6) by moving it up and down until no large pieces were discernable, then dissolving in 10 ml of cold 80/20 EtOH/water [v/v] in a 50 ml tube. The polytron was rinsed with 80/20 EtOH/water between tissue samples. Homogenous slurry were then transferred into the ultracentrifuge (Beckman L8-70M Ultracentrifuge) (Figure 25) and spun at 82000 g (22000 rpm) for 15 min, then tissue supernatant collected and transferred to conical flasks to be evaporated using the Rotavap (Rotavapor, RE111) and afterwards redissolved in 1/99 CH_3CN/water containing 0.4 g/ml urea. The final solution was filtered twice with the 0.2 μm syringe filters and injected

into the HPLC system. Tissue controls were spiked with ~ 50 μCi [^{18}F]FPyKYNE-Losartan right before injection, similarly to plasma control samples.

3.6.2. Pig Metabolism Studies

Test and retest studies (normal) as well as blocking studies were carried out on three pigs, by which they were performed separately on consecutive weeks for each pig (Figure 26). Only plasma samples were collected from pigs. Trunk blood samples were collected, centrifuged, mixed with 1 g urea, filtered, and injected onto HPLC. Samples were prepared similarly to the preparation procedure of rat plasma samples. HPLC data was corrected for noise, radioactive decay, and unretained peak of parent tracer (control).

3.6.2.1. Normal Studies

Pigs were tested the first week (Figure 26). 5 MBq/Kg of [^{18}F]FPyKYNE-Losartan was injected into pig ear vein, and blood was removed from the femoral vein at 0 (control), 1, 2, 5, 10, 20 and 40 min post-injection. Control blood was collected before tracer injection. The same pig was retested the next week following same procedure, to validate reproducibility.

3.6.2.2. Blocking Studies

On the third week of the study (Figure 26), a blocking scan was performed for the pigs to assess any change in tracer-to-metabolite ratio due to specific binding of metabolites to AT_1Rs. 10 mg/Kg Candesartan were administered (i.v.) 15 min prior to tracer injection to ensure blockage of AT_1Rs, followed by 5 MBq/Kg of [^{18}F]FPyKYNE-Losartan (i.v.). Blood was collected at -5 (control), 1, 2, 5, 10, 20 and 40 min post-tracer injection.

3.7. Dosimetry Studies

3.7.1. Pilot Study

3.7.1.1. Gamma Counter Standard Curve

Before executing the actual study, some pilot studies were done to ensure accuracy of our final results and precision of our procedure. The first step towards proving so was developing a standard curve for the gamma counter which was the sole counting method for radioactivity of tissues; so accurateness of this instrument was crucial. By plotting a standard curve, radioactivity in counts per minute (CPM) was related to amount of activity measured in samples in μCi. This graph was referred to later during the final calculations of our full-scale study, when converting activity from CPM to μCi was needed.

The F-18 labeled ligand FDG was used for the standard curve. Dilutions of the stock were made to obtain activities of 0, 1, 2, 4, 6, 8, 10, 12 and 20 μCi. Volumes to remove from the stock for each activity were calculated, then added to gamma counter tubes and toped up with saline/water until 1 ml. The gamma counter was set up and results were obtained (CPM) and back corrected to the time of measuring stock FDG activity.

3.7.1.2. FDG Trial

A dosimetry trial was performed with FDG before the actual study was commenced. One female rat was used for the study and sacrificed 5 min after FDG injection. Its organs were dissected out and tissues of interest samples were transferred to gamma counter tubes to be counted. A more detailed description of the study is depicted in the following section.

3.7.2. Full-Scale Study

To determine the dosimetry profile of [^{18}F]FPyKYNE-Losartan, ex vivo biodistribution in rats was implemented (Figure 27). Sprague-Dawley rats (3 males and 3 females for each data point) (Loevinger et al., 1988; Lourenco et al., 2001). Rats were injected with ~ 0.5 mCi of [^{18}F]FPyKYNE-Losartan (at time of first injection) into tail vein then sacrificed by decapitation without anesthesia at 5, 15, 30 and 60 min

post-injection, which were the time points chosen for this study. A blood sample from each rat (~ 1.5 mL) was collected from the trunk right after decapitation in heparinized vacutainers. Contents of each animal were dissected: brain, eyes, thymus, thyroid, heart, lungs, pancreas, spleen, esophagus, red marrow, bone (trabecular + cortical), adrenal glands, kidneys, liver, bladder, urine, blood, stomach wall and contents, lower large intestine wall and contents, upper large intestine wall and contents, and small intestine wall and contents, in addition to testes from males and ovaries, breasts and uterus from females. Urine was collected directly from the bladder by a syringe. Tissue samples were collected in pre-weighed and labeled gamma counter tubes. The rest of the organ was left aside to be weighed for total organ weights were required for the calculations. Standards were needed for this study to transfer unit of activity into percentage of injected dose (%ID), knowing that the standard corresponded to 1% of ID. Therefore, 3 standards (aliquots of the injected solution) were created by drawing the same *volume* of tracer as injected into the rats by a syringe and adding it to a bottle containing 100 ml of 10% EtOH/H_2O. From this solution, 1 ml was removed into each of 3 gamma counter tubes labeled STD to correspond to standards. Radioactivity remaining in the tails, and syringes was counted in a dose-calibrator, and taken into account in the calculation of the injected dose. Activity of the carcass was used to account for "remaining activity" of each rat at the end of the experiment (Lourenco et al., 2001), and added to activity of brown paper used throughout the procedure, which could contain radioactivity, to calculate percentage of activity recovery of the study. All activity data was back-corrected (decay corrected) to the time of the first injection (reference time) and that activity at time zero was assumed to be zero. When tubes were ready to be counted, gamma counter was set by entering reference time and date. Tissue samples were counted along with standards. After counting, tubes were post-weighed to determine net weight of samples to which back-corrected counts were normalized.

Mean activity data of each organ was calculated as %ID per tissue and %ID/g of tissue, and plotted against time. Fractional activity was then calculated per unit time by the following equation:

(% ID/g x mass of organ) / 100

Exponential functions were fitted for each graph then integrated (from 0 to $+\infty$) to obtain rat residence times (Bq-h/Bq), also called "time integrated activity" which is the newer term (Chad Hunter; OHI). "Residence times" is a probability distribution function that describes the amount of time a fluid element (i.e. the tracer) spends inside the reactor (i.e. the organ). Residence time is defined to be the total integrated activity in a tissue (usually in Becquerel Hours or Bq-h) per unit total injected activity (or Bq-h/ Bq). The next step was converting rat residence times into human residence times. This was done by applying the Feller equation (Feller et al., 1975):

$$\left(\frac{\%ID}{organ}\right)_{human} = \left[\left(\frac{\%ID}{organ}\right)_{rat} \times \left(\frac{m_{TB}}{m_{organ}}\right)_{rat} \times \left(\frac{m_{organ}}{m_{TB}}\right)_{human}\right]$$

Where m_{TB} is total body mass of rat or human, m_{organ} is mass of tissue or organ of rat or human, and %ID/organ the % of injected dose for the organ in question for rat or human.

The total marrow and bone values were divided into red and yellow marrow and cortical and trabecular bone respectively in equal ratios as per guidelines (ICRP, 1975). Safety limits were applied as published in FDA regulations Code of Federal Regulations Title 21, Volume 5, Section 361.1

Human residence times were then entered into the OLINDA/EXM software to obtain the absorbed doses to selected target organs per unit of administered activity, referred to as the effective dose (ED) and effective dose equivalent (EDE) (mSv/MBq). OLINDA/EXM is a software program from the RADAR group, which uses the MIRD method in conjunction with the ICRP 30/60 protocols to calculate effective doses (ICRP 1987; ICRP 1998). Effective doses of [^{18}F]FPyKYNE-Losartan were calculated using ICRP 60 and 103 protocols.

3.8. Statistical Analysis

Results are presented as mean ± standard deviation (SD) calculated as the average from data of each animal. Student's t-test (paired or unpaired, as appropriate) was used to determine statistical

significance. A p-value of <0.05 was considered significant for all tests. N values for each comparison are given in the text or in the figure/table. Bland-Altman plots were used to display inter-user variability or test-retest results. Test-retest variability (TRV) was assessed by calculating the ratio of absolute value of the difference between repeated measurements and the mean of repeated measurements:

$$TRV = \frac{|V1 - V2|}{(V1 + V2)^2} \cdot 100\ (\%)$$

3.9. Figures

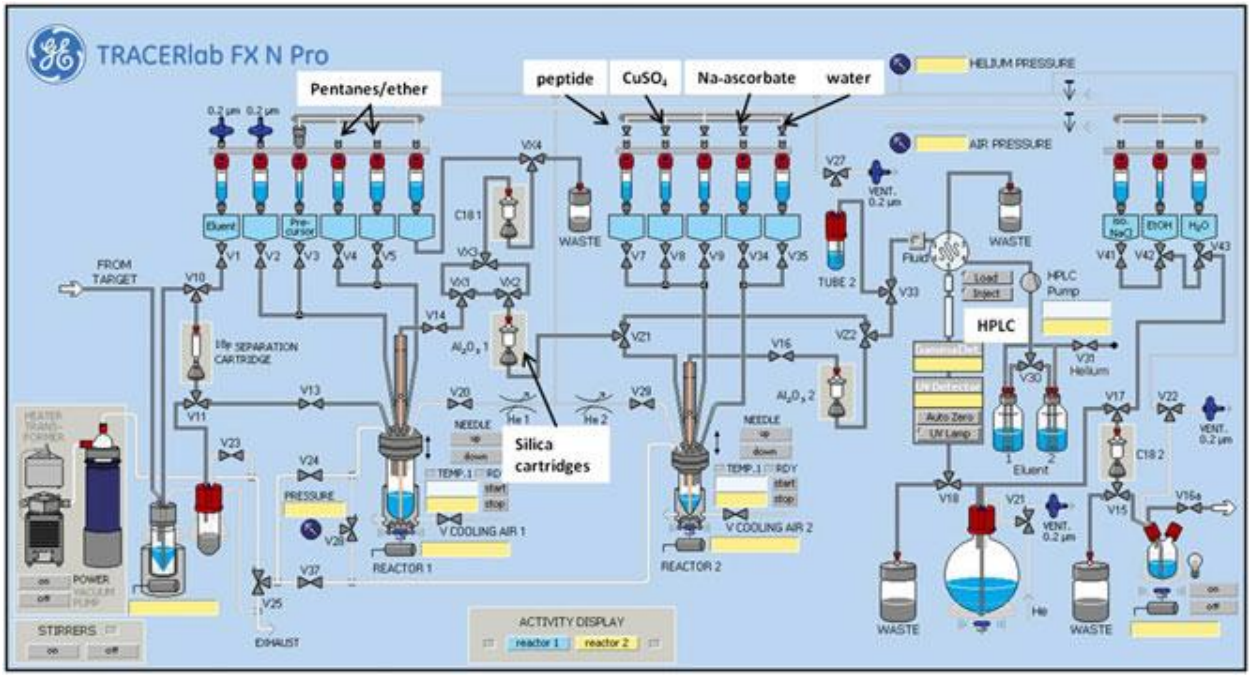

FIGURE 15- SCHEMATIC OF THE TRACERLAB FX N PRO (BY GE HEALTHCARE) USED TO SYNTHESIZE [^{18}F]FPYKYNE-LOSARTAN. MODIFICATIONS ARE INDICATED WITH ARROWS. SCHEMATIC WAS PROVIDED BY GE HEALTHCARE.

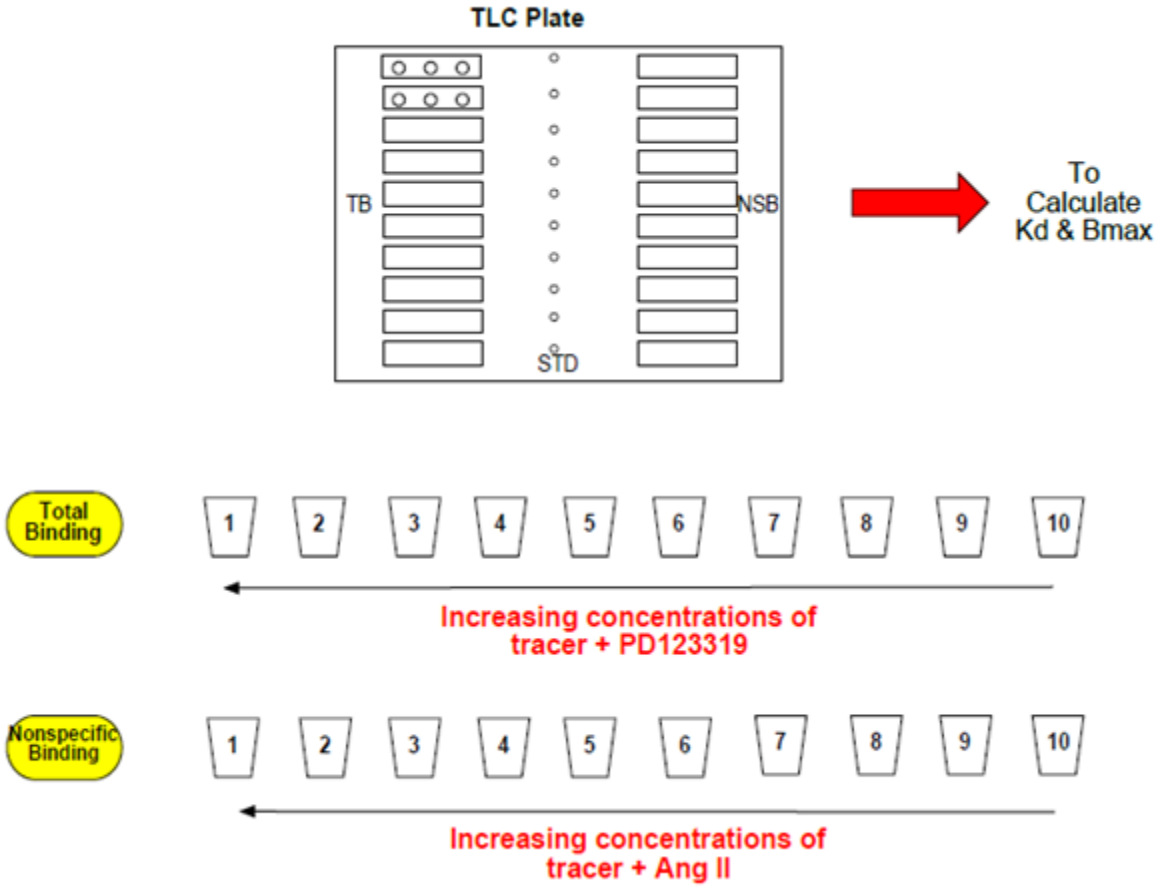

FIGURE 16- A SCHEMATIC DIAGRAM FOR BINDING AFFINITY PROTOCOL OF THE BINDING STUDIES.

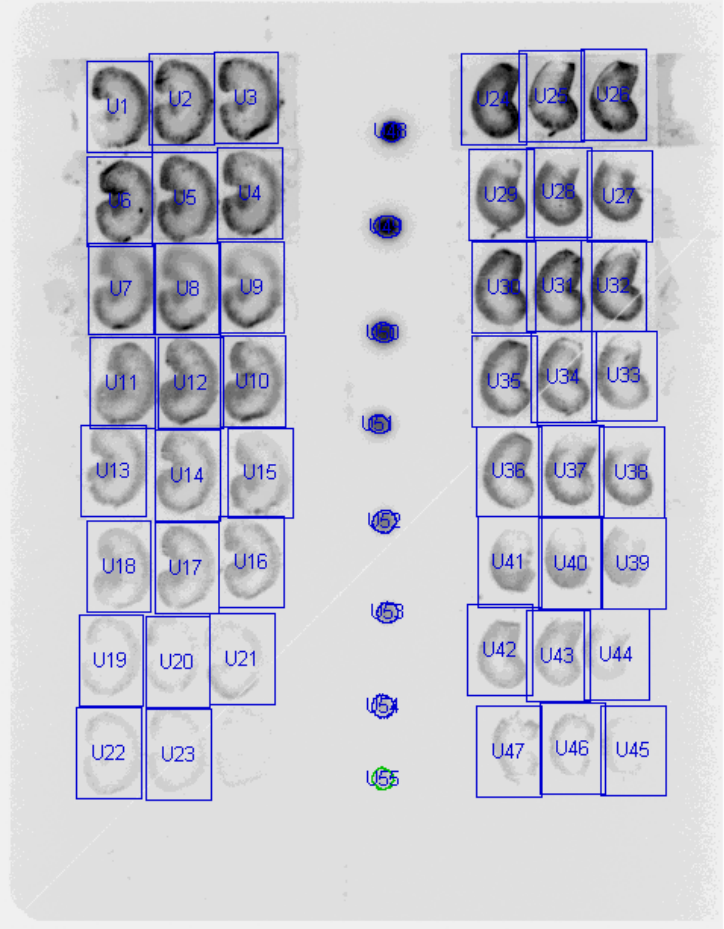

FIGURE 17- IMAGE ANALYSIS OF BINDING ASSAYS IS DONE USING QUANTITYONE SOFTWARE. EQUAL RECTANGLES ARE DRAWN BY THE "VOLUME RECTANGLE TOOL" AROUND THE WHOLE KIDNEY AREA FOR QUANTIFICATION. THE SAME APPROACH IS APPLIED FOR THE STANDARD BY WHICH EQUAL CIRCLES ARE DRAWN AROUND THE DOTS OF RADIOACTIVITY. THEN, A VOLUME ANALYSIS REPORT IS EXPORTED TO AN EXCEL SHEET.

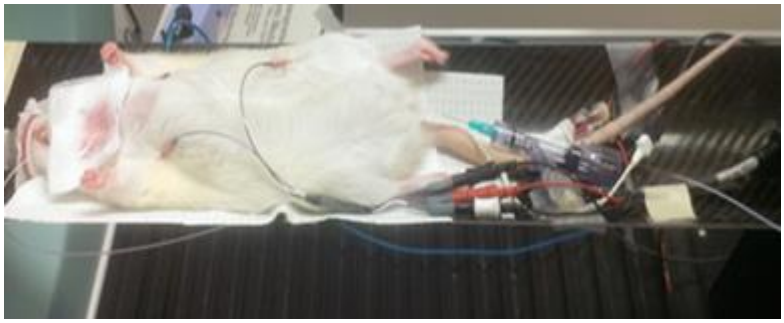

FIGURE 18- A PHOTOGRAPH SHOWING THE PREPARATIONS FOR BLOOD PRESSURE MEASUREMENTS DURING ANTAGONISTIC STUDIES. A RAT THAT HAS UNDERGONE SURGERY IS SHOWN ON THE SCANNER BED CONNECTED TO THE PC-SAM DEVICE.

FIGURE 19- HUMAN PET SCANNER (GE DISCOVERY D690 PET-VCT SCANNER).

FIGURE 20- MICROPET SCANNER USED FOR IMAGING SMALL ANIMALS (SIEMENS INVEON TM).

FIGURE 21- THE PERKIN-ELMER (PACKARD) COBRA II GAMMA COUNTER.

FIGURE 22- JOUAN CR3I REFRIGERATED BENCH TOP CENTRIFUGE.

FIGURE 23- CENTRIFREE (R) ULTRAFILTRATION DEVICE USED FOR ASSESSING PLASMA PROTEIN BINDING. IT WORKS BY SEPARATING FREE FROM PROTEIN-BOUND MICROSOLUTES IN SMALL VOLUMES (0.15- 0.1 ML) OF SERUM, PLASMA AND OTHER BIOLOGICAL SAMPLES THROUGH A LOW-ADSORPTIVE HYDROPHILIC MEMBRANE AND USING A METHOD CALLED ULTRAFILTRATION.

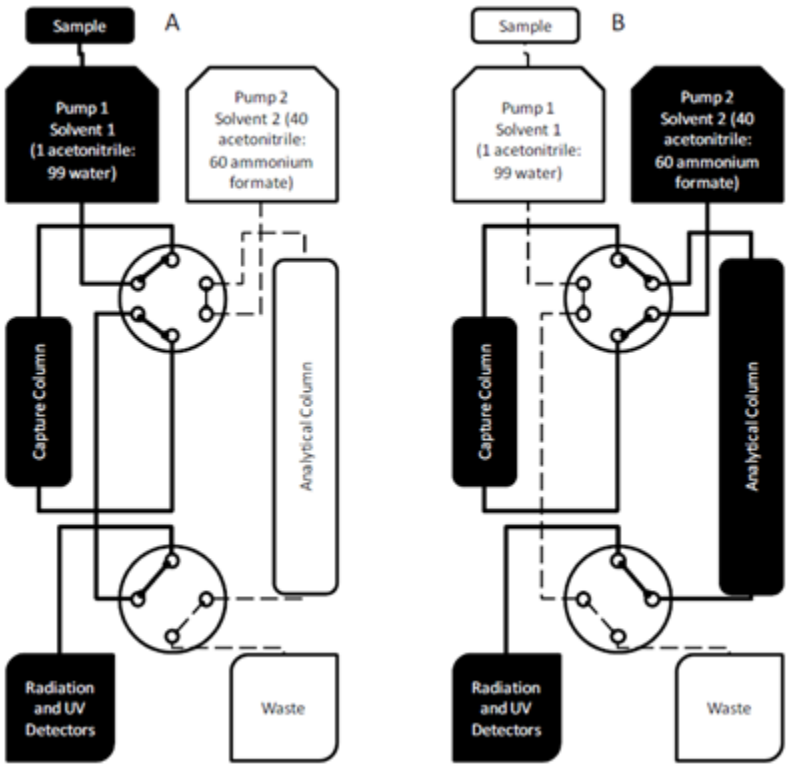

FIGURE 24- FLOW DIAGRAM OF HPLC SWITCH SYSTEM USED FOR METABOLITE ANALYSIS OF PLASMA AND TISSUES. IN **(A)**, SAMPLE IS INJECTED AND IS TRANSFERRED WITH SOLVENT 1 ONTO THE CAPTURE COLUMN (CAPTURE COLUMN ELUATES ARE DETECTED). IN **(B)**, BOTH VALVES ARE SWITCHED AND CAPTURED COMPONENTS ARE BACK-FLUSHED USING SOLVENT 2 ONTO THE ANALYTICAL COLUMN (ANALYTICAL COLUMN ELUATES ARE DETECTED). ADAPTED FROM HILTON (HILTON ET AL., 2000).

FIGURE 25- BECKMAN L8-70M ULTRACENTRIFUGE USED FOR CENTRIFUGING HOMOGENIZED RAT KIDNEY TISSUE DURING METABOLISM STUDIES.

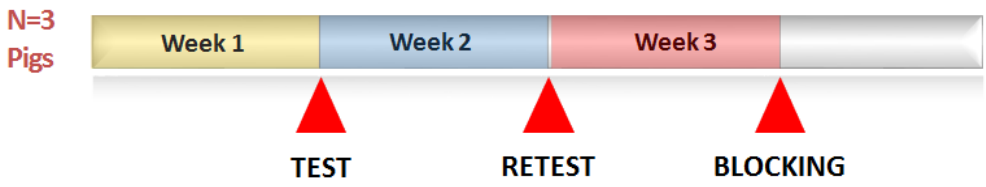

FIGURE 26- PIG METABOLISM STUDIES TIMELINE. N=3 PIGS WERE USED FOR THESE STUDIES. EACH PIG WAS TESTED ON THE FIRST WEEK, THEN RETESTED ON THE SECOND. FOR THESE 2 STUDIES [^{18}F]FPYKYNE-LOSARTAN (5 MBQ/KG) WAS INJECTED I.V. AND BLOOD WAS COLLECTED AT SPECIFIC TIME POINTS. ON THE THIRD WEEK, A BLOCKING STUDY WAS PERFORMED BY INJECTING 10 MG/KG OF CANDESARTAN 15 MIN PRIOR TO TRACER INJECTION.

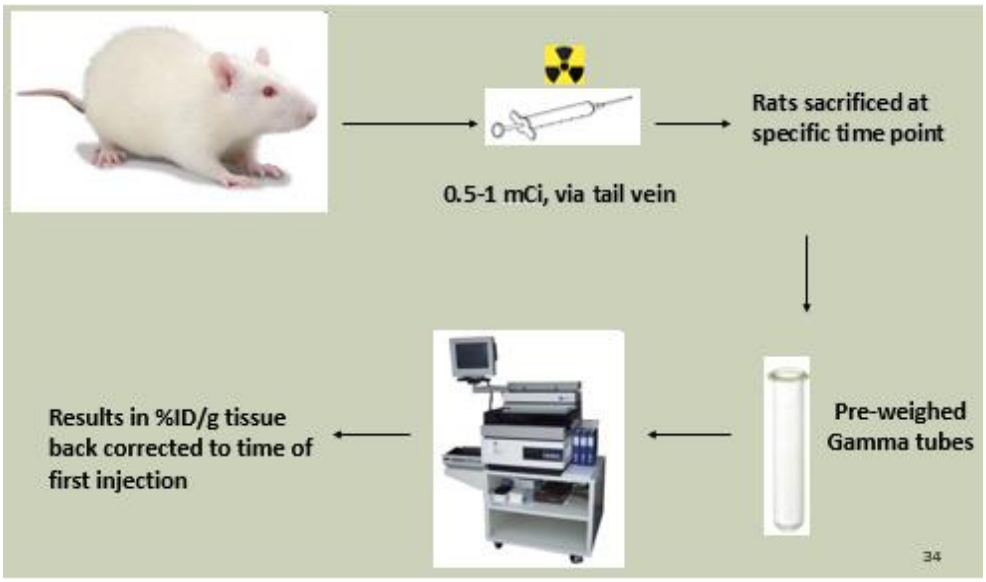

FIGURE 27- FLOW DIAGRAM DISPLAYING EX VIVO BIODISTRIBUTION PROCEDURE. AFTER TRACER INJECTION, RATS WERE DECAPITATED AT DESIRED TIME POINTS. PRE-WEIGHED GAMMA TUBES CONTAINING TISSUE WERE COUNTED RADIOACTIVITY IN A GAMMA COUNTER (PACKARD, COBRA II) AND POST-WEIGHED. DECAY CORRECTED COUNTS WERE CALCULATED AS A PERCENT OF THE INJECTED DOSE PER GRAM OF TISSUE (%ID/G), AND BACK CORRECTED FOR RADIOACTIVE DECAY BY SETTING THE REFERENCE TIME AS THE TIME OF FIRST INJECTION.

4. Results

4.1. In Vitro Binding Studies

4.1.1. Exposure Time and Image Resolution

Phosphor imaging screens were tested with FDG to validate the procedure and assess maximal dose that would saturate the screen. The three tested screens provided linear results exhibiting increasing intensity/density with increasing concentration shown both visually and numerically (Figure 28).

FDG was exposed against phosphor imaging screens for 30 minutes, 1 hour and 3 hours, and the corresponding standard curve plotted to determine which exposure time was the best to obtain linearity, hence using it as the time of exposure for our images. Comparing the result of the different exposure times showed that 1 hour was the best as 30 minutes was not enough to expose the highest densities of activity, and 3 hours was too much exposure thereby causing saturation of the screen at high activity (Figure 29).

Because the phosphor imager gives the option of reading images at different resolutions (50 μm, 100 μm, 200 μm and 800 μm), it was important to decide which resolution was optimal. The aim was to choose the resolution providing clearer images (high resolution), yet not too high causing saturation of activities. 50 μm represents the highest resolution, while 800 μm is the least. 800 μm was excluded from the testing because it refers to the lowest resolution and images obtained would be blurred and unclear. Similarly for this experiment, increasing concentrations of FDG were added on TLC plates and exposed by phosphor screens. In the first set of experiments, the differentiation was between 50 μm and 100 μm: 100 μm displayed better linearity than 50 μm. However, 200 μm provided better results than 100 μm in the second set of experiments (Figure 30). Thus, the choice of resolution was 200 μm.

Therefore, a 1 hour exposure and 200 μm resolution were applied for imaging kidney slices in the binding studies.

4.1.2. Binding Affinity Study

Images obtained showed higher density of activity in kidney cortex compared to medulla. This was more obvious in the TB group compared to NSB, where the latter displayed less pronounced binding with minor difference between cortex and medulla densities (Figure 31). Less dense kidney images were obtained with less activity concentrations of the radioligand, and standard curves showed good linearity (Figure 32). Nonlinear curve fitting using a global fit was applied by GraphPad Prism® to plot best fitted graphs for total binding, nonspecific binding and specific binding for each assay (Figure 33). However, because using TB and NSB curves provided less variable results than using SB curve only, this was the approach relied on for the final results to determine the specific binding parameters of [^{18}F]FPyKYNE-Losartan (Figure 34). The average values of K_d and B_{max} from the 5 assays were 49.4 nM and 348 ± 112 fmol/mm^2, respectively (Table 1).

4.2. Antagonistic Studies

4.2.1. Angiotensin II Dose-Response Effect

For n=4 rats, Ang II caused a dose-dependent increase in blood pressure, and the submaximal dose was determined graphically to be 3 μg/Kg (Figure 35) which goes in line with the literature (Almansa et al., 1996; Almansa et al., 1997), thus, confirming our methodology.

4.2.2. Group I: No Treatment

The control group (n=3) injected with 3 μg/Kg Ang II (submaximal dose) at t=15 min caused an increase in BP of ~ 50 mmHg (Figure 36). This was considered the normal Ang II pressor response. The effect of treatment compounds was determined as the percentage of inhibition of this response.

4.2.3. Group II: Treatment

4.2.3.1. ARBs

Losartan exhibited a dose-dependent antagonism of AT_1Rs upon i.v. injection. Approximately 70% blockage was obtained with a 10 mg/Kg dose and ~ 80% with 20 mg/Kg (n=1 each). A 30 mg/Kg dose (n=3) produced nearly 100% blockage of the receptors (Figure 37; Table 2). So, Losartan is considered a full AT_1R antagonist with 30 mg/Kg being a full saturating dose. The half maximal inhibitory dose (ID_{50}) of Losartan determined from its dose-response curve was 6.4 mg/Kg.

Similarly, Candesartan, which is a more potent AT_1R antagonist than Losartan, blocked AT_1Rs dose-dependently. As the Candesartan dose response curve displays, blocking increases from 78% to 95% by increasing the dose from 2.5 mg/Kg to 7.5 mg/Kg (n=1 each), respectively. At a dose of 10 mg/Kg, Candesartan fully blocks AT_1Rs (n=3) (Figure 38; Table 3), thus showing full AT_1R antagonism with an ID_{50} of 0.71 mg/Kg.

4.2.3.2. FPyKYNE-Losartan

Vehicle 2 (i.e. 5% EtOH + 20% propylene glycol + 50% saline + 25% $NaHCO_3$) produced an average increase of 51 mmHg following Ang II injection (n=3) (Figure 39) in untreated rats, indicating no effect of its additional constituents on blood pressure compared to vehicle 1 (50 mmHg increase). Thus, it is reasonable to compare the subsequent results with those of the other doses. Using this vehicle, the highest doses 30 and 50 mg/Kg of FPyKYNE-Losartan were assessed.

To determine the ED_{50} of our compound and whether it is a partial or complete antagonist as Losartan, a dose-response curve was plotted. With increasing doses of FPyKYNE-Losartan, an increasing blocking effect of AT_1Rs was obtained, however, not reaching 100% with the doses investigated. The blocking effect attained at the highest dose used (50 mg/kg) was 72% (Figure 40; Table 4). At the maximum blocking dose of its parent compound Losartan (30 mg/Kg), FPyKYNE-Losartan did not produce full blockage (46%). Likewise, at 10 mg/Kg, Losartan blocked AT_1Rs with a 70% effect, whereas FPyKYNE-

Losartan had a 26% (n=3). One would think that FPyKYNE-Losartan is therefore a partial antagonist. However, comparing the dose-response curves of Losartan, Candesartan and FPyKYNE-Losartan, FPyKYNE-Losartan displays lower potency than the other two blockers, but would also probably reach a 100% blockage (Figure 41). An ED_{50} of 25.5 mg/Kg was determined for FPyKYNE-Losartan from the curve fit, which represents the dose producing 50% of maximum response. Half maximal inhibition doses of the blockers were determined by GraphPad Prism® software using a four-parameter logistic equation (bottom, top, hill slope, $logID_{50}$), whereby the dose giving 0% or 100% effect was set to 0.01 mg/Kg so that a log transformation of the dose could be computed for the 0% and 100%. As shown in Table 5, the half maximal blocking dose of FPyKYNE-Losartan in vivo is around 4 times and 36 times less than that of Losartan and Candesartan, respectively (Table 5). Hence, like Losartan and Candesartan, FPyKYNE-Losartan is likely a full antagonist, yet not as potent.

4.3. PET/MicroPET Imaging and Analysis

4.3.1. Rat Studies

In previous work (Natasha Arksey), baseline microPET scans of rats injected with [^{18}F]FPyKYNE-Losartan displayed greatest accumulation of activity in the liver and kidneys, respectively. The time-activity curves (TAC) derived from the kidneys displayed a sharp increase in activity uptake in the first few minutes following blood input, then washed out slowly to background levels (at around 55 min) (Arksey et al., 2014). The average distribution volume in the left kidney of control rats obtained from Logan was measured at 2.7 ± 0.68 ml/cm^3 (n=7). When the rats were co-injected with the AT_1R antagonist Candesartan, tracer uptake in the left kidney was reduced in a dose-dependent manner. But to obtain "Inter-User Variability" another user had to repeat the DV calculation for baseline and blocking scans using their own ROIs (Maryam Hachem). For n=21, the average difference between our values was found to be 0.08 ± 1.52. Inter-user variability (calculated as: average [(difference/mean) x 100]) was 15.9%. This data

was plotted in a Bland-Altman plot and all data was in between the mean ± 1.96 standard deviations (Figure 42). From a paired two-tailed t-test, a p-value of 0.81 was found (>0.05), indicating that the difference between our results was not statistically significant and that there is an 81% chance that the difference between the 2 sets of data is due to random chance.

Based on re-analyzed data (User: Maryam), rat PET data showed DVs of 3.2 ± 1.04 on average in normal scans which decreased to 1.1 ± 0.31 in blocking scans at a Candesartan blocking dose of 10 mg/Kg. Thus, a blocking percentage of 67% could be calculated, also referring to specific binding of the tracer, whereas the remaining 33% referring to nonspecific binding as it represents the binding signal of [^{18}F]FPyKYNE-Losartan while AT_1Rs are blocked with Candesartan.

4.3.2. Pig Studies

Normal scans (test and retest) (n=3; 6 scans) displayed high kidney-to-blood contrast and slow clearance from kidneys (Figure 43). Highest uptake (SUV RK: 14.1 ± 6.15; SUV LK: 13.5 ± 5.64) was displayed at a 10-15 min time-frame (specifically 12.5 min) with an uptake ratio of 2.7 ± 0.68 on average for RK relative to blood (Figure 44). Upon blocking AT_1Rs, kidneys displayed reduced uptake (Figure 45). Results of blocking study 1 were excluded because of the improper injection of the blocker (it was co-injected with the tracer instead of being injected prior to it), so blocking percentages were based on blocking scans 2, 3 and 4. Blocking % derived from the SUV decrease was calculated to be around 60% in both RK and LK (Table 6).

As the AT_1R should be fully blocked at the 10 mg/kg dose, any tracer retention observed should be from nonspecific binding. The specific binding is thus represented as the reduced peak retentions in the renal cortex, and can be calculated as the difference in DV values obtained at baseline and when fully blocked with the 10 mg/kg dose over the DV at baseline. Blocking % based on DVs was 60.8% in RK and in 53.3% LK (Table 7). However, these are the percentages using the initial values of DV, that is, before correction for arterial input function and partial volume loss.

4.3.2.1. Arterial Input Function Corrections

Following partial volume corrections, input function was corrected for pig plasma activity by multiplying with the ratio of plasma to blood activity: 1.4 (Section: 4.4.), then imported into the IRW software and taken as the reference for Logan's graphical method. Corrected DV of normal scans (6 scans) was 5.4 ± 1.83 ml/cm^3 for LK and 5.5 ± 1.83 ml/cm^3 for RK.

Retest scans were performed to determine reproducibility of the DV calculation. Right kidney TRV and p-value (2-tailed t-test) of test and retest DVs were calculated to be 1.3 ± 0.05% and 0.98, respectively, showing no significant difference between the datasets (TRV << 15%, and p-value >> 0.05) (Table 8). Bland-Altman plot displayed a good fit of the data within +1.96 SD and -1.96 SD (Figure 46).

Based on corrected DVs, specific binding determined from blocking AT_1Rs in RK is ~ 55%, having a p-value of 0.03 (<0.05; 1-tailed t-test) (Table 8).

Typically, correction for metabolites in plasma should also be done for the input function by multiplying with the unmetabolized fraction of tracer (Section: 4.6.). Since the average number of data points for the uncorrected input function was 35 compared with only 6 data points for HPLC, an exponential correction function was derived to fit the blood metabolite data (Figure 47), then used to determine the unmetabolized tracer fraction at each time point. This fraction was multiplied with the arterial plasma input values to obtain corrected values for metabolites. The equation used was the following (19 degrees of freedom):

$$F_{unmet}(t) = \frac{1}{1 + \exp(-\frac{a}{t^3} + bt)}$$

Where: t is in time, and a and b are fitting constants.

For the normal case: a = 199.239 [min^3]; b = 0.1721 [min^{-1}]. Whereas, in the blocked case: a = 143.0 [min^3]; b = 0.3857 [min^{-1}].

However, because the Logan DV model did not seem to fit the data following metabolite correction, correction for metabolites was not performed.

4.3.2.2. Partial Volume Effect Correction

A curve relating aorta diameter and partial volume recovery factor was fitted. Using the curve equation, a mean correction factor of 2.5 (i.e. partial-volume recovery coefficient = 0.4) was calculated for an average of 10 mm diameter vessel.

4.4. Blood and Plasma Sampling

[^{18}F]FPyKYNE-Losartan injected into three pigs (i.v.) had a slightly higher concentration in plasma than whole blood over time (90 min) (Figure 48). When plotted over time, the ratio of activity per gram in plasma to that of blood remained almost unchanged over time. Based on this constant trend, an average ratio was calculated from all the time points. The plasma-to-whole-blood ratio was approximately 1.4 and was applied as a correction factor for the plasma input in calculation of DV values from PET images (Figure 49). The constant ratio facilitates whole-blood correction for radioactivity in plasma over time (arterial input corrections), as fitting an equation to the ratio data was unnecessary.

4.5. Plasma Protein Binding

The mean proportion of [^{18}F]FPyKYNE-Losartan binding to plasma proteins in rat plasma (n=5), primarily albumin, was assessed by the ultrafiltration device to be 97%, while 3% was free. Thus, [^{18}F]FPyKYNE-Losartan displays high plasma protein binding and a small fraction of the tracer is freely available for binding to AT_1Rs and metabolism by enzymes (Table 9).

4.6. Metabolite Analysis

4.6.1. Rat Metabolism Studies

4.6.1.1. Controls

Unaltered control samples of plasma and kidney tissue homogenate spiked with authentic [^{18}F]FPyKYNE-Losartan and injected onto HPLC had a small proportion of activity lost by the capture cartridge; this is referred to as the unretained tracer. However, radioactivity present in control samples was solely representative of unchanged [^{18}F]FPyKYNE-Losartan. Because HLB sorbent has been shown to be unable to completely capture authentic tracer, the addition of urea was necessary as it was shown to disrupt plasma protein binding (Hilton et al., 2000). On average, 6% of the total radioactivity signal was not captured in the initial phase of the study from plasma and 4% from kidney tissue homogenate (Figure 50). The proportion of tracer not retained by the capture cartridge was needed to correct the peak areas of the unretained metabolites and of unchanged tracer in the experimental runs (see section 3.7. for calculations).

4.6.1.2. Plasma

[^{18}F]FPyKYNE-Losartan exhibited three distinct radioactive peaks in rat plasma, with retention times of approximately 0.5-1 min (peak 1), 6.8 min (peak 2) and 10 min (peak 3) post-switch, respectively. Any radioactivity not trapped by the capture column, and hydrophilic metabolites, which are unlikely to bind to AT_1R, eluting in the initial phase of the study were designated peak 1. The peaks eluting after the column switch were any metabolites retained by the capture column as well as unchanged [^{18}F]FPyKYNE-Losartan. Peak 2 corresponded to a hydrophobic labeled metabolite that can potentially bind to AT_1R. The third peak was unchanged [^{18}F]FPyKYNE-Losartan (Figure 51). The proportion of unretained radioactivity (peak 1) rapidly increased over time from 18 ± 9% to 76 ± 10% between 5 and 30 minutes. Peak 2 was observed as a very small proportion of the total radioactivity and narrowly varied over time (4 ± 1% at 5 min to 1 ± 1% at 30 min). The total proportion of radioactivity of unchanged [^{18}F]FPyKYNE-Losartan (peak

3) decreased over time (78 ± 11% at 5 min to 23 ± 10% at 30 min) (Figure 52). All proportions were noise- and decay-corrected.

4.6.1.3. Kidney

In rat kidney, three total peaks were observed in HPLC chromatograms, corresponding to plasma samples. The retention times for these peaks were respectively: 1.7 min (peak 1), 7.5 min (peak 2) and 11.3 min (peak 3) post-switch (Figure 53). The proportion of unretained radioactivity (peak 1) increased less rapidly over time than in plasma (5 ± 4% at 5 min to 39 ± 20% at 30 min). Peak 2 proportion was very small and slightly varied over time (between 2 ± 1% at 5 min and 3 ± 2% at 30 min), similarly to plasma. However, unchanged [^{18}F]FPyKYNE-Losartan (peak 3) seemed to be more stable in kidney tissue than plasma since it decreased less rapidly over time and accounted for more than 50% of the total proportion of radioactivity (58 ± 19%) at 30 min post-injection (Figure 54).

4.6.2. Pig Metabolism Studies

4.6.2.1. Normal Studies

HPLC chromatograms of pig plasma in baseline studies displayed the presence of two peaks. The first peak has a retention time of 1.0-1.5 min and represents hydrophilic metabolite(s) which are very polar and thus elute from the capture column in the initial phase of the study. The second peak represents unchanged [^{18}F]FPyKYNE-Losartan which has a retention time of ~ 8.7 min post-switch (Figure 55). Analysis showed the presence of unchanged tracer until 20 min post-injection (6%), and thus [^{18}F]FPyKYNE-Losartan exhibited fast metabolism in pig plasma but it was solely representative of the labeled binding species to AT_1Rs (Figure 56).

4.6.2.2. Blocking Studies

When the AT_1Rs were blocked with Candesartan (10 mg/Kg), pig plasma showed the same radioactive peaks as in baseline studies, however, a faster clearance of [^{18}F]FPyKYNE-Losartan from

plasma. In essence, hydrophilic metabolite proportions rapidly increased with time (to 96% at 10 min) while [^{18}F]FPyKYNE-Losartan decreased to 4% by 10 min (Figure 57).

In normal and blocking studies, control samples revealed an average of 6% of authentic tracer unretained in the initial phase of the study (pre-switch), and thus, was used to correct unchanged [^{18}F]FPyKYNE-Losartan proportions in every run.

4.7. Dosimetry Studies

An FDG standard curve for the gamma counter was done to ensure linearity and accuracy of the procedure. The curve, displaying increasing CPM with increasing activity, was perfectly linear (Figure 58). Activities (in μCi) were determined from this graph whenever their corresponding counts per minute were known (from gamma counting).

The dosimetry trial with FDG helped adjust the procedure and ensure reliable data would be obtained by this protocol. A female rat was decapitated at 5 min and corrected counts were determined per gram of sample weight. [^{18}F]FPyKYNE-Losartan was distributed across the whole body as activity was detected is all organs, though blood, stomach, kidney, urine and adrenal gland exhibited the highest uptake at this time point.

Full-scale dosimetry studies were done subsequently to collect rodent data for estimations of human radiation dose equivalents and residence times of [^{18}F]FPyKYNE-Losartan. Tracer tissue uptake at 5, 15, 30, and 60 minutes post-injection in male and female rats correlate with the time-course data from in vivo PET imaging for tissues-of-interest. Similar trends were observed for both males and females. At 5 minutes post-injection, several organs displayed retention: liver, kidneys, lungs, adrenals, small intestine contents, heart, pancreas, spleen, ovaries, urine and blood. From 15 to 60 minutes post-injection, uptake levels in several of these tissues returned closer to baseline: ovaries, heart, pancreas, spleen and blood. Kidney, liver and urine maintained uptake until 60 minutes post-injection. Metabolism related tissues (liver, small intestine contents, upper and lower intestine contents, and urine) generally increased over

time (Table 10; Table 11; Figure 59; Figure 60; Figure 61). Similar residence times were observed for males and females (Table 12; Table 13). Highest uptake was by the liver (~ 80% at 5 min, increases to 90% at 10 min then decreases to 60-70% by 60 min). Its %ID/organ was in both sexes over 3 times more than the rest of the organs and accounted for an average of 39% of the effective dose (ED) (36% in males and 41% in females).

The sex averaged effective doses were calculated according to ICRP 60 and 103 protocols: 2.97E-02 (mSv/MBq) and 3.06E-02 (mSv/MBq), respectively (Table 14; Table 15). A mean of 85% of the total injected dose was recovered in the organs and carcass at the time points studied. All tissue and whole body dose values of [^{18}F]FPyKYNE-Losartan, however, were well below the 3-5 rem safety limits allowed by the FDA.

4.8. Tables and Figures

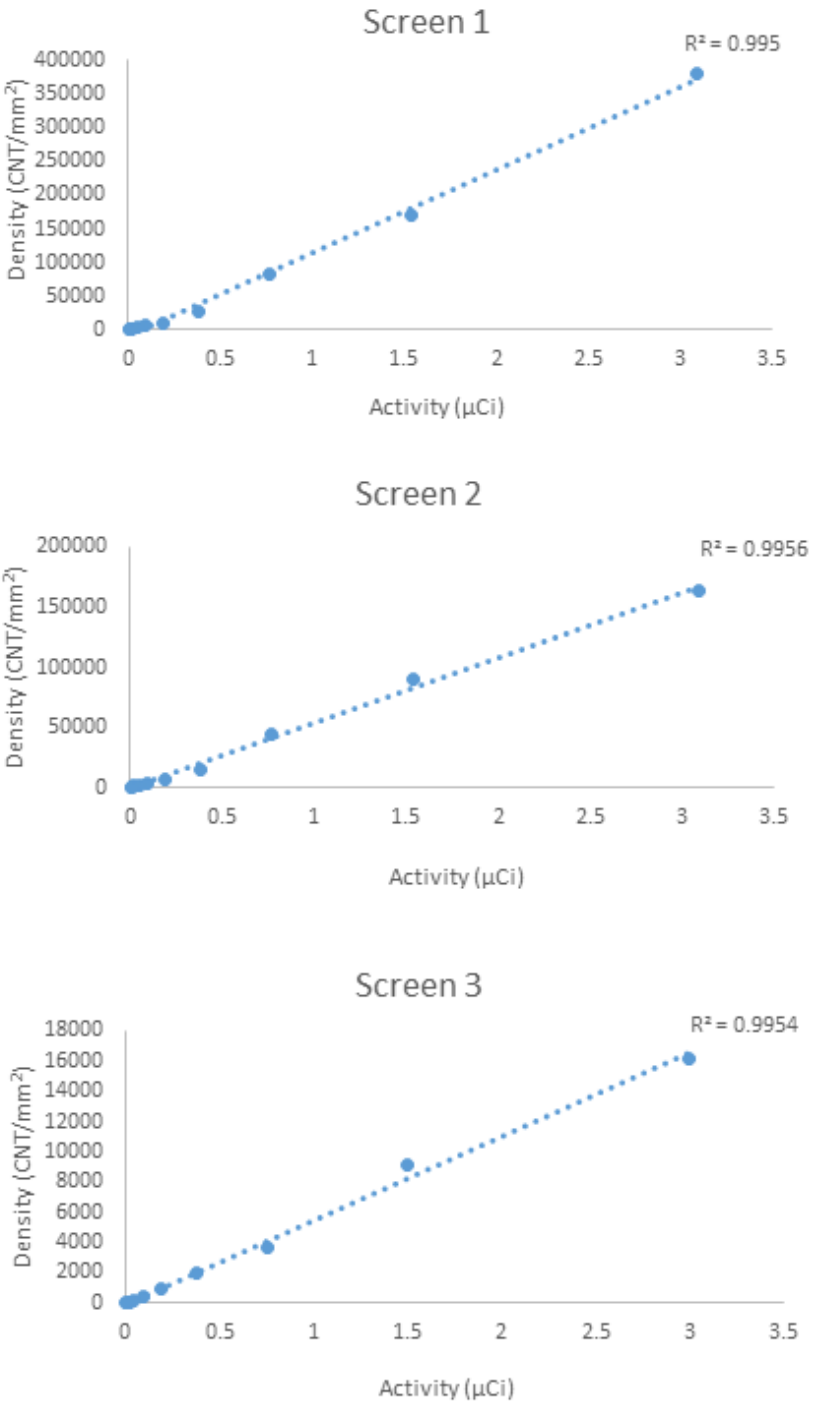

FIGURE 28- SCREEN TESTING. TESTING SCREENS 1, 2 AND 3 WITH INCREASING CONCENTRATIONS OF FDG SHOWED A LINEAR STANDARD CURVE IN THE 3 CASES AT THE TESTED DOSES, IMPLYING THAT ALL 3 SCREENS ARE WELL FUNCTIONAL FOR USE IN BINDING STUDIES.

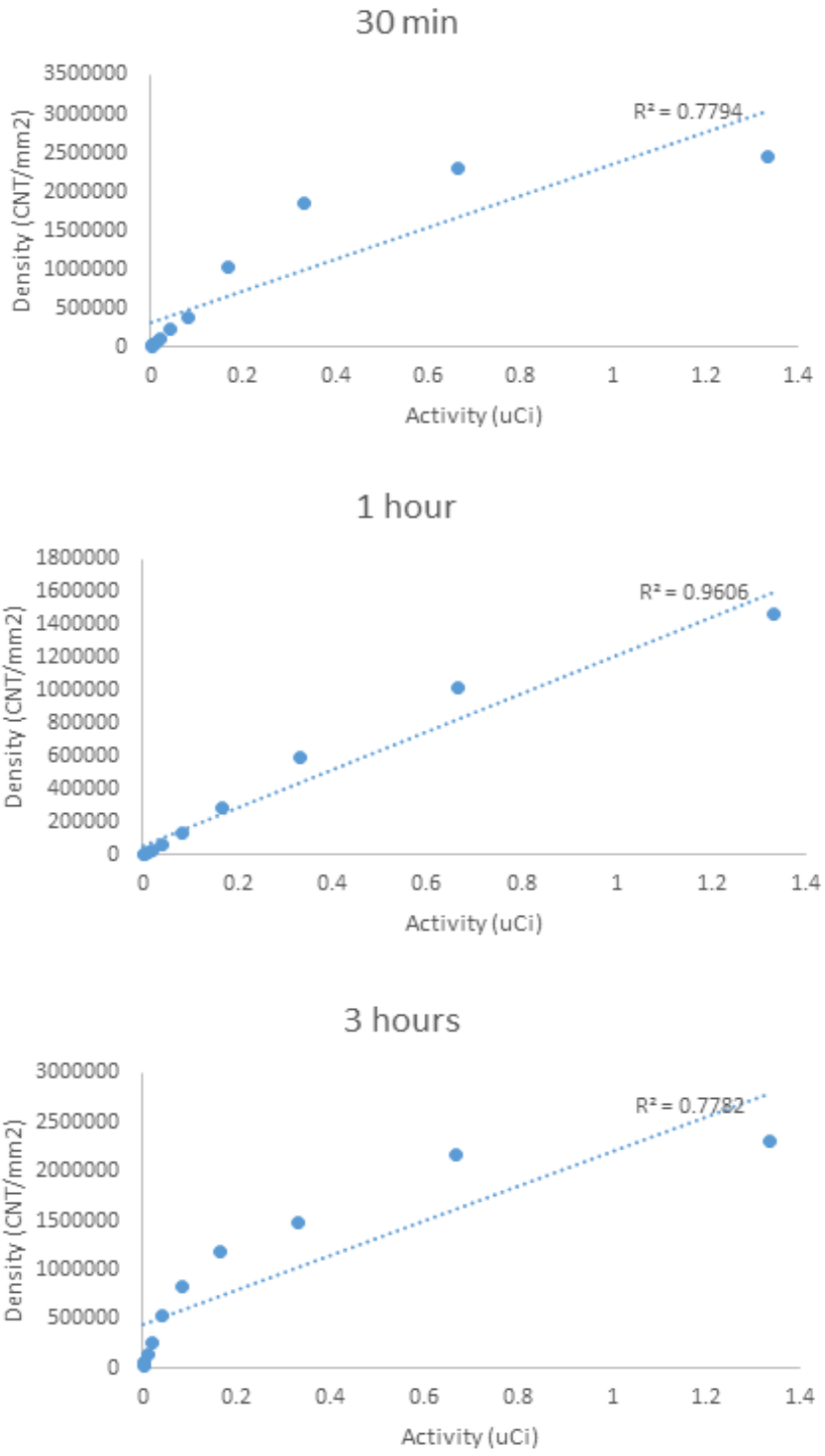

FIGURE 29- CHOICE OF EXPOSURE TIME. VARIATION IN DENSITY (CNT/MM^2) AS A FUNCTION OF ACTIVITY (µCI) IN 3 DIFFERENT SCREENS EXPOSED TO FDG FOR 30 MIN, 1 HOUR AND 3 HOURS. IMAGES WERE ANALYZED AT 100 µM. BEST LINEARITY WAS ACHIEVED UPON A 1 HOUR EXPOSURE COMPARED TO 30 MIN AND 3 HOURS.

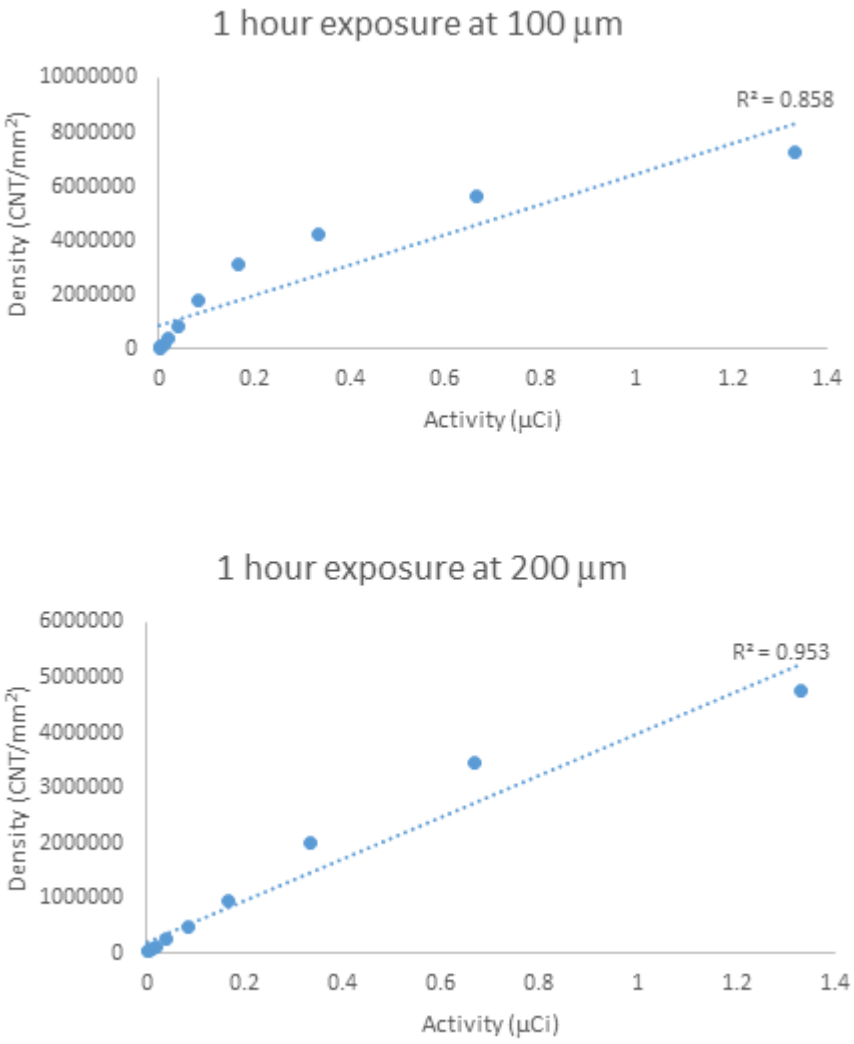

FIGURE 30- CHOICE OF RESOLUTION. COMPARING IMAGE ANALYSIS BY THE MOLECULAR IMAGER® FX AT DIFFERENT RESOLUTIONS WITH A CONSTANT TIME OF EXPOSURE OF 1 HOUR WITH FDG. BEST RESULTS WERE OBTAINED WHEN SCREENS WERE READ AT 200 µM COMPARED TO 50 µM (NOT SHOWN) AND 100 µM.

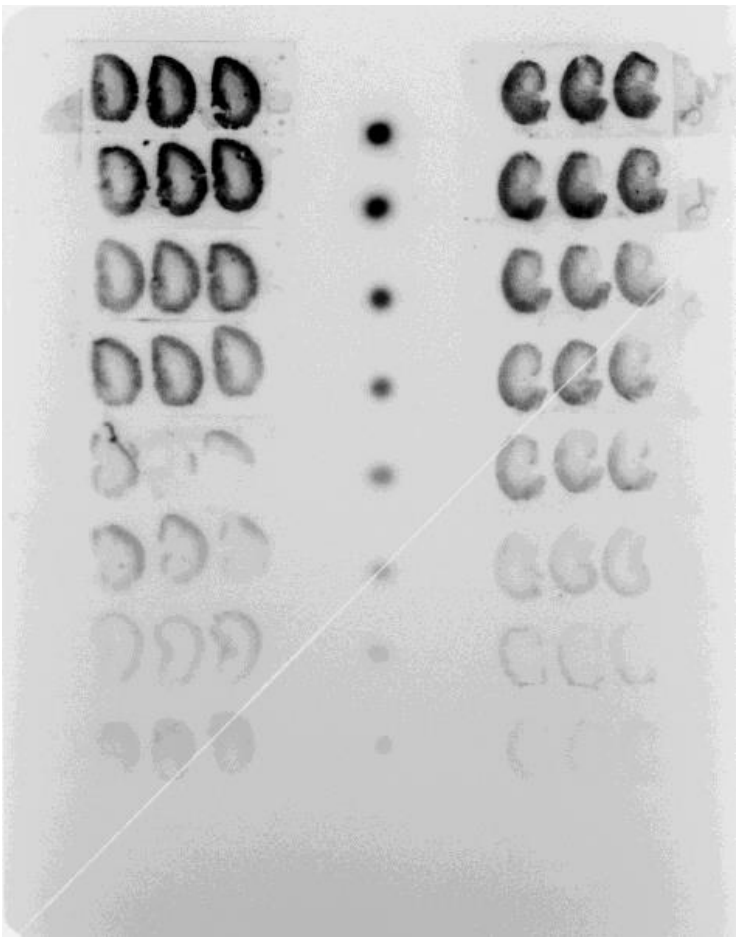

FIGURE 31- REPRESENTATIVE BINDING ASSAY IMAGE SHOWING TOTAL BINDING (TB; **LEFT**) AND NONSPECIFIC BINDING (NSB; **RIGHT**) OF [^{18}F]FPYKYNE-LOSARTAN TO RAT KIDNEY SLICES (20 μM). TB IS HIGHLY DENSE IN KIDNEY CORTEX, WHEREAS, NSB IS DISPERSED IN MEDULLA AND CORTEX, WITH CORTEX DENSITY LESS PROMINENT COMPARED TO TB. IMAGE DENSITY (CNT/MM^2) OF STANDARDS (**MIDDLE**) DISPLAYED PROPORTIONAL DECREASE WITH DECREASING RADIOLIGAND CONCENTRATION.

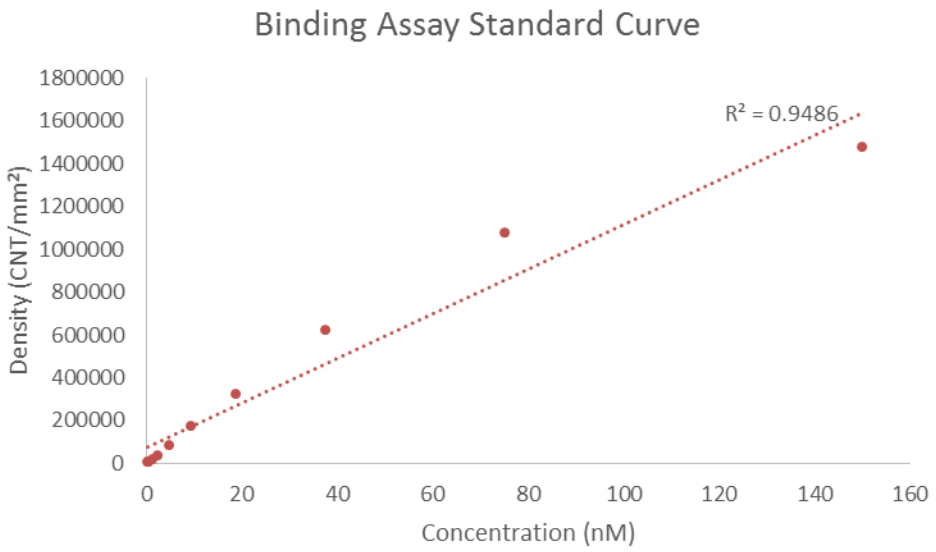

FIGURE 32- A REPRESENTATIVE STANDARD CURVE OF [^{18}F]FPYKYNE-LOSARTAN FOR A BINDING ASSAY. RADIOLIGAND CONCENTRATIONS DISPLAYED GOOD LINEARITY THUS DEMONSTRATING RELIABILITY OF RESULTS.

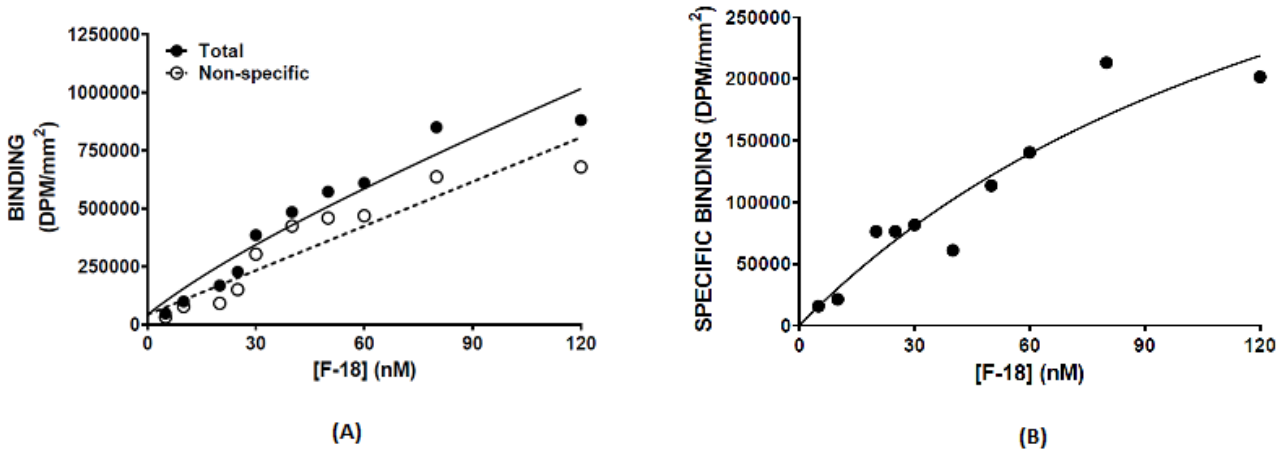

FIGURE 33- NONLINEAR CURVE FITTING OF A REPRESENTATIVE BINDING ASSAY (SA= 880 MCI/ΜMOL) WITH THE GRAPHPAD PRISM 6.02 SOFTWARE. ANALYSIS WAS PERFORMED USING A GLOBAL FIT WITH TB AND NSB **(A)**, AND SB ONLY **(B)**. THE METHOD IN **(A)** PROVIDES MORE DATA POINTS, THUS, MORE ACCURATENESS AND LESS VARIABLE RESULTS.

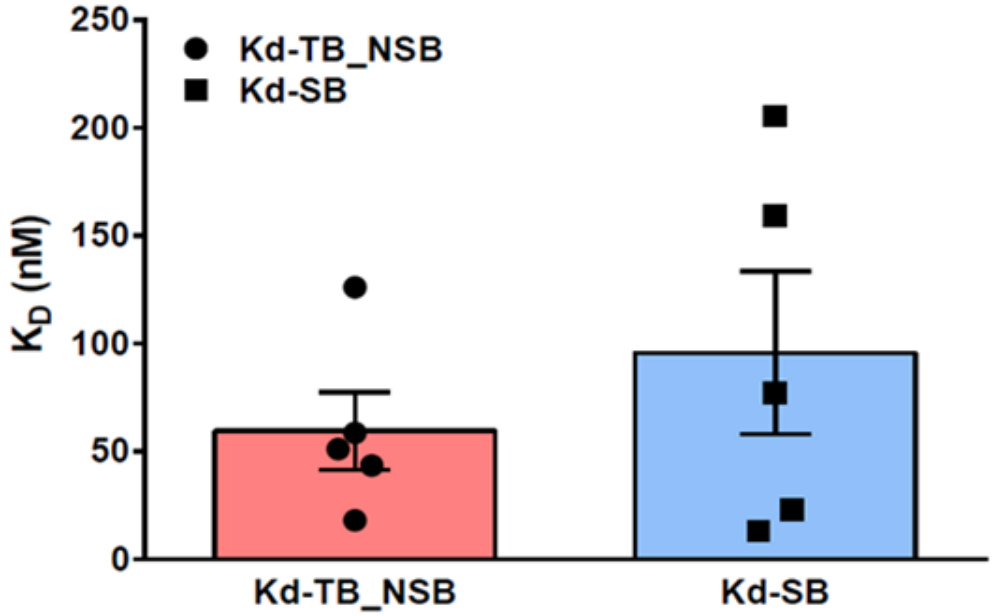

(A)

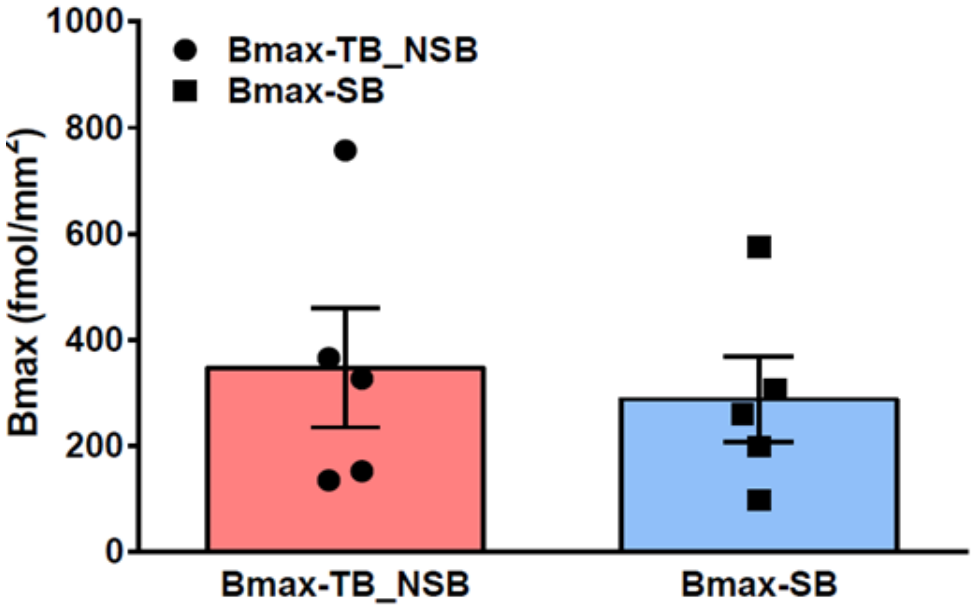

(B)

FIGURE 34- AVERAGE K_D **(A)** AND B_{MAX} **(B)** VALUES USING TB AND NSB VERSUS USING SB ONLY. LESS VARIABILITY IS OBTAINED AMONG K_D VALUES USING THE GLOBAL FIT OF TB AND NSB CURVES.

TABLE 1- AVERAGE K_D AND B_{MAX} VALUES (N=5). RESULTS ARE EXPRESSED AS ARITHMETIC MEAN ± SEM (STANDARD ERROR OF THE MEAN) AND pK_D= -LOG K_D IN MOLAR. 95% CONFIDENCE INTERVAL IS SHOWN IN BRACKETS. OVERALL, THE K_D VALUE IS ABOUT 50 NM USING THE GLOBAL FIT OF TB AND NSB CURVES.

Average of best-fit values (n=5)	
pK_d	7.31 ± 0.14 [6.93 - 7.68]
K_d	4.94×10^{-8} M
Bmax	348 ± 112 [36 - 659]

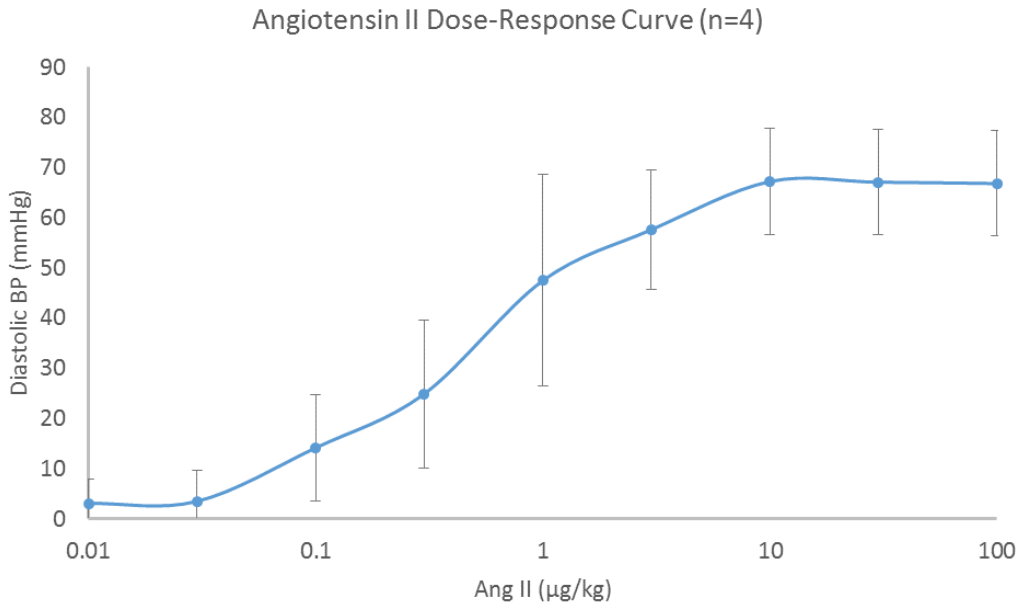

FIGURE 35- DOSE-RESPONSE EFFECT OF ANG II ON DIASTOLIC BP. VALUES REPRESENT THE MEAN ± STANDARD DEVIATION AND N=4 PER GROUP. ANG II SUBMAXIMAL DOSE IS DETERMINED GRAPHICALLY AS THE DOSE PRODUCING THE SUBMAXIMAL EFFECT WHICH REFERS TO 3 µG/KG. VALUES REPRESENT MEAN BP ± SD.

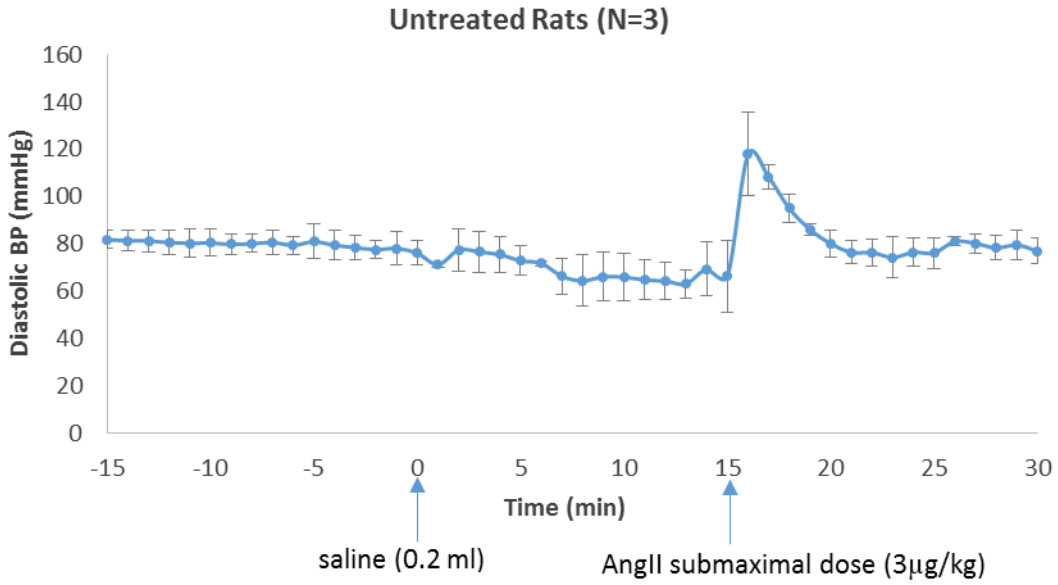

FIGURE 36- ANG II PRESSOR EFFECT IN UNTREATED RATS (USING VEHICLE 1). RATS (N=3) PRETREATED WITH SALINE VEHICLE (0.2 ML) DISPLAYED AN INCREASE OF ~ 50 MMHG IN DIASTOLIC BLOOD PRESSURE UPON ADMINISTRATION OF ANG II SUBMAXIMAL DOSE (3 µG/KG). VALUES REPRESENT MEAN BP ± SD.

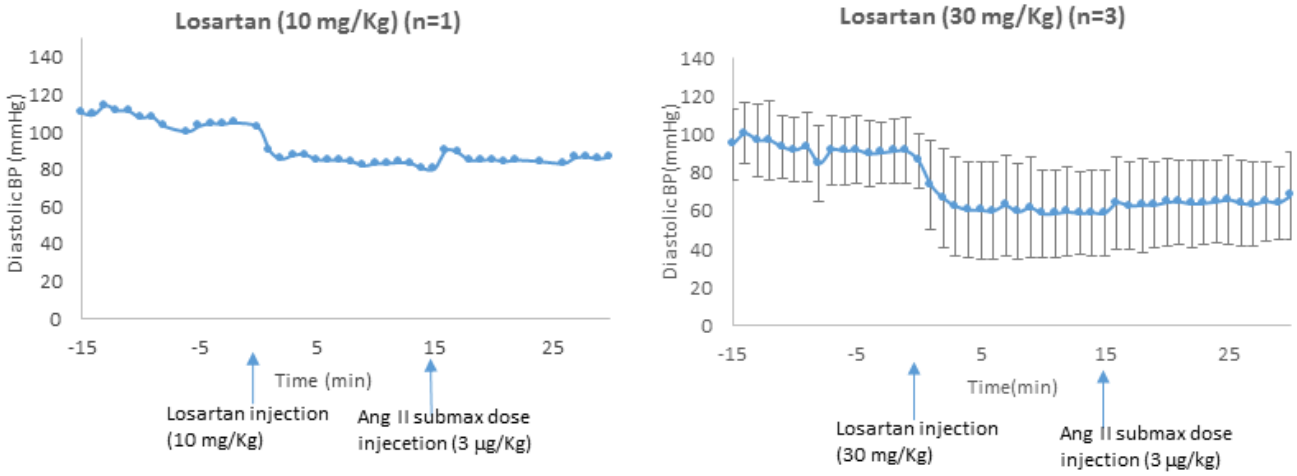

FIGURE 37- ANTAGONISTIC EFFECT OF LOSARTAN. LOSARTAN DOSES WERE INJECTED I.V. IN RATS 15 MIN PRIOR TO ANG II SUBMAXIMAL DOSE INJECTION. THE PRESSOR EFFECT PRODUCED BY ANG II WAS COMPARED WITH THE UNTREATED GROUP TO DETERMINE THE BLOCKING % PRODUCED BY THE ARB. APPROXIMATELY 70% BLOCKAGE OF ANG II EFFECT WAS OBTAINED WITH A 10 MG/KG DOSE OF LOSARTAN (N=1) AND CLOSELY TO 100% BLOCKAGE WITH A 30 MG/KG DOSE (N=3) (VALUES REPRESENT MEAN BP ± SD). LOSARTAN IS A FULL AT_1R BLOCKER WITH A MAXIMUM BLOCKING DOSE OF 30 MG/KG.

TABLE 2- DOSE-DEPENDENT ANTAGONISM OF LOSARTAN. BLOCKING PERCENTAGE INCREASES FROM AROUND 20% AT A 1 MG/KG DOSE TO ALMOST FULL BLOCKAGE OF ANG II PRESSOR EFFECT AT A DOSE OF 30 MG/KG.

Dose (mg/Kg)	Block (%)	Ang II increase (mmHg)	Ang II Effect (%)
0	0	50	100
1	19	41	81
2.5	24	38	76
5	34	33	66
10	69	10	31
20	78	11	22
30	90	5	10

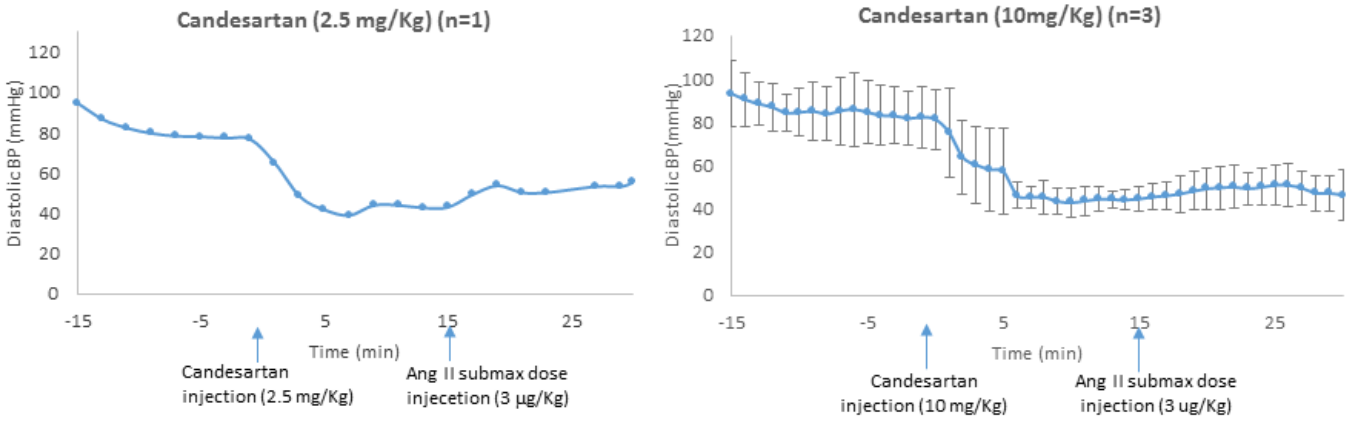

FIGURE 38- ANTAGONISTIC EFFECT OF CANDESARTAN. CANDESARTAN, A VERY POTENT AT_1R ANTAGONIST, BLOCKS AT_1RS DOSE-DEPENDENTLY. AS THE CANDESARTAN DISPLAYS 78% BLOCKAGE OF ANG II EFFECTS ON BLOOD PRESSURE WITH A DOSE OF 2.5 MG/KG (N=1). AT A DOSE OF 10 MG/KG, CANDESARTAN FULLY BLOCKS AT_1RS (N=3) THUS SHOWING FULL AT_1R ANTAGONISM (VALUES REPRESENT MEAN BP ± SD).

TABLE 3- DOSE-DEPENDENT ANTAGONISM OF CANDESARTAN. BLOCKING PERCENTAGE INCREASES FROM AROUND 65% AT A DOSE OF 1 MG/KG TO FULL BLOCKAGE OF ANG II PRESSOR EFFECT WITH A DOSE OF 10 MG/KG.

Dose (mg/Kg)	Block (%)	Ang II increase (mmHg)	Ang II Effect (%)
0	0	50	100
1	65	18	35
2.5	78	11	22
5	90	5	10
7.5	95	3	5
10	100	0	0

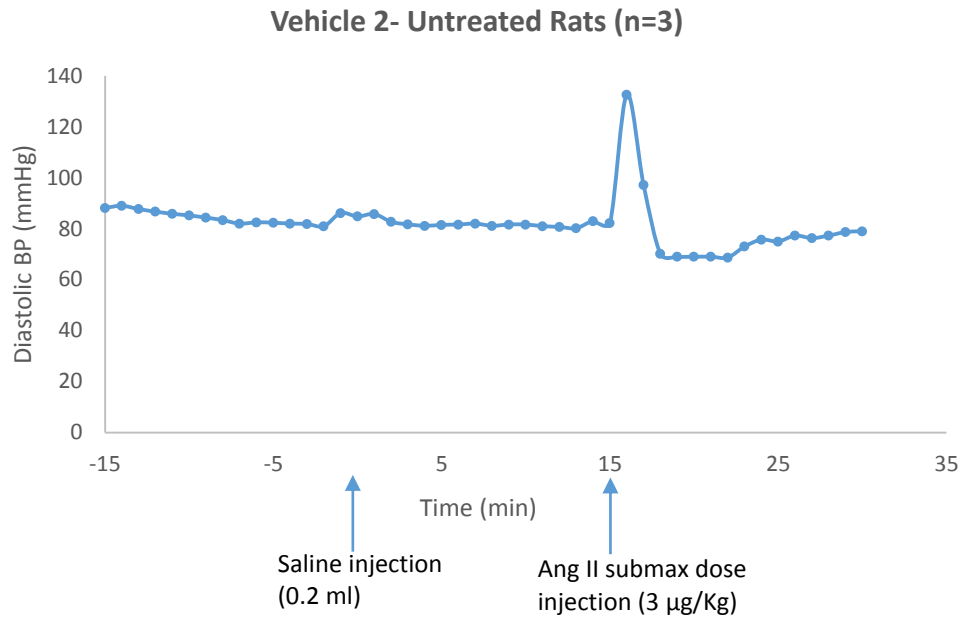

FIGURE 39- ANG II PRESSOR EFFECT USING VEHICLE 2 (I.E. 5% ETOH + 20% PROPYLENE GLYCOL + 50% SALINE + 25% $NAHCO_3$). THIS VEHICLE PRODUCED AN AVERAGE INCREASE OF 51 MMHG FOLLOWING ANG II INJECTION IN UNTREATED RATS (N=3), WHICH IS ALMOST THE SAME EFFECT ON BLOOD PRESSURE AS VEHICLE 1 (50 MMHG INCREASE).

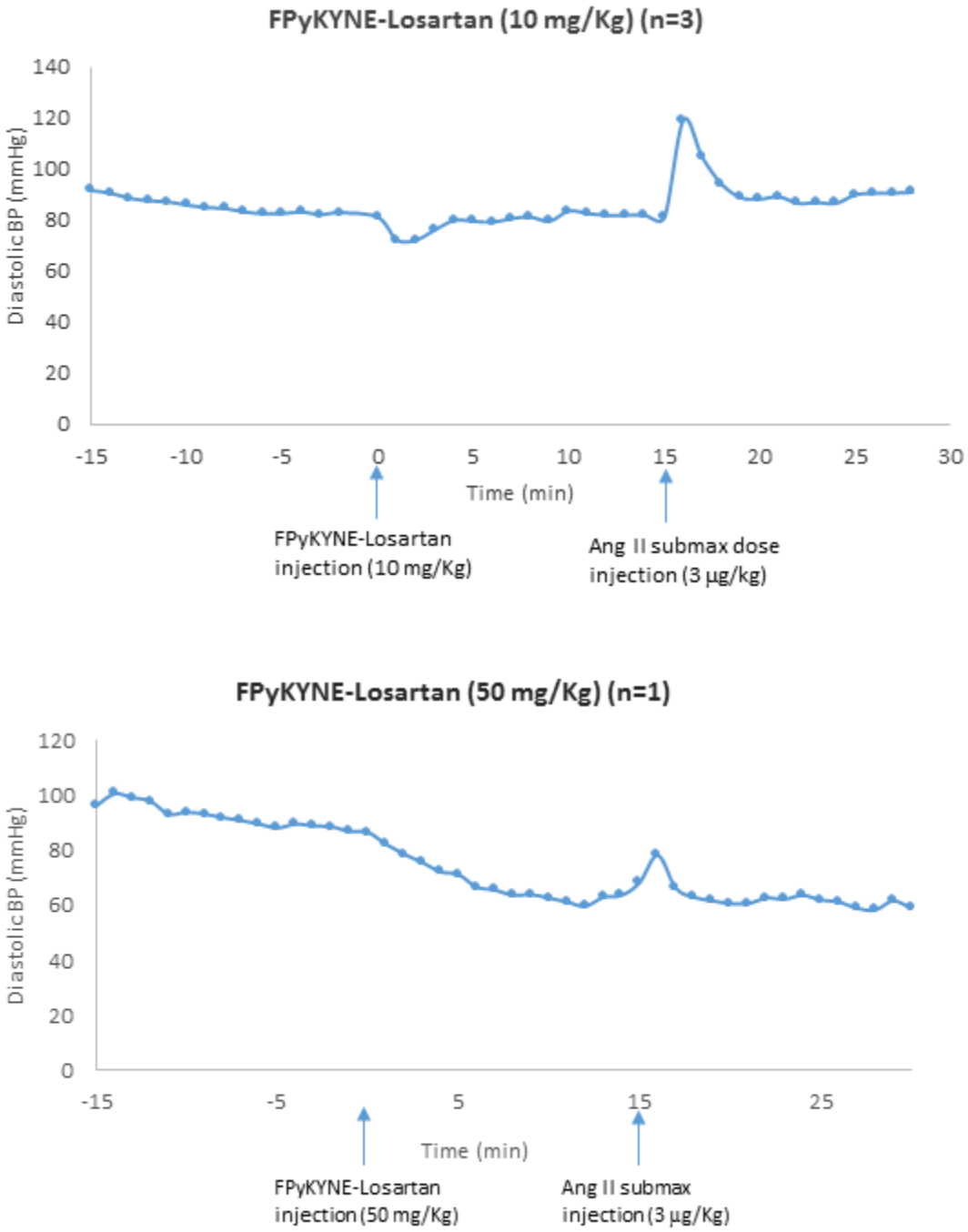

FIGURE 40- ANTAGONISTIC EFFECT OF FPYKYNE-LOSARTAN. WITH INCREASING DOSES OF FPYKYNE-LOSARTAN, AN INCREASING BLOCKING EFFECT OF AT_1Rs WAS OBTAINED. THE BLOCKING EFFECT ATTAINED AT THE HIGHEST DOSE USED (50 MG/KG) WAS 72%. AT 10 MG/KG, FPYKYNE-LOSARTAN HAD A BLOCKING EFFECT OF 26% (N=3), EXPRESSED AS THE PERCENTAGE OF ANG II PRESSOR RESPONSE.

TABLE 4- DOSE-DEPENDENT BLOCKING EFFECT OF FPYKYNE-LOSARTAN ON THE PRESSOR RESPONSE OF ANG II. BLOCKING PERCENTAGE INCREASED FROM 16% TO 72% WITH DOSES RANGING FROM 3 MG/KG TO 50 MG/KG, WHILE THE EFFECT OF ANG II DECREASED FROM 84% TO 28%, RESPECTIVELY.

Dose (mg/Kg)	Block (%)	Ang II increase (mmHg)	Ang II Effect(%)
0	0	50	100
3	16	42	84
10	26	37	74
15	34	33	66
30	46	27	54
50	72	14	28

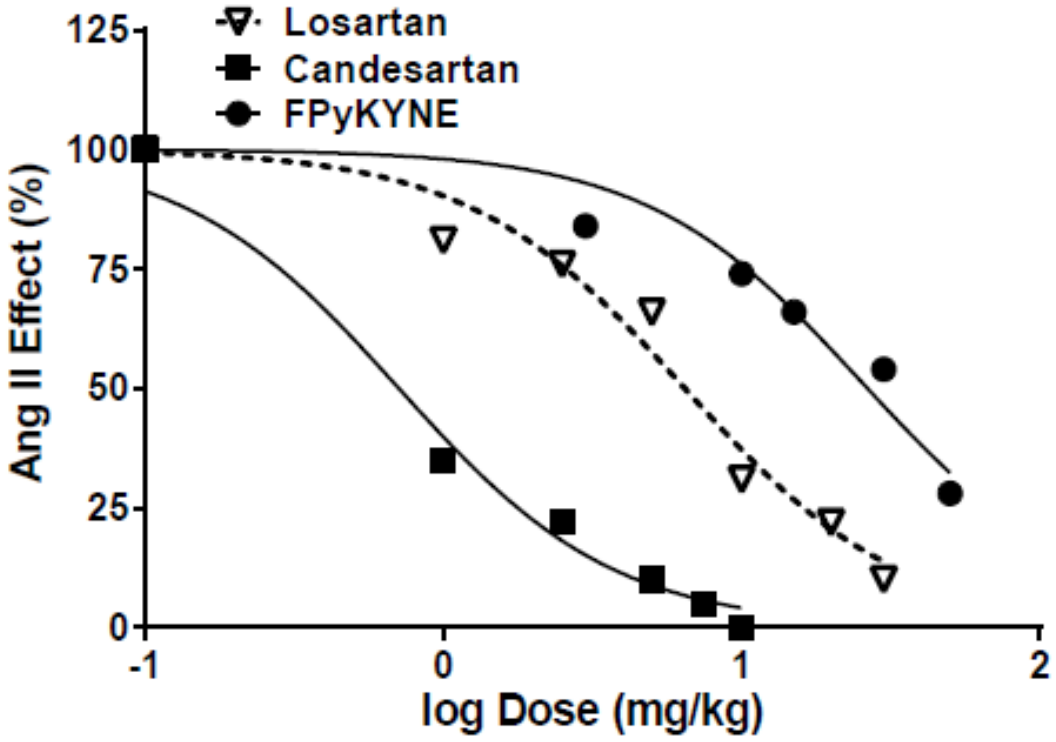

FIGURE 41- DOSE-RESPONSE CURVES OF THE AT_1R BLOCKERS: CANDESARTAN, LOSARTAN AND FPYKYNE-LOSARTAN. THE GRAPH DISPLAYS THE EFFECT OF ANG II (SUBMAXIMAL DOSE: 3 µG/KG I.V.) WHEN THESE BLOCKERS ARE PRESENT, IN ANESTHETIZED RATS. CURVES WERE FITTED USING NONLINEAR CURVE FITTING (GRAPHPAD PRISM 6.02).

TABLE 5- BEST-FIT VALUES OF BOTTOM, TOP AND ID_{50} VALUES OF LOSARTAN, CANDESARTAN AND FPYKYNE-LOSARTAN. IN THE MODEL USED, BASAL VALUES WERE CONSTRAINED TO "0" AND THE TOP FITTED TO A VALUE THAT EQUALED TO OR WAS LOWER THAN 100%. THIS WAS THE PREFERRED MODEL BASED ON STATISTICAL ANALYSIS. ID_{50}'S WERE DETERMINED TO BE 6.4 MG/KG, 0.7 MG/KG AND 25.5 MG/KG FOR LOSARTAN, CANDESARTAN AND FPYKYNE-LOSARTAN, RESPECTIVELY.

	Losartan	Candesartan	FPyKYNE
Best-fit values			
Bottom	1.517e-010	~ 2.220e-016	2.107
Top	= 100.0	= 100.0	= 100.0
LogID50	0.8098	-0.1489	1.407
HillSlope	-1.197	-1.197	-1.197
ID50	6.4	0.7	25.5

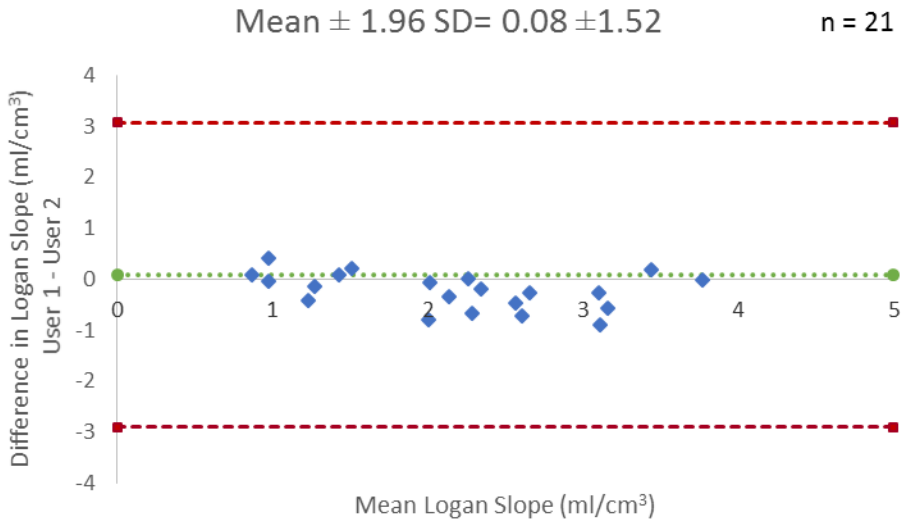

FIGURE 42- BLAND-ALTMAN PLOT COMPARING LOGAN SLOPE VALUES BETWEEN USER 1 AND USER 2 (INTER-USER VARIABILITY). MEAN DIFFERENCE BETWEEN LOGAN SLOPE REPEATED MEASURES (N=21, USER 1- USER 2) WAS 0.08 ± 1.52, WITH A TRV OF 15.9%.

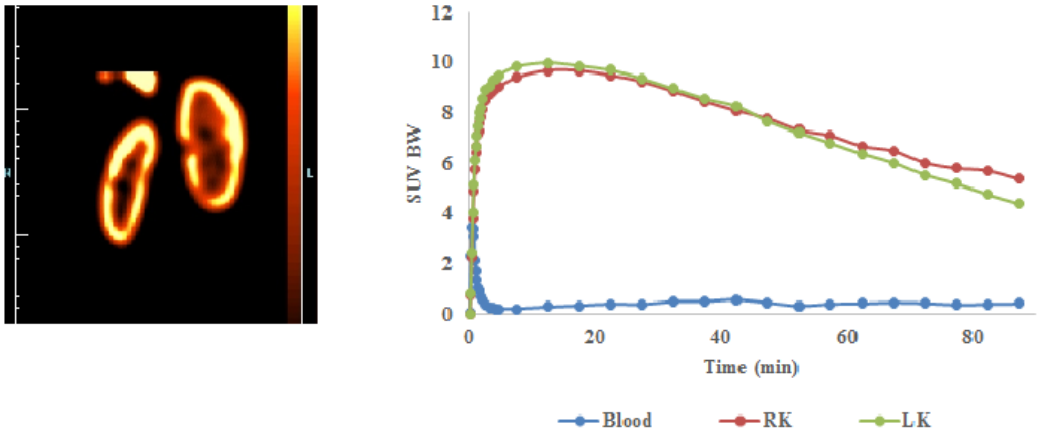

FIGURE 43- REPRESENTATIVE PET IMAGE (CORONAL VIEW) OF PIG KIDNEYS DISPLAYING [^{18}F]FPYKYNE-LOSARTAN UPTAKE. GOOD CONTRAST IMAGES ARE OBTAINED WITH HIGH RENAL RETENTION OF THE TRACER IN KIDNEY CORTEX AND SLOW CLEARANCE FROM KIDNEYS. TRACER TIME-ACTIVITY CURVES FOR BLOOD INPUT (AORTA), RIGHT KIDNEY (RK) AND LEFT KIDNEY (LK) ARE PRESENTED AS STANDARDIZED UPTAKE VALUES NORMALIZED TO BODY WEIGHT (SUV_{BW}) FROM 0 TO 90 MIN.

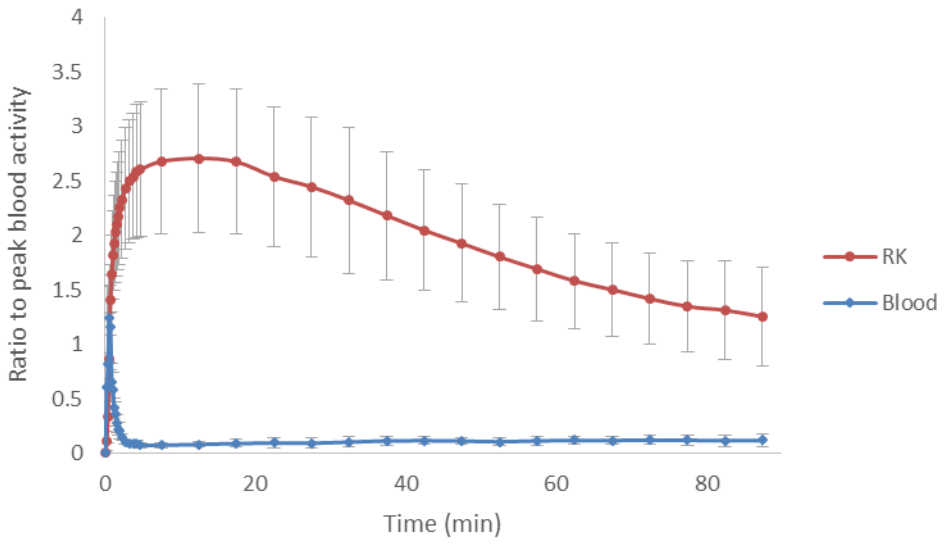

FIGURE 44- PIG KIDNEY-TO-BLOOD ACTIVITY RATIO. NORMAL PIG PET SCANS (N=3; 6 SCANS) DISPLAYED HIGH KIDNEY-TO-BLOOD CONTRAST (2.7 ± 0.68 AT 12.5 MIN) AND SLOW CLEARANCE FROM KIDNEYS.

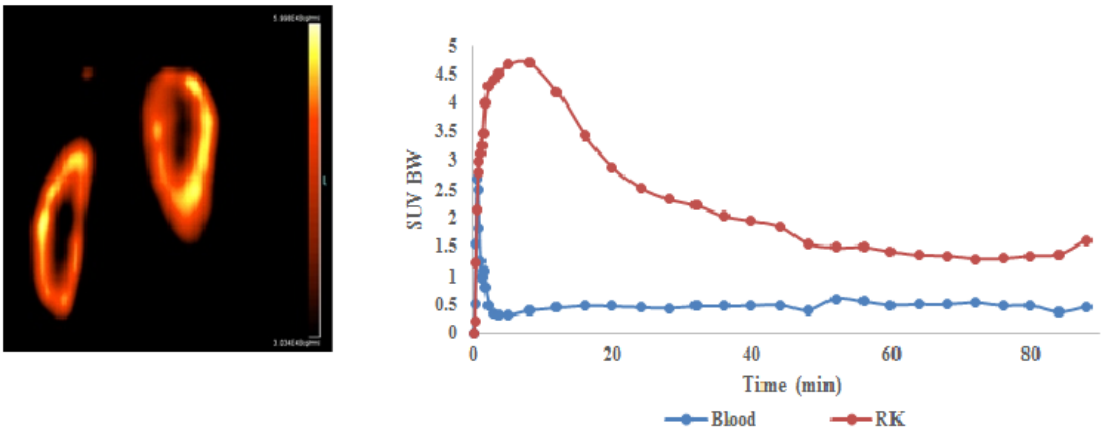

FIGURE 45- REPRESENTATIVE PET CORONAL IMAGE OF PIG KIDNEYS INJECTED WITH [^{18}F]FPYKYNE-LOSARTAN FOLLOWING CANDESARTAN INJECTION (10 MG/KG) 15 MIN LATER, AND THE CORRESPONDING TIME-ACTIVITY CURVE FOR BLOOD INPUT (AORTA) AND RIGHT KIDNEY (RK). REDUCED TRACER RETENTION IS OBSERVED IN THE KIDNEY CORTEX, INDICATING SPECIFIC BINDING TO AT_1R. PEAK STANDARDIZED UPTAKE VALUE (SUV) IN RIGHT KIDNEY DECREASES TO AROUND 4.7 AT ~ 10 MIN POST-INJECTION.

TABLE 6- TABLE REPRESENTING PEAK SUV AT A 10-15 MIN TIME FRAME IN NORMAL AND BLOCKING CONDITIONS FOR PIG LEFT KIDNEY (LK) AND RIGHT KIDNEY (RK), AND THE CORRESPONDING BLOCKING %.

Peak SUV	LK			RK		
Normal	13.5	±	5.64	14.1	±	6.16
Blocked	5.4	±	3.89	5.8	±	4.59
Blocking %		60			59	

TABLE 7- TABLE SHOWING LOGAN SLOPE VOLUMES FOR NORMAL (N=3) AND BLOCKING SCANS (N=3), AND THE CORRESPONDING BLOCKING PERCENTAGE FOR LEFT (LK) AND RIGHT KIDNEYS (RK), BEFORE APPLYING PARTIAL VOLUME AND ARTERIAL INPUT CORRECTIONS.

DV	LK	RK
Average Normal	18.5 ± 5.79	19.1 ± 5.92
Average Blocked	8.6 ± 3.53	7.5 ± 3.79
Blocking %	53	61

TABLE 8- DV VALUES OF PIG RIGHT KIDNEY AFTER CORRECTION FOR ARTERIAL INPUT FUNCTION AND PARTIAL VOLUME LOSS, FOR NORMAL AND BLOCKING SCANS. TEST AND RETEST VALUES SHOW REPRODUCIBILITY WITH A TRV OF 1.3% (<<15%) AND A P-VALUE OF 0.98 (>>0.05), WHILE BLOCKED DV VALUES WERE SIGNIFICANTLY DECREASED AND DISPLAYED A P-VALUE OF 0.03 AND A BLOCKING % OF ~ 55%.

Normal DV (n=3)	5.6	±	1.83
Blocked DV (n=3)	2.5	±	1.10
Blocking %	55		
TRV	1.3	±	0.05
P-value (Test-Retest)	0.98		
P-value (Normal-Blocked)	0.03		

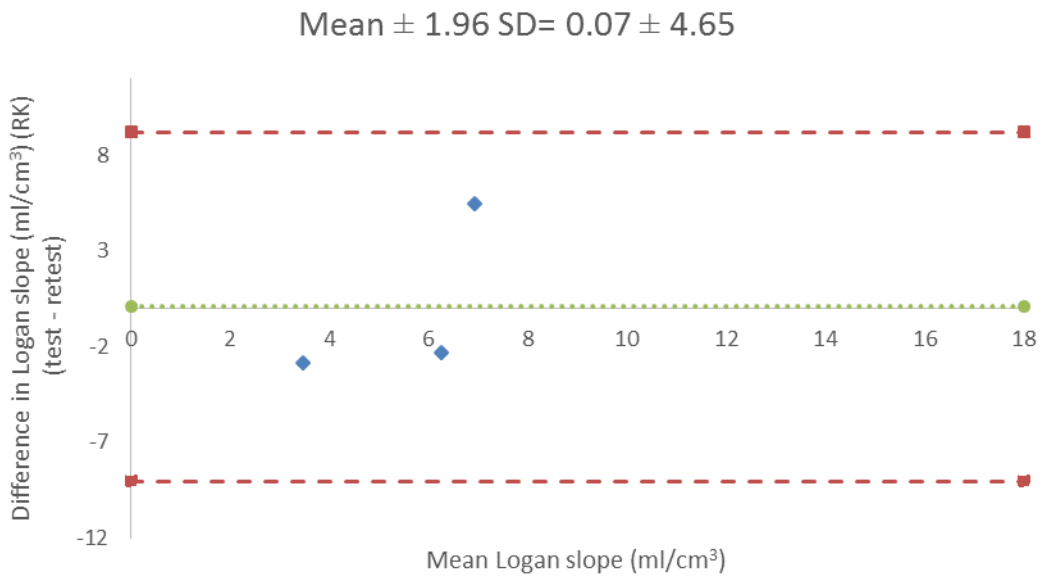

FIGURE 46- BLAND-ALTMAN PLOT COMPARING TEST-RETEST LOGAN SLOPE VALUES FOR [^{18}F]FPYKYNE-LOSARTAN IN PIG RIGHT KIDNEYS. MEAN DIFFERENCES BETWEEN LOGAN SLOPES REPEATED MEASURES (N=3, TEST-RETEST) WAS 0.18. P-VALUE= 0.97 AND TRV= 1.3 ± 0.13.

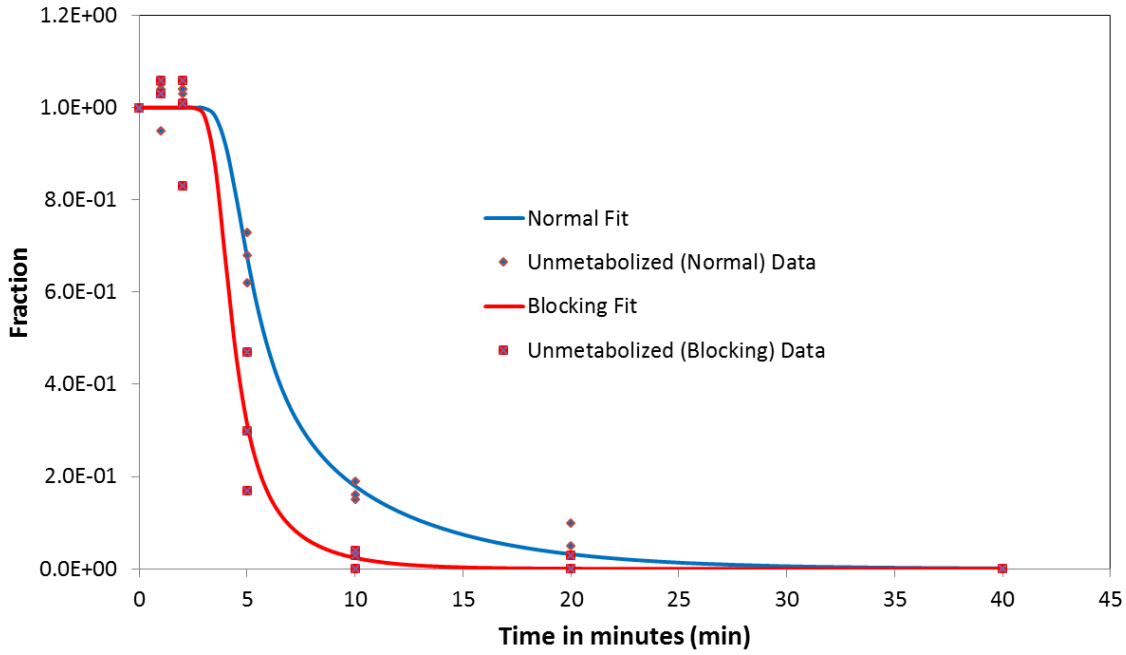

FIGURE 47- BEST FITTED GRAPHS FOR UNMETABOLIZED [^{18}F]FPYKYNE-LOSARTAN IN PIG PLASMA IN BOTH NORMAL AND BLOCKING CONDITIONS. THE CHI-SQUARED VALUES ARE VERY LOW (AROUND 0.02 FOR BOTH DATA SETS) FOR 19 DEGREES OF FREEDOM, WHICH IS A GOOD FIT. THE FUNCTION OBTAINED WOULD BE USED TO DETERMINE UNMETABOLIZED TRACER FRACTION AT EACH TIME POINT. ACCORDINGLY, CORRECTING INPUT FUNCTION FOR UNALTERED PARENT TRACER IN PLASMA WOULD BE POSSIBLE.

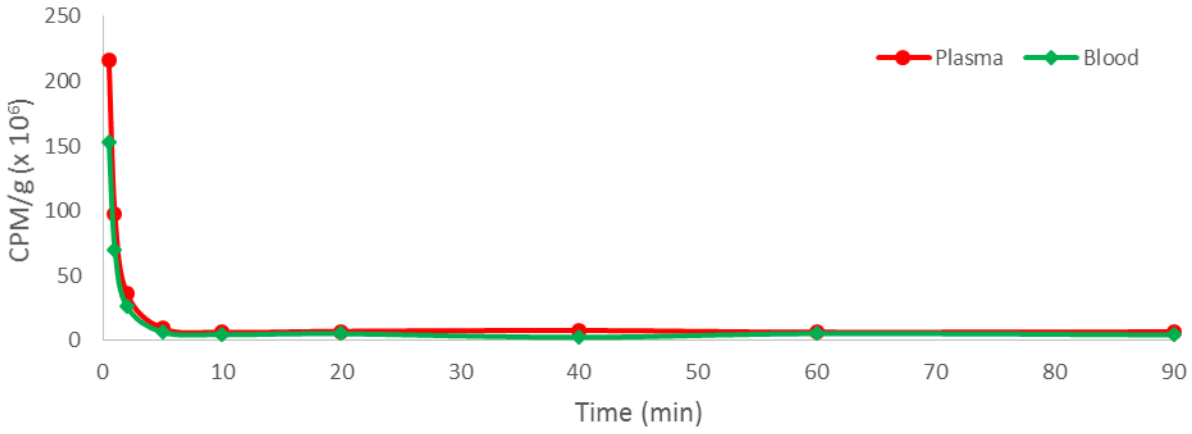

FIGURE 48- PIG BLOOD AND PLASMA RADIOACTIVITY. CONCENTRATION OF [^{18}F]FPYKYNE-LOSARTAN WAS SLIGHTLY HIGHER IN PIG PLASMA THAN IN WHOLE BLOOD ALONG 90 MIN.

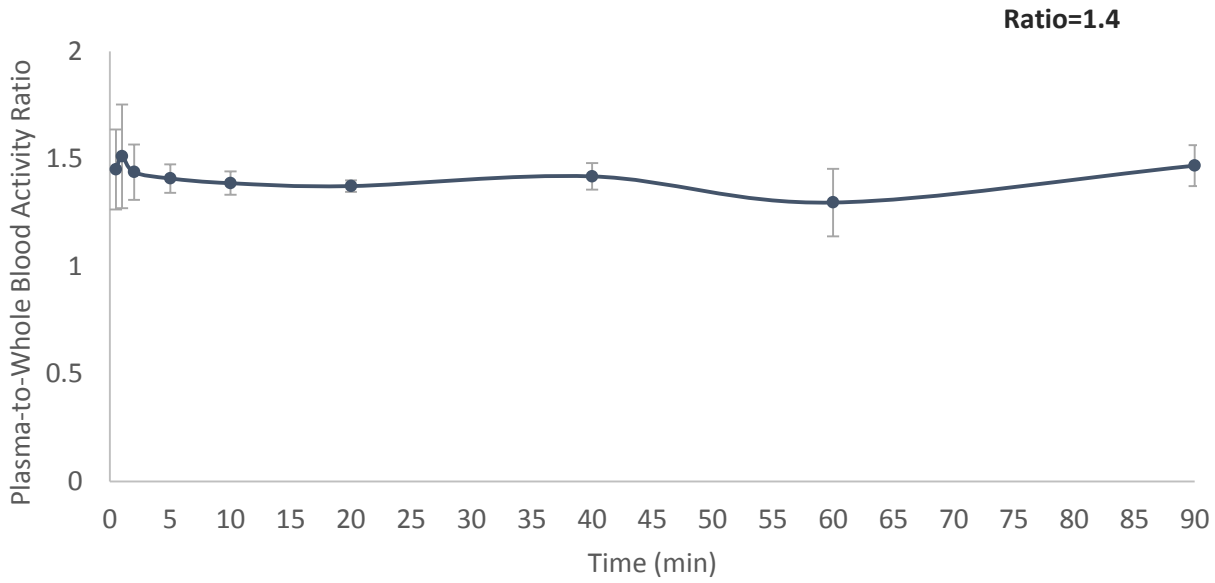

FIGURE 49- RATIO OF PLASMA-TO-WHOLE BLOOD ACTIVITY OVER TIME (MIN) IN PIGS FOR [^{18}F]FPYKYNE-LOSARTAN AS MEASURED BY FEMORAL ARTERY BLOOD SAMPLING. DATA ARE PRESENTED AS MEAN ± SD (N=3 AT EACH DATA POINT). A CONSTANT VARIATION OVER TIME WAS OBTAINED DISPLAYING AN AVERAGE RATIO OF 1.4, WHICH WAS USED FOR WHOLE-BLOOD-TO-PLASMA CORRECTIONS.

TABLE 9- FREE AND PROTEIN BOUND PROPORTIONS OF [^{18}F]FPYKYNE-LOSARTAN IN RAT PLASMA (N=5).

	Free %		Plasma Protein Bound %
Assay 1	3.5		96.5
Assay 2	2.5		97.5
Assay 3	2.6		97.4
Assay 4	2.4		97.6
Assay 5	2.8		97.2
Average	2.8		97.2
Final Result	**3**	**±0.43**	**97**

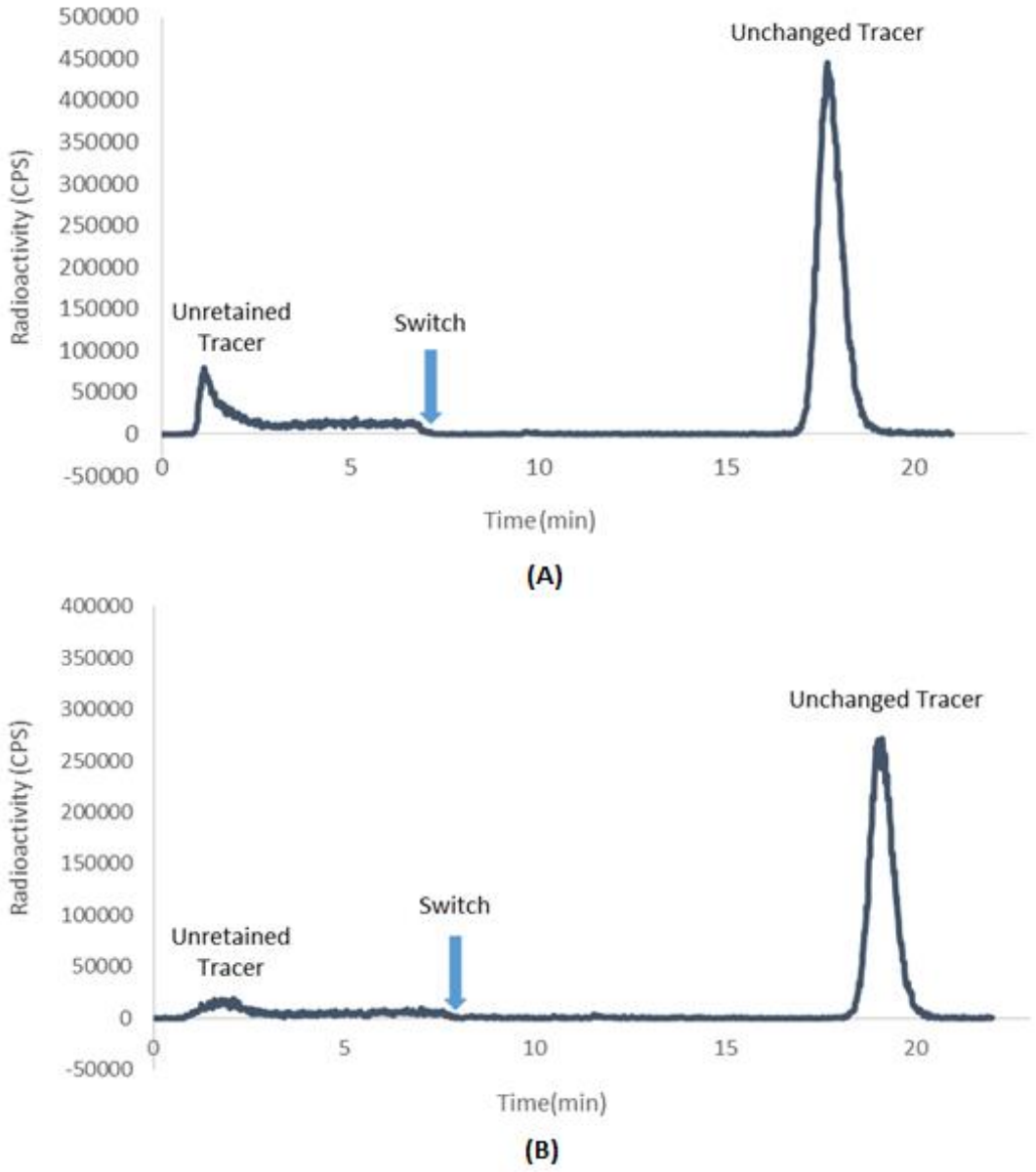

FIGURE 50- REPRESENTATIVE HPLC CHROMATOGRAMS DISPLAYING RETENTION TIME OF UNCHANGED/AUTHENTIC [^{18}F]FPYKYNE-LOSARTAN IN CONTROL RAT PLASMA (A) AND KIDNEY (B). RADIOACTIVITY IN CONTROL SAMPLES IS SOLELY REPRESENTATIVE OF [^{18}F]FPYKYNE-LOSARTAN. THE FIRST PEAK REPRESENTS RADIOACTIVITY OF THE TRACER NOT CAPTURED BY THE CAPTURE COLUMN. ON AVERAGE, 6% WAS UNRETAINED IN PLASMA (A) AND 4% IN KIDNEY TISSUE SAMPLES (B). THIS PERCENTAGE IS USED TO CORRECT TRACER PROPORTIONS. PEAK 2 REPRESENTS AUTHENTIC [^{18}F]FPYKYNE-LOSARTAN ELUTING AT 10 MIN POST-SWITCH IN RAT PLASMA (A) AND 11.3 MIN POST-SWITCH IN RAT KIDNEYS (B).

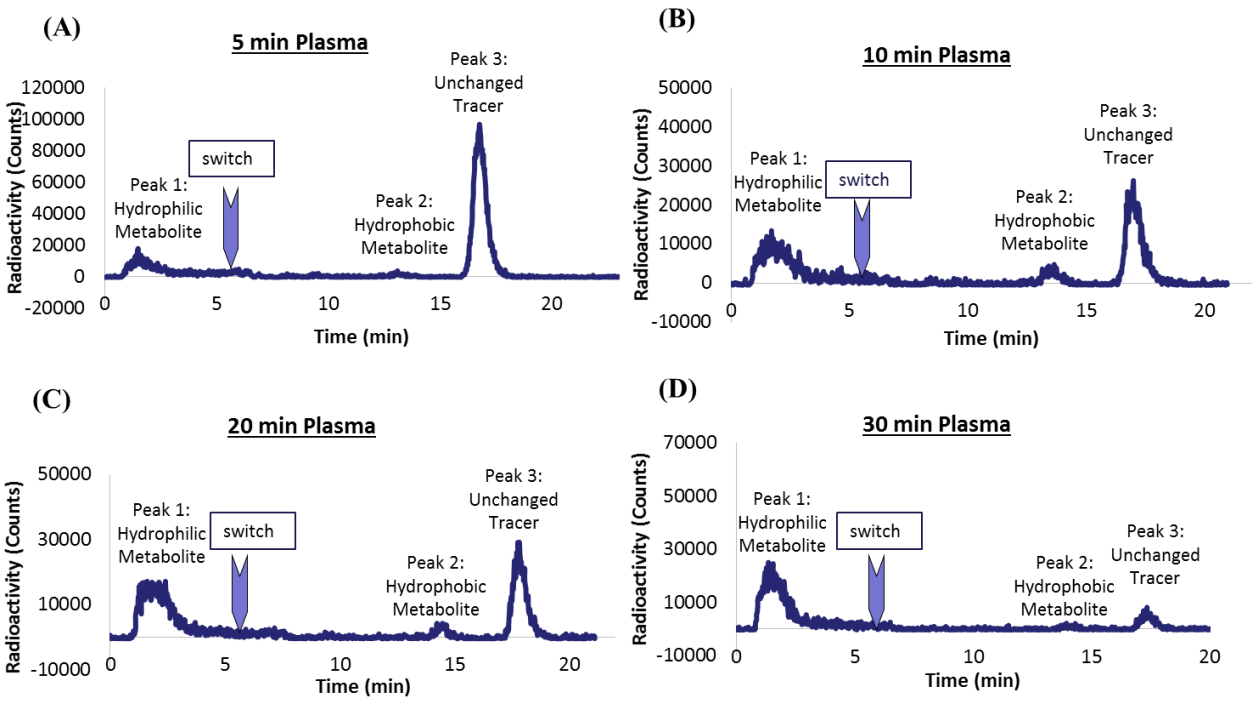

FIGURE 51- REPRESENTATIVE HPLC CHROMATOGRAMS DISPLAYING UNCHANGED [^{18}F]FPYKYNE-LOSARTAN AND ITS LABELED METABOLITES IN RAT PLASMA AT RESPECTIVE TIME POINTS. [^{18}F]FPYKYNE-LOSARTAN (PEAK 3) IS METABOLIZED INTO A HYDROPHILIC METABOLITE(S) (PEAK 1) AND A HYDROPHOBIC METABOLITE (PEAK 2). PLASMA SAMPLES WERE ANALYZED AT 5 MIN **(A)**, 10 MIN **(B)**, 20 MIN **(C)** AND 30 MIN **(D)** POST-TRACER INJECTION (N=3 PER TIME POINT). RETENTION TIMES WERE APPROXIMATELY: 0.5-1 MIN (PEAK 1), 6.8 MIN (PEAK 2) AND 10 MIN (PEAK 3) POST-SWITCH.

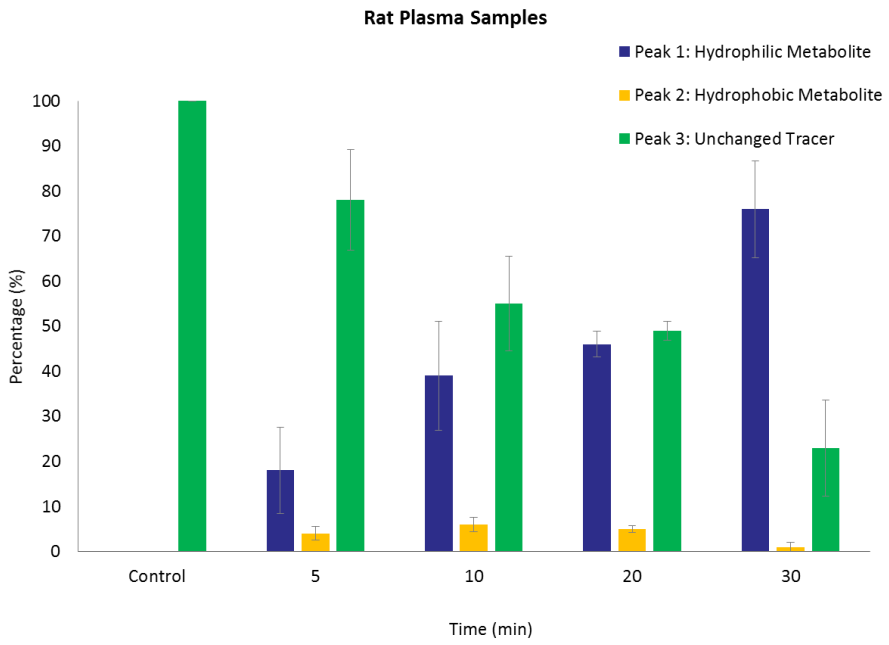

FIGURE 52- METABOLITE ANALYSIS OF [^{18}F]FPYKYNE-LOSARTAN IN RAT PLASMA (N=3 PER TIME POINT). PEAK AREA WAS QUANTIFIED, CORRECTED FOR NOISE, RADIOACTIVE DECAY AND UNRETAINED TRACER PROPORTION, AND EXPRESSED AS A PERCENTAGE OF TOTAL AREA PER SAMPLE.

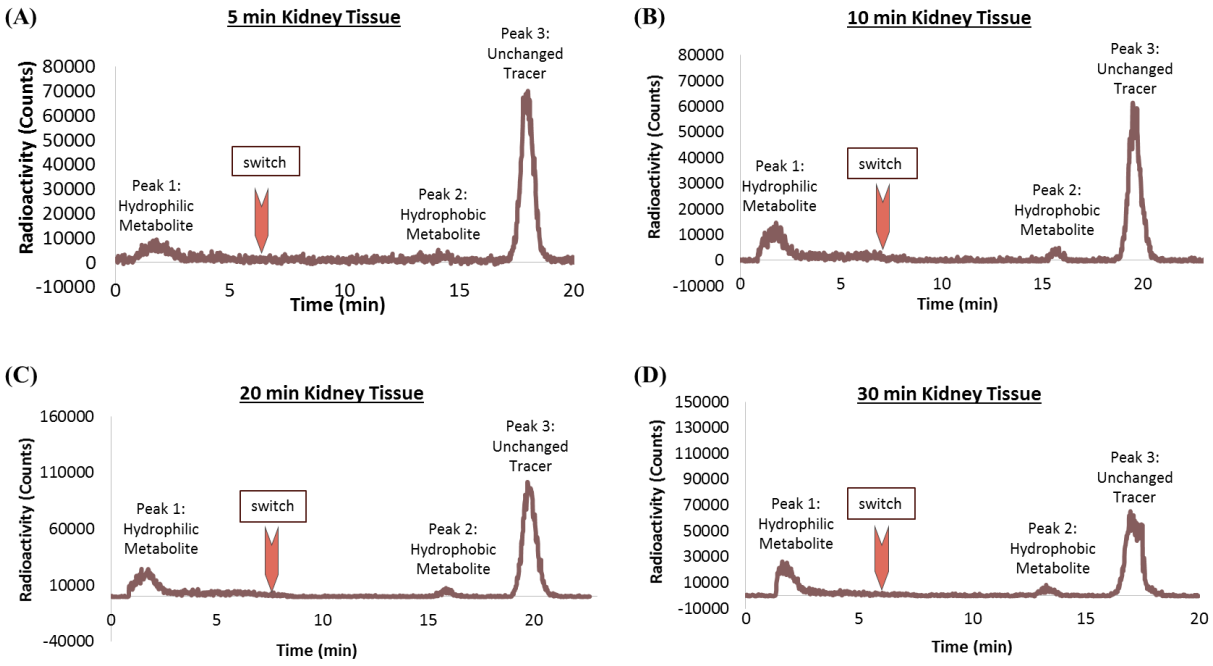

FIGURE 53- REPRESENTATIVE HPLC CHROMATOGRAMS DISPLAYING UNCHANGED [^{18}F]FPYKYNE-LOSARTAN AND ITS LABELED METABOLITES IN RAT KIDNEY TISSUE AT RESPECTIVE TIME POINTS. [^{18}F]FPYKYNE-LOSARTAN (PEAK 3) IS METABOLIZED INTO A HYDROPHILIC METABOLITE(S) (PEAK 1) AND A HYDROPHOBIC METABOLITE (PEAK 2). KIDNEY TISSUE SAMPLES WERE ANALYZED AT 5 MIN **(A)**, 10 MIN **(B)**, 20 MIN **(C)** AND 30 MIN **(D)** POST-TRACER INJECTION (N=3 PER TIME POINT). RETENTION TIMES WERE APPROXIMATELY: 1.7 MIN (PEAK 1), 7.5 MIN (PEAK 2) AND 11.3 MIN (PEAK 3) POST-SWITCH.

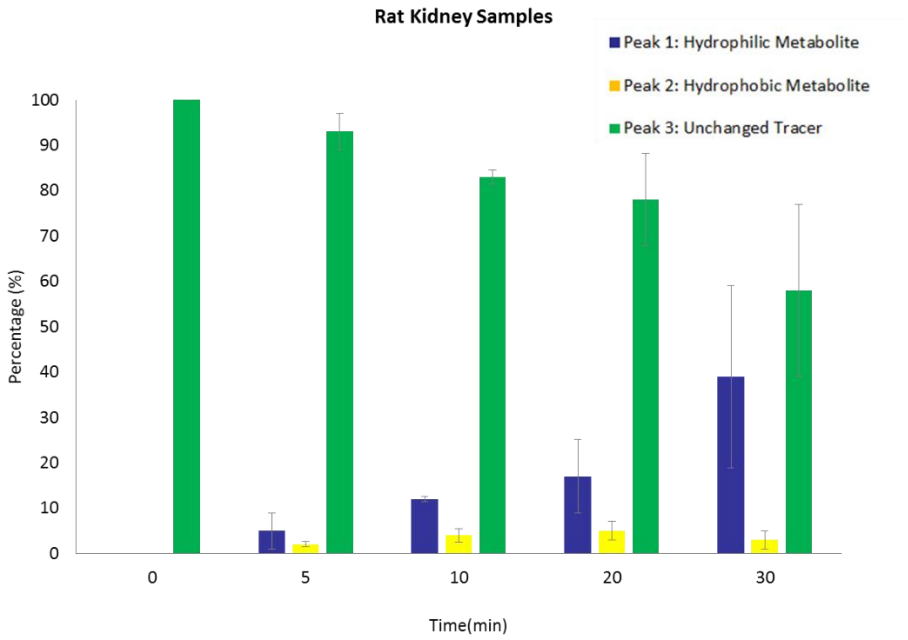

FIGURE 54- METABOLITE ANALYSIS OF [^{18}F]FPYKYNE-LOSARTAN IN RAT KIDNEY TISSUE HOMOGENATE (N=3 PER TIME POINT). PEAK AREA WAS QUANTIFIED, CORRECTED FOR NOISE, RADIOACTIVE DECAY AND UNRETAINED TRACER PROPORTION, AND EXPRESSED AS A PERCENTAGE OF TOTAL AREA PER SAMPLE.

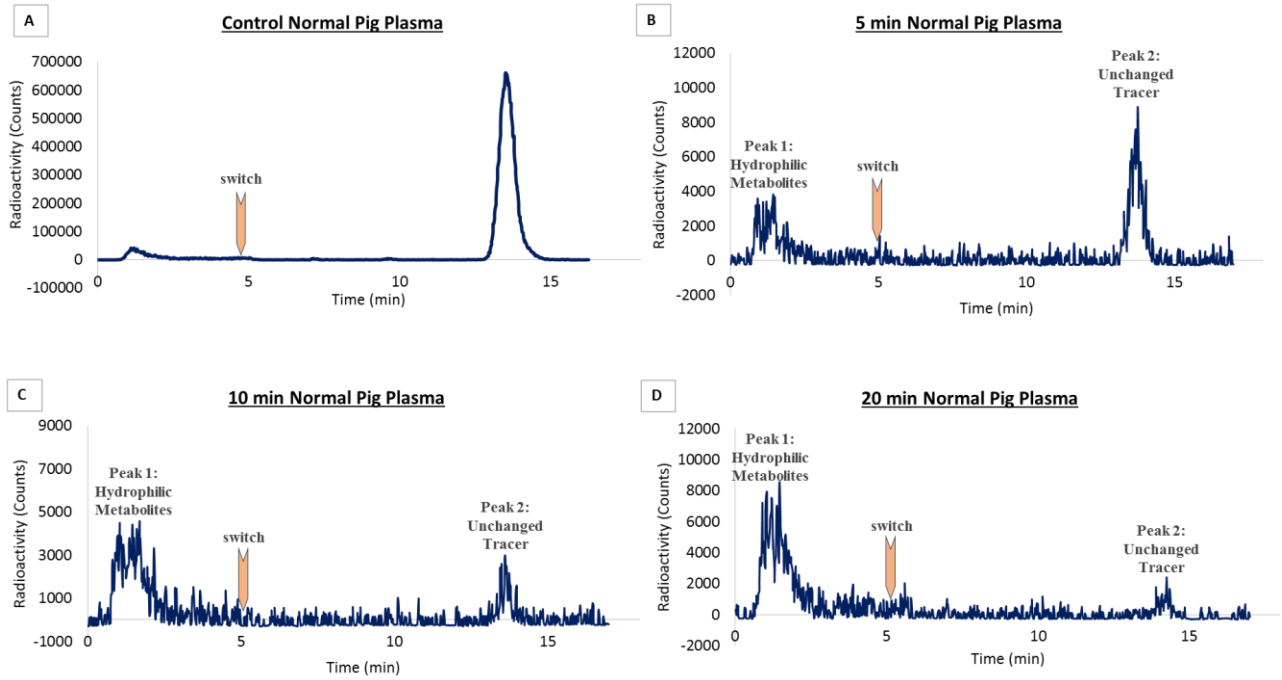

FIGURE 55- REPRESENTATIVE HPLC CHROMATOGRAMS DISPLAYING UNCHANGED [^{18}F]FPYKYNE-LOSARTAN AND ITS LABELED METABOLITES, IN NORMAL PIG PLASMA AT RESPECTIVE TIME POINTS. CONTROL PLASMA ARE SOLELY REPRESENTATIVE OF UNCHANGED [^{18}F]FPYKYNE-LOSARTAN WHICH HAS A RETENTION TIME OF 8.7 MIN AFTER SWITCH **(A)**. PLASMA SAMPLES WERE ANALYZED AT 1 (NOT SHOWN), 2 (NOT SHOWN), 5 **(B)**, 10 **(C)**, 20 **(D)** AND 40 (NOT SHOWN) MIN POST-INJECTION. [^{18}F]FPYKYNE-LOSARTAN (PEAK 2) IS METABOLIZED INTO HYDROPHILIC METABOLITES (PEAK 1) WHICH ARE ELUTED AT 1.0-1.5 MIN.

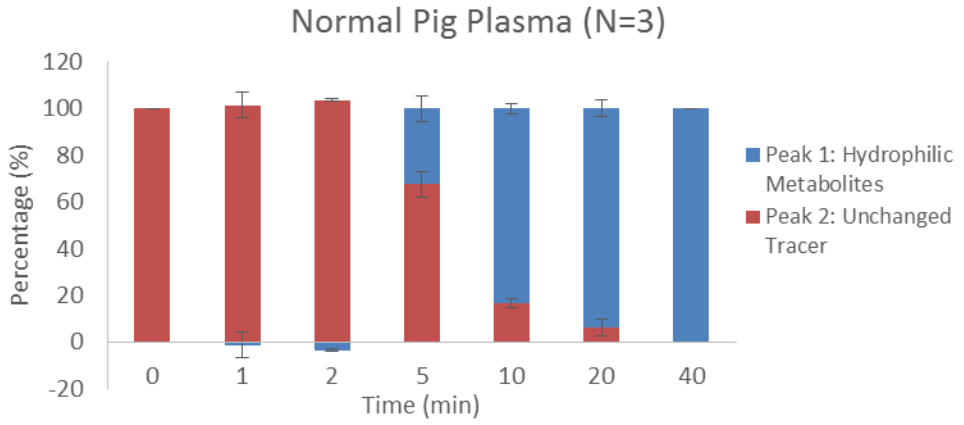

FIGURE 56- PROPORTIONS OF [^{18}F]FPYKYNE-LOSARTAN AND ITS HYDROPHILIC LABELED METABOLITES IN PIG PLASMA UNDER NORMAL CONDITIONS (N=3) OVER TIME. PEAK AREA WAS QUANTIFIED AND EXPRESSED AS A PERCENTAGE OF TOTAL AREA PER SAMPLE. RADIOACTIVITY IN THE CONTROL SAMPLE REPRESENTS UNCHANGED TRACER ONLY (100%). PIG PLASMA EXHIBITED RAPID METABOLISM OF [^{18}F]FPYKYNE-LOSARTAN WHICH WAS REDUCED FROM 68 ± 6% AT 5 MIN TO 6 ± 4% AT 20 MIN POST-INJECTION.

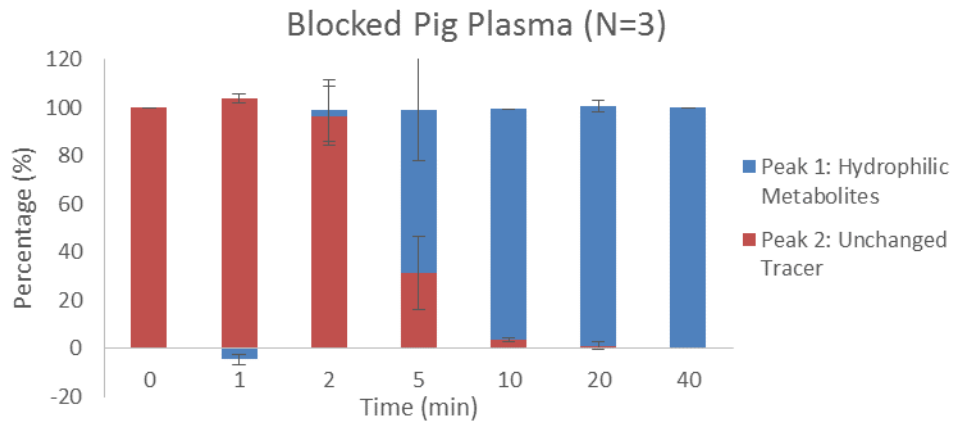

FIGURE 57- [^{18}F]FPYKYNE-LOSARTAN METABOLITE ANALYSIS FOR PIG PLASMA UNDER BLOCKING CONDITIONS (N=3; WITH 10 MG/KG CANDESARTAN). PEAK AREA WAS QUANTIFIED AND EXPRESSED AS A PERCENTAGE OF TOTAL AREA PER SAMPLE. METABOLISM OF [^{18}F]FPYKYNE-LOSARTAN IS FASTER WHEN AT_1RS ARE BLOCKED BY WHICH IT IS WASHED OUT FROM PLASMA WITHIN 10 MIN VS. 20 MIN WHEN AT_1RS ARE AVAILABLE FOR BINDING. THIS GIVES EVIDENCE FOR THE TRACER'S SPECIFICITY TO THE AT_1R.

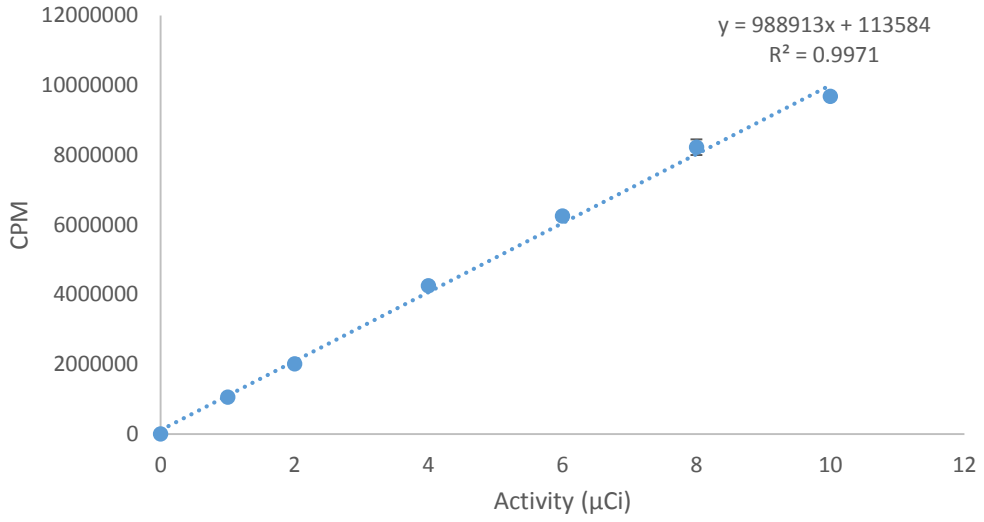

FIGURE 58- [^{18}F]FDG GAMMA COUNTER STANDARD CURVE RELATING COUNTS PER MINUTE (CPM) TO ACTIVITY IN µCI. THE EQUATION OF THIS LINE WAS USED FOR DOSIMETRY STUDIES TO CONVERT MEASURED ACTIVITIES INTO COUNTS.

TABLE 10- TISSUE UPTAKE (%ID/G) OF [^{18}F]FPYKYNE-LOSARTAN FOR ALL TIME POINTS AND TISSUES OF FEMALE SPRAGUE-DAWLEY RATS (N=3 AT ALL TIME POINTS) RECEIVING ~ 0.5 MCI (AT TIME OF FIRST INJECTION). GASTROINTESTINAL CONTENTS WERE COLLECTED FROM THE LOWER LARGE INTESTINE (LLI), UPPER LARGE INTESTINE (ULI), AND SMALL INTESTINE (SI).

Females (n=3 per time point)	5 min (%ID/g)			15 min (%ID/g)			30 min (%ID/g)			60 min (%ID/g)		
Brain	0.005	±	0.002	0.002	±	0.001	0.002	±	0.001	0.000	±	0.000
Eye	0.012	±	0.004	0.006	±	0.002	0.006	±	0.001	0.003	±	0.001
Thyroid	0.065	±	0.007	0.049	±	0.026	0.031	±	0.020	0.012	±	0.004
Thymus	0.022	±	0.009	0.017	±	0.002	0.011	±	0.001	0.005	±	0.001
Heart	0.075	±	0.011	0.025	±	0.002	0.011	±	0.001	0.004	±	0.001
Lung	0.205	±	0.020	0.105	±	0.055	0.054	±	0.019	0.021	±	0.008
Spleen	0.157	±	0.082	0.057	±	0.051	0.033	±	0.015	0.020	±	0.010
Pancreas	0.296	±	0.373	0.067	±	0.074	0.133	±	0.101	0.068	±	0.072
Esophagus	0.092	±	0.036	0.051	±	0.014	0.229	±	0.250	0.012	±	0.003
Stomach Contents	0.016	±	0.001	0.013	±	0.007	0.016	±	0.012	0.014	±	0.011
Stomach Wall	0.046	±	0.000	0.147	±	0.101	0.042	±	0.028	0.022	±	0.019
LLI Contents	0.006	±	0.002	0.008	±	0.005	0.010	±	0.007	0.008	±	0.007
LLI Wall	0.056	±	0.007	0.037	±	0.011	0.022	±	0.004	0.014	±	0.005
ULI Contents	0.040	±	0.025	0.837	±	1.418	0.056	±	0.039	0.231	±	0.300
ULI Wall	0.052	±	0.006	0.161	±	0.184	0.026	±	0.005	0.028	±	0.032
Small Intestine Contents	0.248	±	0.245	2.017	±	1.491	1.126	±	0.950	0.068	±	0.090
Small Intestine Wall	0.071	±	0.023	0.285	±	0.257	0.145	±	0.078	0.013	±	0.002
Bladder	0.061	±	0.052	0.062	±	0.022	0.049	±	0.038	0.102	±	0.049
Red Marrow	0.005	±	0.024	0.019	±	0.016	0.079	±	0.074	0.012	±	0.011
Bone	0.027	±	0.016	0.021	±	0.004	0.014	±	0.003	0.032	±	0.027
Muscle	0.015	±	0.003	0.018	±	0.009	0.023	±	0.015	0.019	±	0.022
Breast	0.050	±	0.042	0.027	±	0.015	0.056	±	-	0.015	±	0.012
Ovary	0.103	±	0.012	0.039	±	0.019	0.033	±	0.024	0.017	±	0.003
Uterus	0.020	±	0.003	0.026	±	0.015	0.026	±	0.022	0.033	±	0.021
Adrenal Gland	0.076	±	0.013	0.045	±	0.035	0.023	±	0.010	0.031	±	0.033
Kidney	1.832	±	0.357	1.143	±	0.232	0.466	±	0.091	0.108	±	0.075
Liver	7.617	±	1.881	7.967	±	2.535	6.467	±	1.020	6.795	±	0.997
Urine	0.974	±	1.459	0.225	±	0.192	0.124	±	0.161	0.407	±	0.542
Blood	0.084	±	0.018	0.036	±	0.002	0.020	±	0.000	0.008	±	0.001

TABLE 11- TISSUE UPTAKE (%ID/G) OF [^{18}F]FPYKYNE-LOSARTAN FOR ALL TIME POINTS AND TISSUES OF MALE SPRAGUE-DAWLEY RATS (N=3 AT ALL TIME POINTS) RECEIVING ~ 0.5 MCI (AT TIME OF FIRST INJECTION). GASTROINTESTINAL CONTENTS WERE COLLECTED FROM THE LOWER LARGE INTESTINE (LLI), UPPER LARGE INTESTINE (ULI), AND SMALL INTESTINE (SI).

Males (n=3 per time point)	5 min (%ID/g)			15 min (%ID/g)			30 min (%ID/g)			60 min (%ID/g)		
Brain	0.011	±	0.007	0.002	±	0.001	0.002	±	0.001	0.001	±	0.000
Eye	0.012	±	0.005	0.009	±	0.004	0.004	±	0.004	0.005	±	0.003
Thyroid	0.039	±	-	0.046	±	0.045	0.011	±	0.009	0.025	±	0.013
Thymus	0.038	±	0.015	0.022	±	0.007	0.014	±	0.001	0.008	±	0.002
Heart	0.119	±	0.041	0.029	±	0.003	0.014	±	0.003	0.010	±	0.006
Lung	0.276	±	0.072	0.107	±	0.011	0.058	±	0.008	0.036	±	0.018
Spleen	0.152	±	0.077	0.055	±	0.040	0.051	±	0.028	0.025	±	0.009
Pancreas	0.158	±	0.134	0.216	±	0.194	0.107	±	0.015	0.050	±	0.009
Esophagus	0.100	±	0.031	0.051	±	0.051	0.026	±	0.012	0.042	±	0.020
Stomach Contents	0.012	±	0.009	0.067	±	0.071	0.017	±	0.006	0.008	±	0.003
Stomach Wall	0.097	±	0.040	0.060	±	0.022	0.055	±	0.014	0.027	±	0.015
LLI Contents	0.027	±	0.007	0.004	±	0.001	0.032	±	0.026	0.014	±	0.011
LLI Wall	0.068	±	0.028	0.034	±	0.010	0.032	±	0.009	0.016	±	0.006
ULI Contents	0.039	±	0.038	0.023	±	0.017	0.037	±	0.025	0.045	±	0.046
ULI Wall	0.070	±	0.016	0.026	±	0.002	0.024	±	0.004	0.458	±	0.772
Small Intestine Contents	0.273	±	0.353	0.947	±	1.543	0.465	±	0.698	0.070	±	0.039
Small Intestine Wall	0.156	±	0.125	0.115	±	0.151	0.097	±	0.136	1.077	±	1.846
Bladder	0.075	±	0.034	0.538	±	0.520	0.308	±	0.214	0.108	±	0.120
Red Marrow	0.051	±	0.029	0.018	±	0.009	0.018	±	0.010	0.036	±	0.042
Bone	0.027	±	0.010	0.016	±	0.005	0.018	±	0.008	0.029	±	0.011
Muscle	0.033	±	0.004	0.029	±	0.012	0.016	±	0.003	0.014	±	0.007
Testis	0.018	±	0.003	0.023	±	0.008	0.019	±	0.010	0.013	±	0.002
Adrenal Gland	0.161	±	0.068	0.041	±	0.007	0.047	±	0.033	0.028	±	0.007
Kidney	1.804	±	0.356	0.760	±	0.206	0.224	±	0.078	0.094	±	0.025
Liver	6.076	±	1.193	7.189	±	0.398	5.716	±	1.648	4.865	±	1.440
Urine	0.152	±	0.118	1.038	±	0.411	1.095	±	1.027	2.436	±	1.995
Blood	0.176	±	0.066	0.051	±	0.009	0.034	±	0.008	0.020	±	0.006

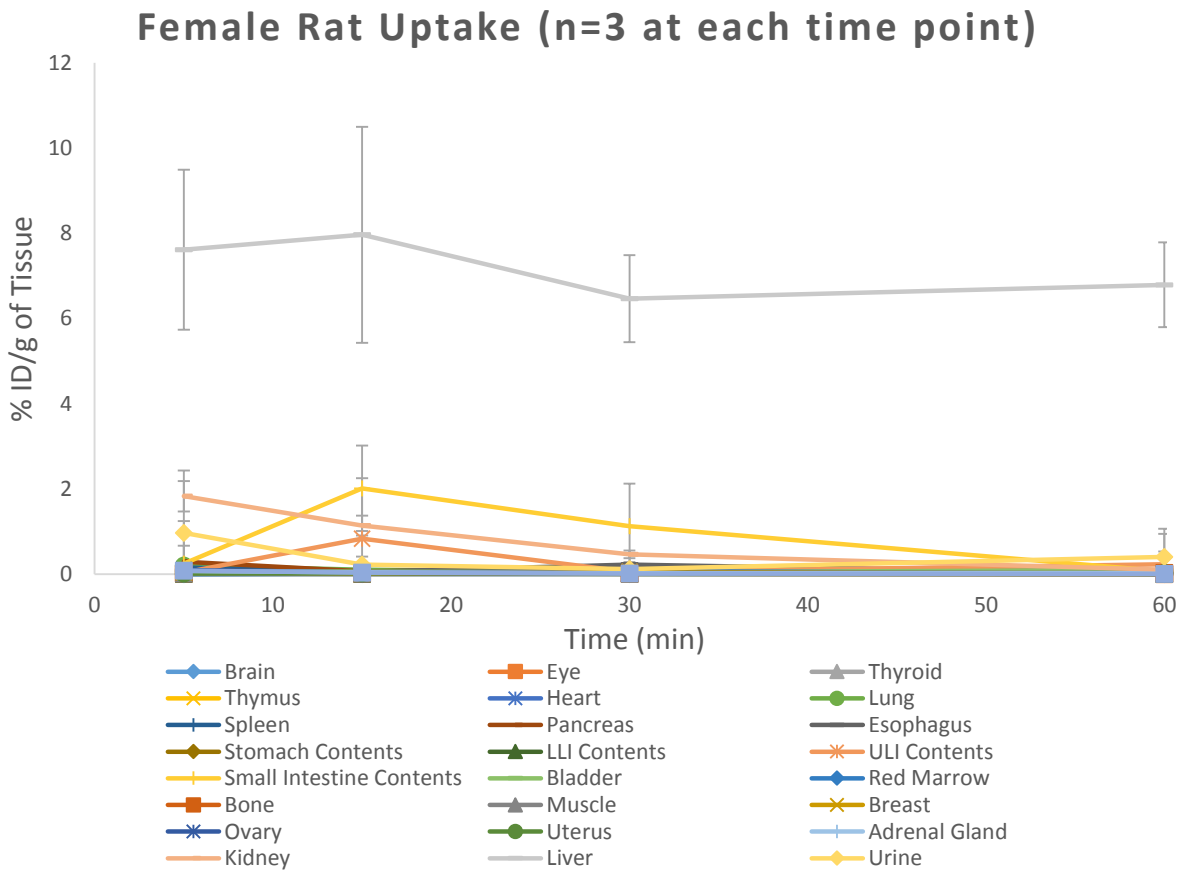

FIGURE 59- FEMALE SPRAGUE-DAWLEY RAT UPTAKE OF [^{18}F]FPYKYNE-LOSARTAN EXPRESSED AS %ID PER GRAM OF TISSUE (N=3 RATS PER TIME POINT). GASTROINTESTINAL CONTENTS WERE COLLECTED FROM THE LOWER LARGE INTESTINE (LLI), UPPER LARGE INTESTINE (ULI), AND SMALL INTESTINE (SI). EXCEPT FOR GASTROINTESTINAL CONTENTS AND URINE WHICH INCREASED OVER TIME, RAPID UPTAKE OF [^{18}F]FPYKYNE-LOSARTAN WAS OBSERVED IN TISSUES GRADUALLY DECREASING 5 MIN FOLLOWING TRACER INJECTION, WITH LIVER SHOWING HIGHEST UPTAKE.

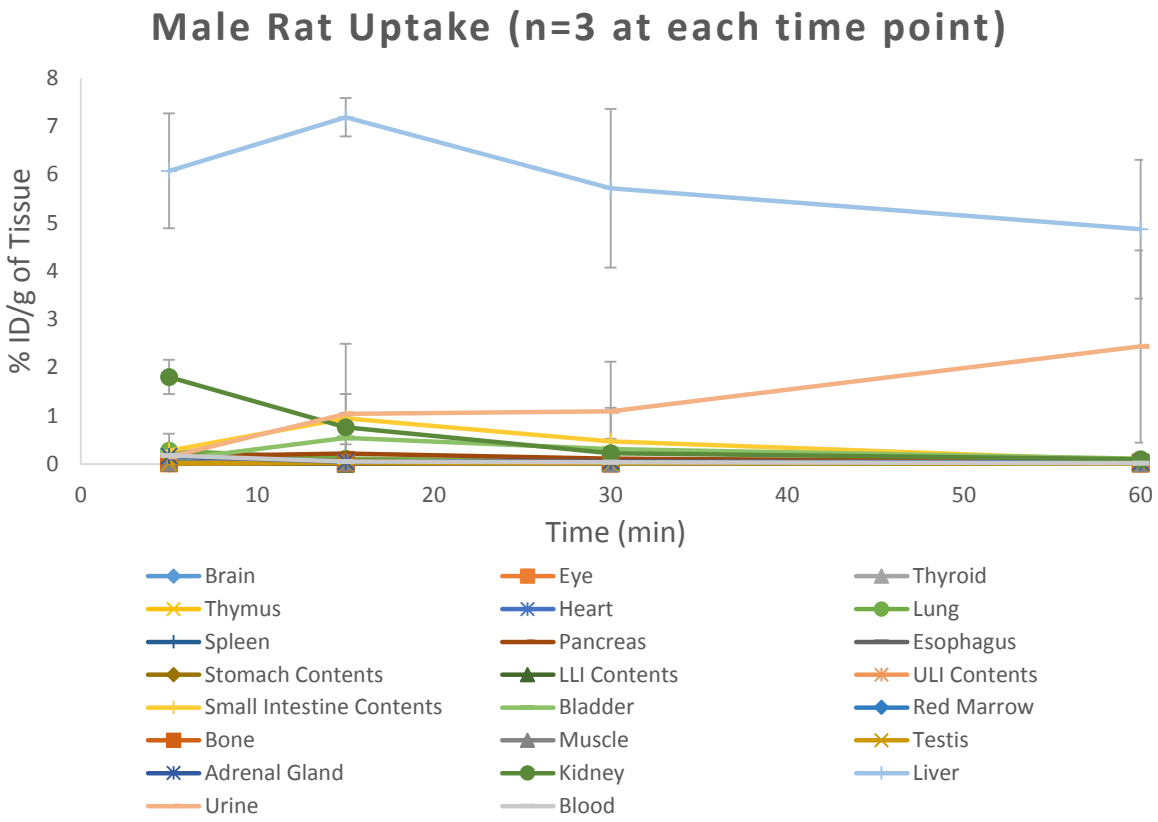

FIGURE 60- MALE SPRAGUE-DAWLEY RAT UPTAKE OF [^{18}F]FPYKYNE-LOSARTAN EXPRESSED AS %ID PER GRAM OF TISSUE (N=3 RATS PER TIME POINT). GASTROINTESTINAL CONTENTS WERE COLLECTED FROM THE LOWER LARGE INTESTINE (LLI), UPPER LARGE INTESTINE (ULI), AND SMALL INTESTINE (SI). EXCEPT FOR GASTROINTESTINAL CONTENTS AND URINE WHICH INCREASED OVER TIME, RAPID UPTAKE OF [^{18}F]FPYKYNE-LOSARTAN WAS OBSERVED IN TISSUES GRADUALLY DECREASING 5 MIN FOLLOWING TRACER INJECTION, WITH LIVER SHOWING HIGHEST UPTAKE.

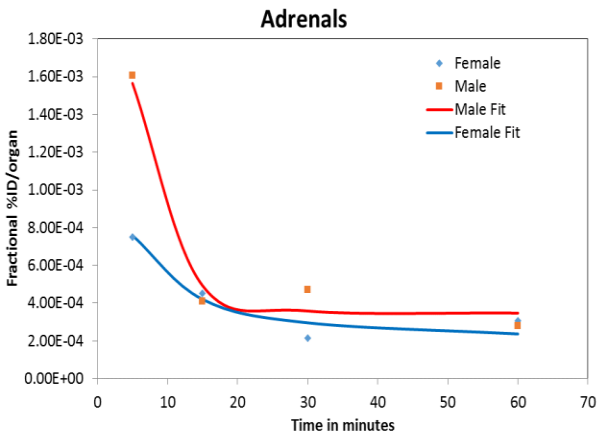
Adrenals
Fractional %ID/organ
Time in minutes
Female
Male
Male Fit
Female Fit

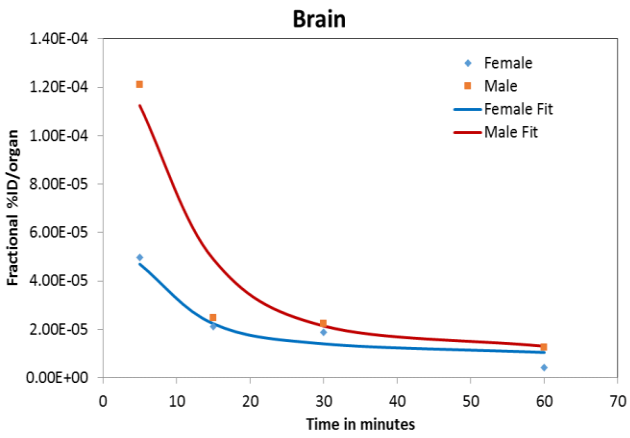
Brain
Fractional %ID/organ
Time in minutes
Female
Male
Female Fit
Male Fit

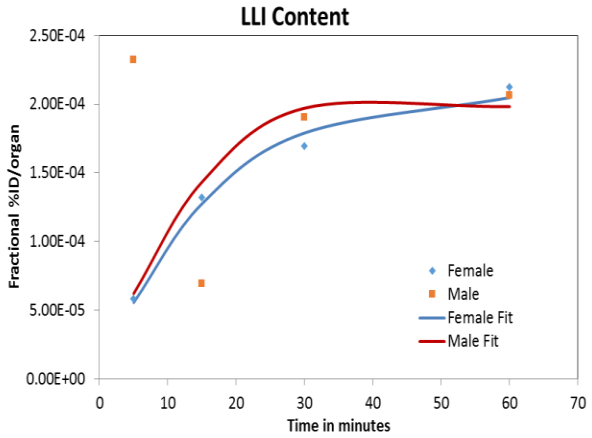
LLI Content
Fractional %ID/organ
Time in minutes
Female
Male
Female Fit
Male Fit

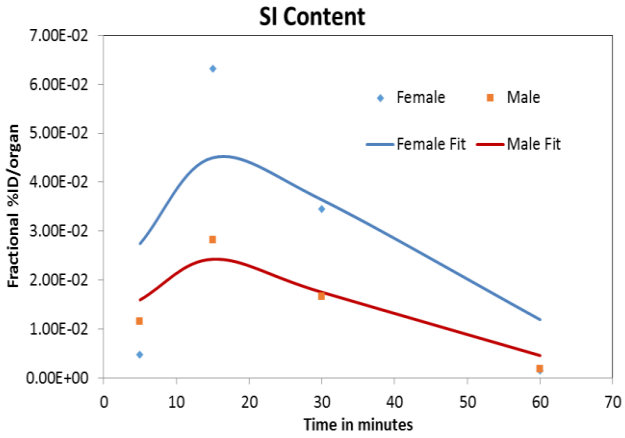
SI Content
Fractional %ID/organ
Time in minutes
Female
Male
Female Fit
Male Fit

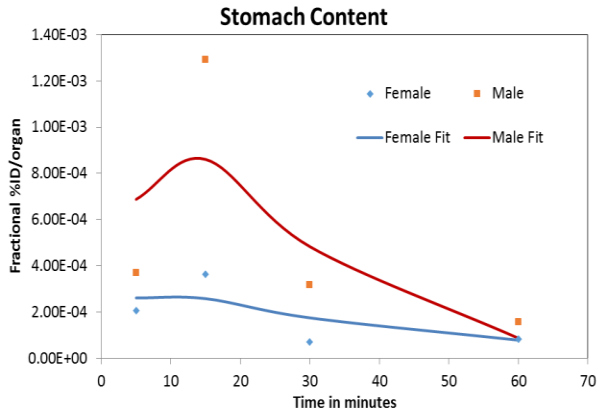
Stomach Content
Fractional %ID/organ
Time in minutes
Female
Male
Female Fit
Male Fit

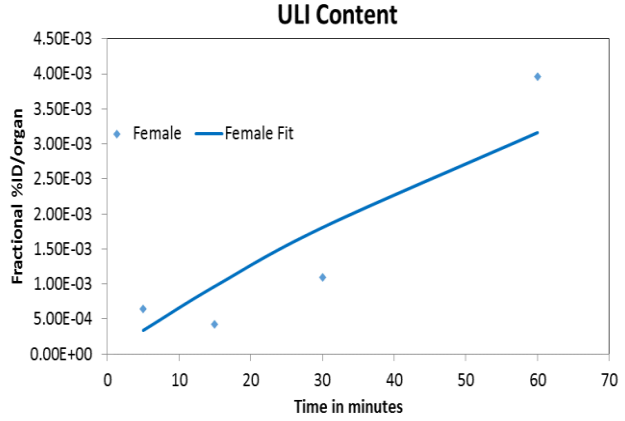
ULI Content
Fractional %ID/organ
Time in minutes
Female
Female Fit

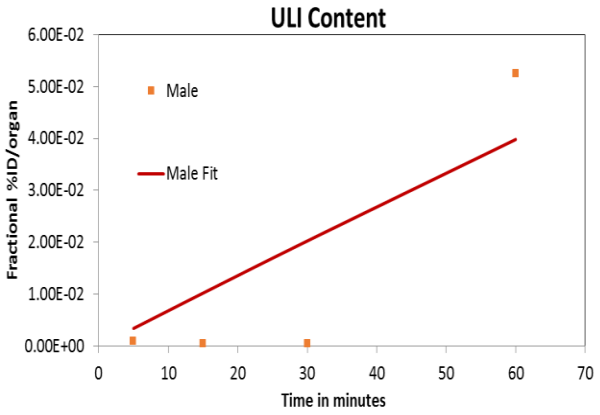
ULI Content
Male
Male Fit
Fractional %ID/organ
Time in minutes

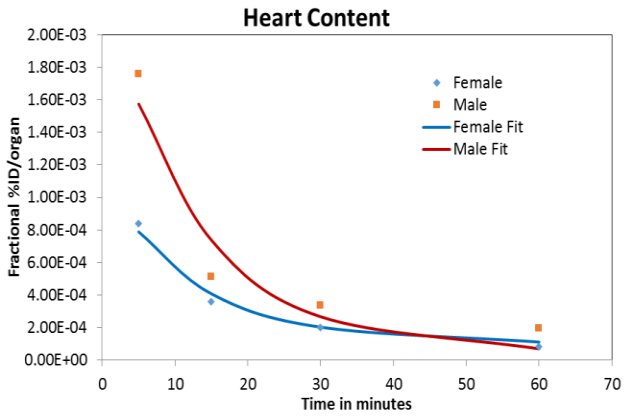
Heart Content
Female
Male
Female Fit
Male Fit
Fractional %ID/organ
Time in minutes

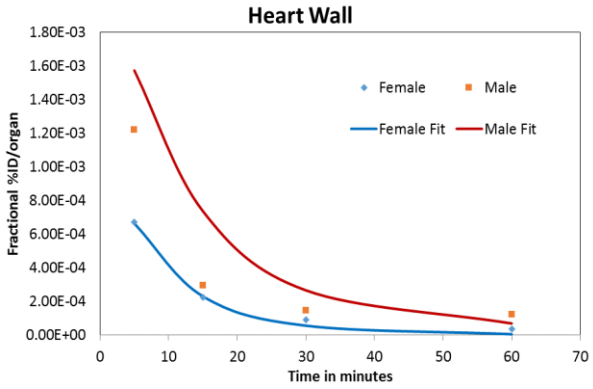
Heart Wall
Female
Male
Female Fit
Male Fit
Fractional %ID/organ
Time in minutes

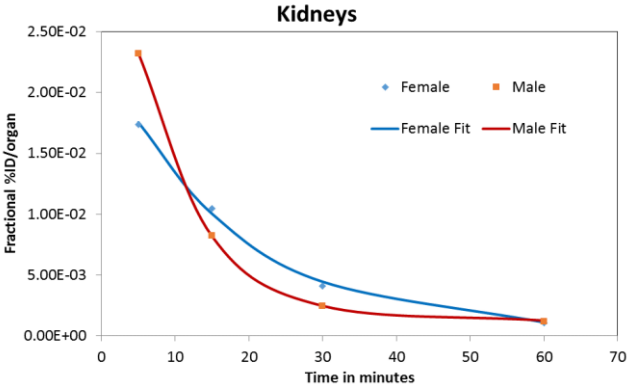
Kidneys
Female
Male
Female Fit
Male Fit
Fractional %ID/organ
Time in minutes

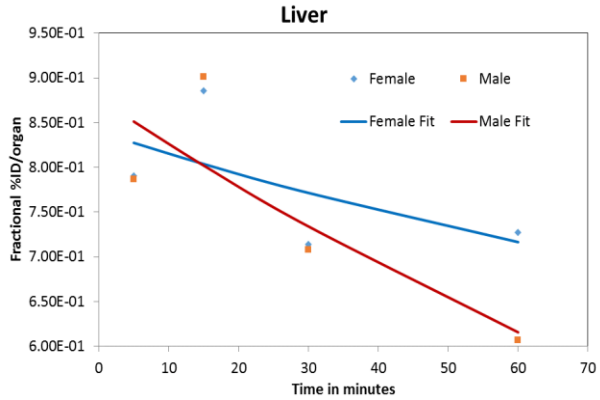
Liver
Female
Male
Female Fit
Male Fit
Fractional %ID/organ
Time in minutes

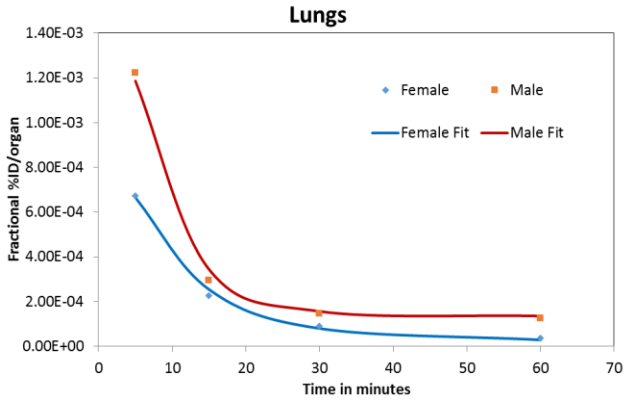
Lungs
Female
Male
Female Fit
Male Fit
Fractional %ID/organ
Time in minutes

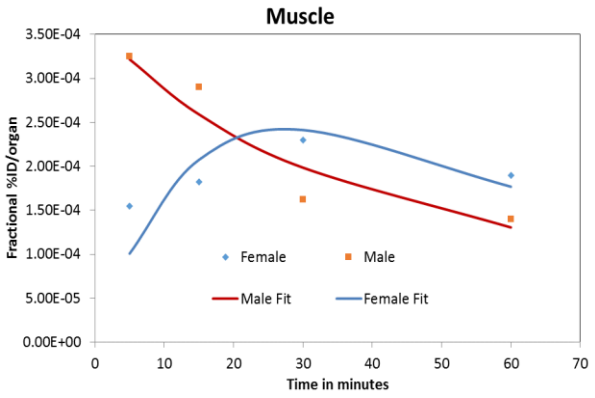
Muscle
Fractional %ID/organ
3.50E-04
3.00E-04
2.50E-04
2.00E-04
1.50E-04
1.00E-04
5.00E-05
0.00E+00
0 10 20 30 40 50 60 70
Time in minutes
Female
Male
Male Fit
Female Fit

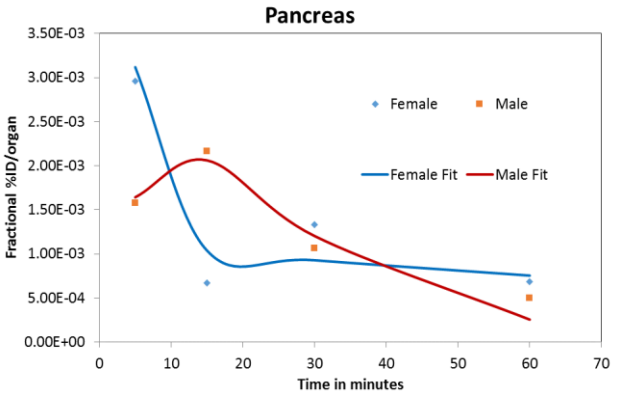
Pancreas
Fractional %ID/organ
3.50E-03
3.00E-03
2.50E-03
2.00E-03
1.50E-03
1.00E-03
5.00E-04
0.00E+00
0 10 20 30 40 50 60 70
Time in minutes
Female
Male
Female Fit
Male Fit

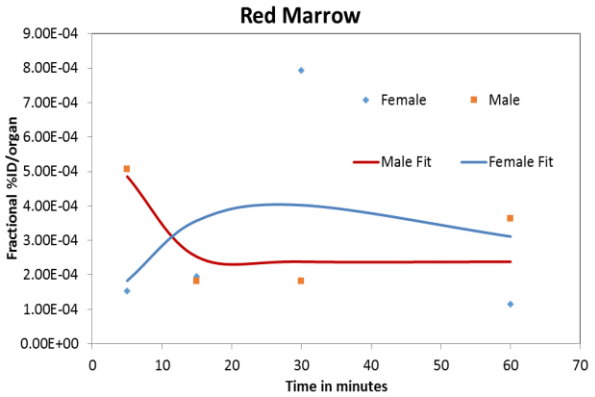
Red Marrow
Fractional %ID/organ
9.00E-04
8.00E-04
7.00E-04
6.00E-04
5.00E-04
4.00E-04
3.00E-04
2.00E-04
1.00E-04
0.00E+00
0 10 20 30 40 50 60 70
Time in minutes
Female
Male
Male Fit
Female Fit

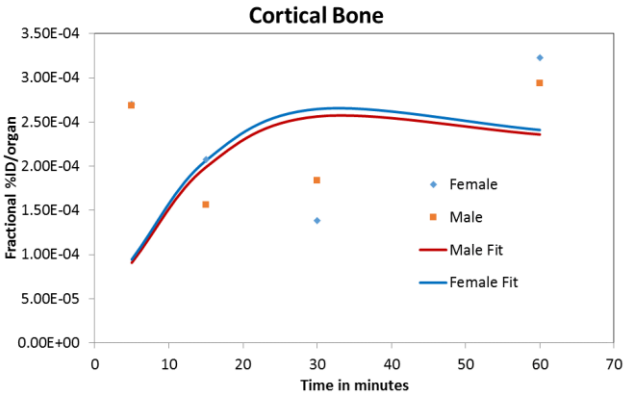
Cortical Bone
Fractional %ID/organ
3.50E-04
3.00E-04
2.50E-04
2.00E-04
1.50E-04
1.00E-04
5.00E-05
0.00E+00
0 10 20 30 40 50 60 70
Time in minutes
Female
Male
Male Fit
Female Fit

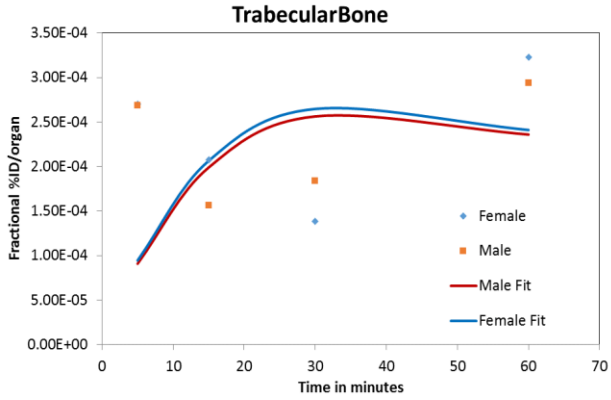
TrabecularBone
Fractional %ID/organ
3.50E-04
3.00E-04
2.50E-04
2.00E-04
1.50E-04
1.00E-04
5.00E-05
0.00E+00
0 10 20 30 40 50 60 70
Time in minutes
Female
Male
Male Fit
Female Fit

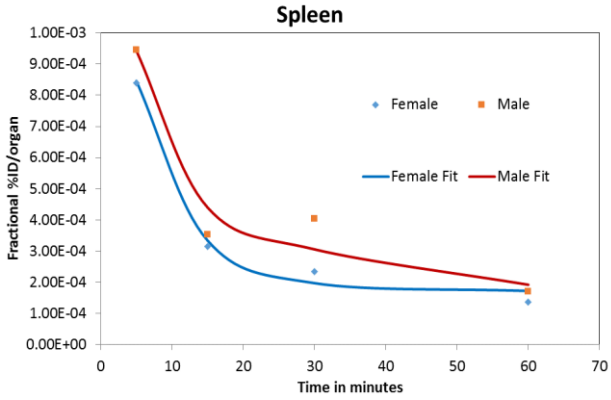
Spleen
Fractional %ID/organ
1.00E-03
9.00E-04
8.00E-04
7.00E-04
6.00E-04
5.00E-04
4.00E-04
3.00E-04
2.00E-04
1.00E-04
0.00E+00
0 10 20 30 40 50 60 70
Time in minutes
Female
Male
Female Fit
Male Fit

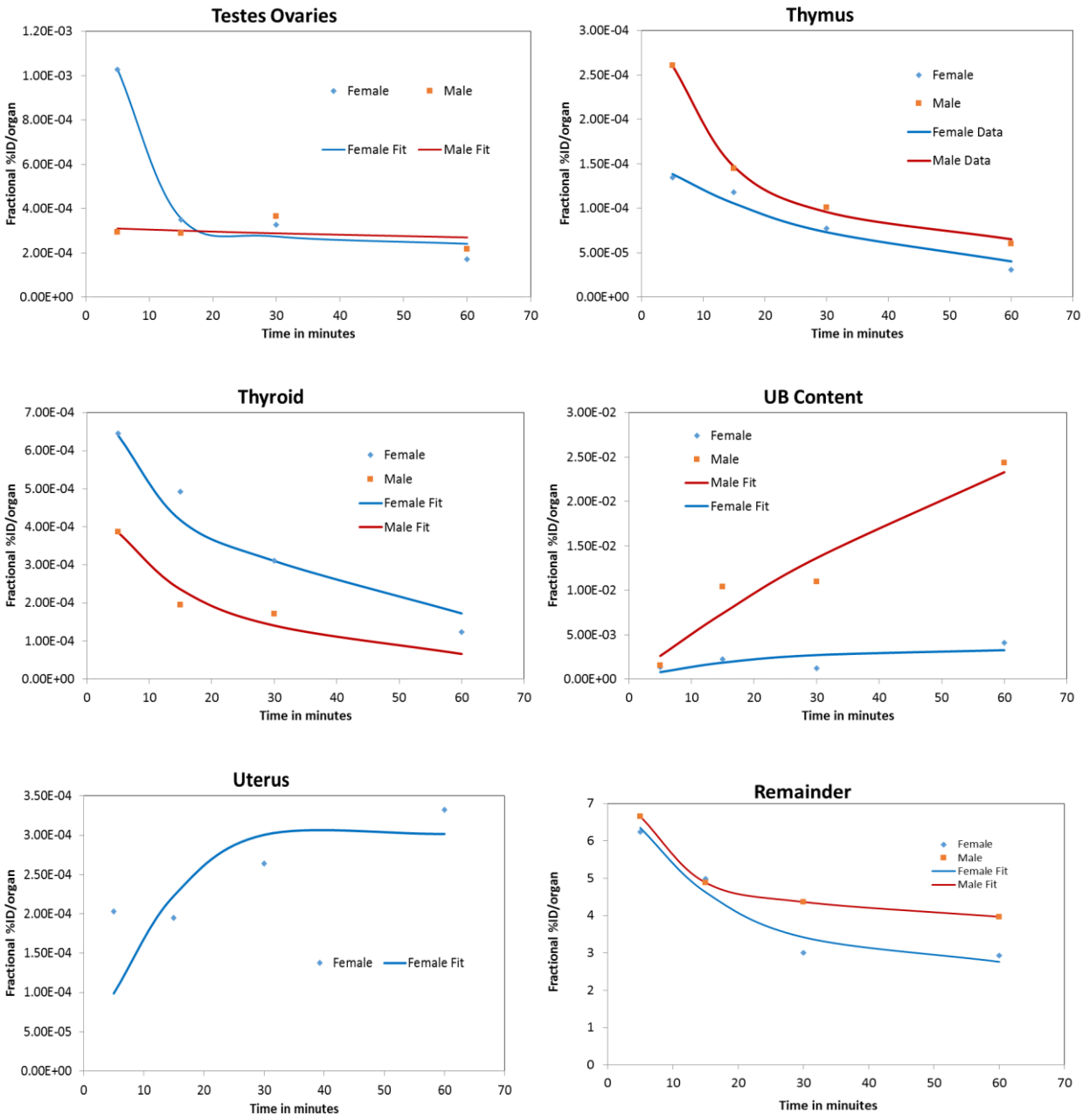

FIGURE 61- ORGAN GRAPHS DISPLAYING BEST FITS OF FEMALE AND MALE ORGAN UPTAKE WITH TIME. UPTAKE IS EXPRESSED AS FRACTIONAL ACTIVITY (%ID/ORGAN) PER TIME (MIN). GASTROINTESTINAL CONTENTS WERE COLLECTED FROM THE LOWER LARGE INTESTINE (LLI), UPPER LARGE INTESTINE (ULI), AND SMALL INTESTINE (SI). IN THE OLINDA/EXM SOFTWARE, HEART IS CONSIDERED "HEART WALL", URINE IS TERMED "URINARY BLADDER CONTENTS" (UB CONTENTS), AND BLOOD IS TERMED "HEART CONTENTS". AS THE GRAPHS SHOW, MALE AND FEMALE RATS DISPLAY SIMILAR TRENDS OF UPTAKE IN COMMON ORGANS (EXCLUDING TESTES, OVARIES AND BREASTS). A MEAN OF 85% OF THE TOTAL INJECTED DOSE WAS RECOVERED IN THE ORGANS AND CARCASS AT THE TIME POINTS STUDIED.

TABLE 12- ORGAN RESIDENCE TIMES (KBQ-H/KBQ) OF [^{18}F]FPYKYNE-LOSARTAN IN FEMALE SPRAGUE-DAWLEY RATS AND MASSES FOR RATS, AND HUMANS (CALCULATED FROM RAT DATA).

Organ residence times and masses for rats and humans - FEMALE				
Organ	Rat	Rat Organs	Human Organs	Human
	kBq-h/kBq	g	g	kBq-h/kBq
Adrenals	1.03E-03	3.95E-02	13	1.33E-03
Brain	2.15E-05	1.39E+00	1300	7.85E-05
Breasts	6.90E-04	7.79E-02	500	1.74E-02
LLI Content	7.16E-04	1.32E+00	130	2.76E-04
SI Content	3.39E-02	3.20E+00	280	1.16E-02
Stomach Content	3.89E-04	1.19E+00	230	2.95E-04
ULI Content	1.22E-02	9.74E-01	190	9.32E-03
Heart Content	3.19E-04	5.18E-01	370	8.94E-04
Heart Wall	1.18E-04	3.50E-01	250	3.31E-04
Kidneys	3.38E-03	9.37E-01	275	3.88E-03
Liver	3.03E+00	1.09E+01	1400	1.52E+00
Lungs	1.18E-04	1.46E+00	950	3.00E-04
Muscle	6.96E-04	3.02E-01	17500	1.58E-01
Pancreas	3.34E-03	5.42E-02	120	2.89E-02
Red Marrow	6.40E-04	1.50E-02	900	1.50E-01
Cortical Bone	8.58E-04	2.75E-01	3200	3.91E-02
Trabecular Bone	2.14E-04	6.88E-02	800	9.77E-03
Spleen	5.30E-04	6.23E-01	130	4.33E-04
Ovaries	6.83E-04	7.17E-02	11	4.11E-04
Thymus	1.15E-04	6.81E-01	20	1.33E-05
Thyroid	4.76E-04	5.44E-02	17	5.82E-04
UB Content	1.31E-02	7.68E-02	200	1.34E-01
Uterus	1.13E-03	5.79E-02	80	6.13E-03
Remainder	1.04E-01	210	31134	6.04E-02
Total Body	-	235	60000	-

TABLE 13- ORGAN RESIDENCE TIMES (KBQ-H/KBQ) OF [^{18}F]FPYKYNE-LOSARTAN IN MALE SPRAGUE-DAWLEY RATS AND MASSES FOR RATS, AND HUMANS (CALCULATED FROM RAT DATA).

Organ residence times and masses for rats and humans - MALE				
Organ	Rat	Rat Organs	Human Organs	Human
	kBq-h/kBq	g	g	kBq-h/kBq
Adrenals	1.09E-03	2.79E-02	14	2.09E-03
Brain	5.26E-05	1.34E+00	1450	2.19E-04
LLI Content	7.11E-04	1.65E+00	110	1.82E-04
SI Content	1.94E-02	4.20E+00	350	6.21E-03
Stomach Content	8.73E-04	1.26E+00	250	6.62E-04
ULI Content	1.59E-01	1.04E+00	190	1.11E-01
Heart Content	5.69E-04	6.50E-01	510	1.71E-03
Heart Wall	3.76E-04	4.21E-01	330	1.13E-03
Kidneys	4.35E-03	1.14E+00	310	4.52E-03
Liver	3.15E+00	1.26E+01	1800	1.73E+00
Lungs	4.63E-04	1.30E+00	1200	1.64E-03
Muscle	5.37E-04	3.20E-01	29000	1.86E-01
Pancreas	2.47E-03	8.27E-02	140	1.60E-02
Red Marrow	1.20E-03	1.29E-02	1170	4.17E-01
Cortical Bone	7.91E-04	1.14E-01	4400	1.17E-01
Trabecular Bone	1.98E-04	2.85E-02	1100	2.93E-02
Spleen	6.08E-04	6.82E-01	150	5.13E-04
Testes	8.56E-04	1.61E+00	35	7.12E-05
Thymus	2.17E-04	7.33E-01	25	2.84E-05
Thyroid	5.07E-04	2.46E-02	20	1.58E-03
UB Content	7.73E-02	1.56E-01	200	3.79E-01
Remainder	1.43E-01	251	30246	6.64E-02
Total Body	-	280	73000	-

TABLE 14- ESTIMATED EFFECTIVE DOSES (MSV/MBQ) FOR [^{18}F]FPYKYNE-LOSARTAN. THE TABLE INCLUDES A LIST OF THE EQUIVALENT AND WEIGHTED DOSES TO THE ORGANS FOR THE MALE AND FEMALE PHANTOMS. DOSES WERE CALCULATED ACCORDING TO ICRP 60 AND 103 PROTOCOLS USING OLINDA/EXM SOFTWARE. THE LIVER ACCOUNTS FOR MORE THAN 36% OF THE ED IN BOTH SEXES SUGGESTING THAT THE HEPATOBILIARY SYSTEM AND THE KIDNEYS ARE RESPONSIBLE FOR ELIMINATING [^{18}F]FPYKYNE-LOSARTAN.

	Male			Female		
Organ	Equivalent Dose to Target Organ mSv/MBq	Weighted Equivalent Dose ICRP 60	Weighted Equivalent Dose ICRP 103	Equivalent Dose to Target Organ mSv/MBq	Weighted Equivalent Dose ICRP 60	Weighted Equivalent Dose ICRP 103
Adrenals	4.34E-02	2.17E-04	4.01E-04	3.80E-02	1.90E-04	3.51E-04
Brain	1.92E-03	9.60E-06	1.92E-05	1.08E-03	5.40E-06	1.08E-05
Breasts	5.24E-03	2.62E-04		1.37E-02	6.85E-04	1.64E-03
Gallbladder	4.17E-02		3.85E-04	4.15E-02		3.83E-04
LLI	1.05E-02	1.26E-03		6.42E-03	7.70E-04	
SI	1.51E-02	7.55E-05	1.39E-04	1.21E-02	6.05E-05	1.12E-04
Stomach	1.08E-02	1.30E-03	1.30E-03	1.14E-02	1.37E-03	1.37E-03
ULI	5.55E-02	2.78E-04		1.62E-02	8.10E-05	
Heart Wall	1.33E-02		1.23E-04	1.41E-02		1.30E-04
Kidneys	1.97E-02	9.85E-05	1.82E-04	1.84E-02	9.20E-05	1.70E-04
Liver	2.15E-01	1.08E-02	8.60E-03	2.46E-01	1.23E-02	9.84E-03
Lungs	1.13E-02	1.36E-03	1.36E-03	1.21E-02	1.45E-03	1.45E-03
Muscle	8.31E-03	4.16E-05	7.67E-05	7.47E-03	3.74E-05	6.90E-05
Ovaries				1.31E-02	2.62E-03	1.05E-03
Pancreas	4.82E-02	2.41E-04	4.45E-04	7.72E-02	3.86E-04	7.13E-04
Red Marrow	3.89E-02	4.67E-03	4.67E-03	1.68E-02	2.02E-03	2.02E-03
Osteogenic Cells	3.06E-02	3.06E-04	3.06E-04	1.71E-02	1.71E-04	1.71E-04
Skin	4.02E-03	4.02E-05	4.02E-05	3.51E-03	3.51E-05	3.51E-05
Spleen	7.08E-03	3.54E-05	6.54E-05	7.76E-03	3.88E-05	7.16E-05
Testes	5.34E-03	1.07E-03	4.27E-04			
Thymus	5.16E-03	2.58E-05	4.76E-05	4.91E-03	2.46E-05	4.53E-05
Thyroid	1.48E-02	7.40E-04	5.92E-04	7.43E-03	3.72E-04	2.97E-04
Bladder	1.83E-01	9.15E-03	7.32E-03	9.21E-02	4.61E-03	3.68E-03
Uterus	1.70E-02	8.50E-05		2.25E-02	1.13E-04	2.08E-04
Colon			4.34E-03			1.44E-03
ED (mSv/MBq)		3.20E-02	3.38E-02		2.74E-02	2.74E-02

TABLE 15- SEX AVERAGED EFFECTIVE DOSES (ED) FOR [^{18}F]FPYKYNE-LOSARTAN IN HUMANS BASED ON ICRP 60 AND ICRP 103 PROTOCOLS (0.030 AND 0.031 MSV/MBQ, RESPECTIVELY). THESE VALUES ARE COMPARABLE TO OTHER ^{18}F-TRACERS SUCH AS [^{18}F]FDG.

Sex Averaged Values	
ED ICRP 60 (mSv/MBq)	2.97E-02
ED ICRP 103 (mSv/MBq)	3.06E-02

5. Discussion

5.1. Binding Affinity Parameters

In the light of characterizing our novel tracer, studying its in vitro characteristics is essential. Binding studies performed aimed to assess the specific binding parameters (K_d and B_{max}) of [^{18}F]FPyKYNE-Losartan on rat kidney tissue in vitro, thus, validating in vivo PET findings. Although in vivo studies ultimately have a greater therapeutic relevance than in vitro studies (Michel et al., 2013), the latter have the advantage of bypassing the animal's systemic factors, so any pharmacokinetic or pharmacodynamic effects on tracer binding could be ignored.

Consistent with AT_1R localization, high levels of binding was observed in the rat renal cortex, however binding to the medulla could not be differentiated from that of the cortex through image analysis due to low image resolution. This is a limitation of the study, as the highest binding should be apparent in the outer medulla similarly to previous reports established using the specific Ang II receptor radioligand [^{125}I]-[Sar^1, Ile^8] Ang II (Fabiani et al., 2000).

On the other hand, the study provides further evidence that [^{18}F]FPyKYNE-Losartan binds specifically to AT_1Rs in in vitro conditions. Specific binding refers to the binding of a ligand to its specific target or receptor, while nonspecific is the binding of a ligand to something other than its designated receptor such as other receptors, or different types of transporters/proteins in the cell membrane (Foreman et al., 2003). In our study, although tracer selectivity for AT_1Rs over AT_2Rs has been reported (Arksey et al., 2014), AT_2Rs were blocked with PD123319 in the total binding group and with Ang II in the nonspecific binding group to ensure any nonspecific binding to AT_2Rs is omitted. Hence, the TB group corresponds to tracer specific binding to the AT_1R plus binding to nonspecific sites other than the AT_2R (which is blocked). Whereas the NSB group correlates with possible binding to any site other than the

AT_1R and AT_2R that are flooded with Ang II. When subtracting the binding obtained from these two groups, specific binding of [^{18}F]FPyKYNE-Losartan to AT_1Rs (only) is determined.

K_d is the reciprocal of K_a which is a measure of the affinity of a drug for the receptor. A low K_d indicates that less drug is needed to occupy 50% of the receptors and that molecules are tightly bound. A high value indicates that more of the drug is required to occupy 50% of the receptors and that molecules are weakly bound to the receptors. A drug with low K_d has high K_a, and vice versa. As previous SAR studies on Losartan (R: CH_2OH) have shown, adding a methyl group at the 5-imidazole position (R: CH_2OCH_3) increased the IC_{50} from 19 nM to 32 nM (Carini et al., 1991), thus by adding a larger group as in FPyKYNE-Losartan (R: FPyKYNE= 2-[F-18]fluoro-3-pent-4-yn-1-yloxypyridine) it was expected that the IC_{50} value or the K_d would be even higher as the compound becomes more bulky. Therefore, the average K_d of $\sim$ 50 nM for FPyKYNE-Losartan is in line with previous SAR studies. Apparently, affinity of the blockers to AT_1Rs is much less than that of its natural ligand Ang II. The K_d of Ang II has been widely studied and that in rat kidney was reported to be around 1-2 nM: 2.2 ± 0.2 nM (Brown et al., 1983); 1.02 nM (Cox et al., 1984); 0.6 ± 0.4 nM (Sechi et al., 1992).

Nonspecific binding, although less than total binding, was higher than expected. Rat in vivo studies with [^{18}F]FPyKYNE-Losartan have displayed nonspecific binding to be around 35% in vivo (Arksey et al., 2014), however, this doesn't seem to be the case in vitro as rat kidney slices revealed very high nonspecific binding, even higher than specific binding in most of the assays. A reason possibly attributing to this outcome is that the tracer, being hydrophobic, sticks tightly to the slices and perhaps to the glass of the slides, such that washing with buffer and distilled water is not sufficient for removing unbound tracer. Accordingly, it is suggested that replacing distilled water with more washes of buffer or washing for a longer time, could have a stronger effect in displacing the free compound from the slices, overall reducing the nonspecific binding proportion.

Comparing the analysis approaches, less variability among K_d values was obtained using the global fit of TB and NSB curves rather than SB curves only, while B_{max} was less altered between both approaches. This is because using both TB and NSB curves provides more data points on the graphs, hence, robustness and certainty are better in terms of K_d. B_{max}, however, is less likely to be affected as the maximum binding is relatively unchanged (refer to Figure 34).

5.2. Full Antagonism

FPyKYNE-Losartan was evaluated for inhibiting the Ang II-induced increase of diastolic arterial blood pressure in normal rats. The percent decrease in the normal effect of Ang II on arterial blood pressure at its submaximal dose of 3 µg/Kg was calculated for each dose. The most frequently used way to determine AT_1R antagonism in vivo is the measurement of blood pressure responses to i.v. injections of Ang II in the presence of one or more doses of an ARB. However, several other in vivo antagonism studies have focused on the inhibition of other Ang II responses. For example, Losartan and Telmisartan were shown to inhibit the Ang II- induced development of pro-inflammatory molecules in the kidneys (Kumar et al., 2010), and Candesartan inhibited the Ang II-induced plasma aldosterone increase (Wada et al., 1994).

The choice of monitoring diastolic blood pressure for antagonistic studies was based on the following literature: Grant et al., 1988; Wong et al., 1989; Christophe et al., 1995. Mean and systolic blood pressures were also recorded. Moreover, diastolic blood pressure (the minimum pressure in the arteries; when heart and blood vessels are relaxed) is known to be a better indication of the risk especially when the drugs used act to decrease blood pressure. To confirm the choice of BP assessed in this study, both diastolic BP and systolic BP were analyzed. Similar variations in blood pressure were obtained here (Figure 62).

In pharmacological studies, it is rather important to differentiate between the terms IC_{50}, ID_{50}, GI_{50}, LD_{50}, and ED_{50} that are often used interchangeably. IC_{50} is the drug concentration causing 50% inhibition

of the maximal inhibitory effect. IC_{50} only applies for inhibition of a specified individual target. It indicates the concentration of a particular product or inhibitor (antagonist) needed to inhibit a given biological process. It is commonly used as a measure of antagonistic drug potency in pharmacological research done in vitro (nM) (using autoradiography assays), whereas, ID_{50} is usually the alternative term for the inhibiting dose of the antagonist in vivo (mg/Kg). GI_{50} is the concentration for 50% of maximal inhibition of cell proliferation in whole-cell assays. LD_{50} is the lethal dose or concentration causing 50% of total cell death, although it is often argued that it should be used for in vivo studies only. ED_{50} (or EC_{50}) is the dose (or concentration) of a drug causing 50% of the maximum effect for any measured biological effect of interest, also referred to as the "potency" of the drug. ED_{50} would be the preferable term for a drug that hasn't yet been identified as an agonist or antagonist, this being the case for FPyKYNE-Losartan. Yet once it is characterized as an antagonist, the term IC_{50} or ID_{50} becomes more accurate.

Dissolving larger doses of FPyKYNE-Losartan was not possible with saline. FPyKYNE-Losartan is a hydrophobic compound, and is not available as a powder for the higher doses but rather as an oily substance hardly soluble in water/saline. A new vehicle solution was necessary to ensure proper dissolution at higher concentrations. Propylene glycol and EtOH increased the solubility of FPyKYNE-Losartan, and importantly, had no effect on blood pressure compared to the original vehicle (saline).

Graph fitting for this study was done based on two models. In the first, curves displayed the effect of Ang II (%) (refer to Figure 41 and Table 5). For this model, basal was constrained to "0" and the top values (maximal inhibitory effect) for Losartan, Candesartan and FPyKYNE-Losartan were set to be equal or lower than 100%. In the second model, graphs displayed the inhibition of Ang II effect (%) rather than the effect of Ang II, so experimental points were fitted with an equation where the basal point was still constrained to a value of "0" (as no inhibition of Ang II effects should be observed) and the top values were set to fit a value ≤ 100 (Figure 63; Table 16). Both models show full antagonism of the blockers and using either one does not change the ID_{50} value.

Losartan (1-30 mg/Kg) and Candesartan (1-10 mg/Kg) produced a dose-dependent inhibition of Ang II receptor binding. FPyKYNE-Losartan (3-50 mg/Kg) also displayed in vivo antagonism of Ang II pressor effect in a dose-dependent manner, but with a lower potency than the other two blockers. Compared to Losartan, FPyKYNE-Losartan is about four-fold less potent in blocking the pressor effect of Ang II. This could be due to the change in structure with the addition of FPyKYNE at the 5-position, leading to lower potency for AT_1R antagonism. Nevertheless, FPyKYNE-Losartan still acts as a full antagonist, with an ID_{50} of 25.5 mg/Kg required to block 50% of the maximal response produced by Ang II. As depicted in its dose-response curve, 100% blockage would likely be attained at higher doses, explicitly at ~ 70 mg/Kg (graphically: logDose= ~ 1.85; refer to Figure 41). Candesartan (ID_{50}= 0.7 mg/Kg), on the other hand, is almost 9 times more potent relative to Losartan (ID_{50}= 6.4) and 36 times relative to FPyKYNE-Losartan (ID_{50}= 25.5). At a dose of 10 mg/Kg, Candesartan completely blocks the receptor as Ang II produced no effect on blood pressure when injected. Similarly, Losartan virtually blocks AT_1Rs at a dose of 30 mg/Kg, also suggesting that Candesartan is more potent than Losartan in antagonizing AT_1Rs in vivo. Such results are in line with previous research (Fabiani et al., 2000). The different influence of ARBs on Ang II receptor inhibition is due to the pharmacokinetic and pharmacodynamic differences that exist between them (Fabiani et al., 2000; Meredith, 2010).

By comparing ID_{50}'s obtained for Losartan and Candesartan with previously published data, our values seemed to be higher. For instance, the ID_{50} of Losartan obtained in pithed rats in vivo was 1.7 mg/Kg in studies performed by Lee and colleagues (1999) and 0.4 mg/Kg by Shibouta et al. (1993). These values are less than our dose (6.4 mg/Kg). Knowing that the route of administration was the same (i.v.), this discrepancy could be attributed to the difference in rat model; pithing the rat, anesthetizing it or leaving it conscious could possibly produce variable effects on the physiology of the rat and more precisely its RAS. Candesartan's ID_{50} obtained in our study (0.7 mg/Kg) was higher compared to that obtained in conscious rats (0.03 mg/Kg) (Shibouta et al., 1993) and pithed (0.02 mg/Kg) (Dendorfer et al., 2002). Thus,

a precise ID_{50} for the blockers cannot be implied from previous research as their findings are difficult to associate. This could be due to the different conditions of each experiment. Overall, our results are comparable to published literature.

5.3. PET/MicroPET Imaging and Evaluation of Binding Properties

5.3.1. Evaluation in Rats

Using PET allows sequential measurements of radioactivity in ROIs in vivo after intravenously injecting a radiolabeled ligand. Usually for radioligands that are known to bind reversibly, a simple two-compartment model can be applied to graphically determine the ratio B_{max}/ K_d from the slope (DV), describing the binding potential. B_{max} represents the concentration of ligand binding sites and K_d the equilibrium dissociation constant of the ligand-binding site complex. This ratio could then be compared with in vitro measures of the same parameters to confirm the results (Logan et al., 1990).

The preliminary evaluation of in vivo binding of [^{18}F]FPyKYNE-Losartan in rats using micro-PET imaging displayed greatest accumulation of activity in the liver and kidneys in normal untreated rats (Arksey et al., 2014). Renal TACs displayed a sharp increase in activity uptake in the first few minutes, following the arterial blood input functions, then washed out slowly to background levels around 55 min. The high liver uptake is due to nonspecific binding and metabolism, as the liver is the primary site of metabolism for large hydrophobic molecules (refer to section 5.6.). However, scans did not display uptake in adrenals although studies have shown the density of AT_1Rs to be the highest in adrenals, followed by kidney, brain, aorta and heart, respectively (Chang et al., 1991). This result could be explained differently. First, due to the very small size of adrenals, the resolution of microPET may not be enough to image them. The shortage in PET resolution could also explain the difficulties to differentiate between kidney cortex and medulla uptake. Additionally, adrenals could also be affected by spillover from the kidney cortex located directly beneath them, or from the liver (high uptake) located right above. Another possibility is

that [^{18}F]FPyKYNE-Losartan binds more specifically to AT_{1A} than AT_{1B} receptors. Both receptor subtypes are known to be present in rats but AT_{1A} is expressed mostly in kidney and liver, while AT_{1B} is merely found in the adrenals in addition to the brain and testes (Burson et al., 1994). Even though the latter possibility is not very critical as only rodents have AT_1R subtypes contrary to pigs and humans, further experiments are required for confirmation.

Another point of notice is the lack of tracer retention in the heart and brain. AT_1Rs are poorly expressed in the heart exhibiting approximately 400 times less AT_1Rs compared to the kidney cortex (Chang et al., 1991). Normal cardiac tissue AT_1R density is probably too low to be imaged by PET, yet in models where cardiac AT_1R expression is increased such as MI (Tan et al., 2004), it may become possible to visualize the increased signal. For example, the AT_1R tracer [^{11}C]KR31173 of the Hopkins group displayed cardiac retention only in an MI model with upregulated AT_1Rs (Zober et al., 2006). It is important to note that low receptor expression combined with the relatively low SA of the tracer (high levels of cold ligand) will result in potential saturation of cardiac AT_1Rs and no images of specific AT_1 retention in the heart. Receptor saturation with the unlabeled compound (cold mass) in tracer formulations will lower the signal-to-noise ratio (Jagoda et al., 2004) in tissues expressing low receptor densities such as the heart (Chang et al., 1991). Cardiac uptake is expected to increase with improved SA of tracer formulations. However, current SA levels of [^{18}F]FPyKYNE-Losartan (200-4200 mCi/µmol; 7.4-155 GBq/µmol) were appropriate to produce excellent signal-to-noise ratios and images of the kidneys which are rich in AT_1Rs.

In order to image the brain, a radioligand must cross the BBB. Typically, molecules of small molecular weight (< 400-600 Daltons) and appropriate lipophilicity are those that normally penetrate the BBB (Sawada et al., 1999; Jong et al., 2005). However, the overwhelming majority of small molecules (<500 Daltons), proteins and peptides do not cross the BBB (Pardridge, 1995; 1998; 2003; 2005; 2007a; 2007b; 2007c). It was henceforth reported that in order to cross the BBB, molecules might need to be carried via specific transporters or proteins expressed at the luminal (blood) side of the endothelial cells along with

having apt weights and hydrophobicity (Gabathuler, 2010). Our compound is hydrophobic but has a MW of 627.11 Da; it was shown to poorly cross the BBB to image brain AT_1Rs.

5.3.2. Evaluation in Pigs

Moving towards large animal imaging, pigs were the chosen animals for this task. The significance of using pigs in translational research is that they share similar anatomic and physiologic characteristics with humans involving the cardiovascular, urinary, integumentary, and digestive systems. In regards to AT_1R imaging, pigs are a good choice of an animal model for human AT_1R imaging since in contrast to rodents, in which two subtypes (AT_{1a} and AT_{1b}) have been discovered, they possess only one subtype of these receptors, i.e., the AT_1R, like humans (Zober et al., 2006). Pigs are increasingly being used alternatively to dogs or monkeys as the choice of nonrodent species in preclinical studies on pharmaceuticals, because they have better anatomic similarities with man than dogs, are easier to deal with, and are less expensive (Thörn et al., 2011; Swindle et al., 2012). PET imaging of pigs with [^{18}F]FPyKYNE-Losartan further confirmed the high uptake, image contrast, binding specificity and slow clearance of the tracer in pig kidneys.

Performing blocking studies with PET imaging is important not only to confirm tracer specificity to the AT_1R, but also to determine whether any plasmatic ^{18}F-labeled metabolites would interfere in the binding signal to AT_1Rs. [^{18}F]FPyKYNE-Losartan metabolism effect on AT_1Rs was evaluated by assessing any change in tracer-to-metabolite ratio due to specific binding of metabolites to AT_1Rs. Blocking AT_1Rs with Candesartan reduced peak retention (average of $\sim$ 57%) in the renal cortex, indicating binding specificity of [^{18}F]FPyKYNE-Losartan to AT_1Rs. This result provides good justification for pursuing the translation of [^{18}F]FPyKYNE-Losartan towards human imaging to monitor AT_1Rs. Co-injection of the tracer with Candesartan did not ensure blockage of the AT_1Rs as shown by the blocking scan of pig 1 (Figure 64), which did not display reduced SUV or DV values compared to the normal scans. Candesartan is a very

potent ARB and an insurmountable antagonist that works by inactivating the receptor (see section 1.6.2.), such that no AT_1R ligand could further bind as long as it is present. However, co-injecting it with the tracer was not the perfect protocol for our blocking studies as a binding signal was still observed at the level of the kidneys even with the full blocking dose of Candesartan (10 mg/Kg), whereas pre-treatment 15 min prior to the tracer produced better blocking results. This could imply that the tracer binds irreversibly to the receptors and acts as an insurmountable antagonist to AT_1Rs, similarly to Candesartan. Nevertheless, some inconsistencies were still obtained among renal TACs of the blocking scans even when Candesartan was pre-injected. So, increasing the number of pigs and performing additional blocking scans would be preferable to increase the significance with regards to the blocking effect on the kidney cortex signal. Furthermore, the final DV values for the normal scans (5.56 ± 1.83 ml/cm^3) and the blocking scans (2.51 ± 1.10 ml/cm^3) reflect high variability ($\sim$ 33% and 44%, respectively) among the individual pigs (regardless of the fact that their differences were not significant). Addition of more animals would likely reduce result variability.

Arterial Input Function Corrections

The arterial input function is critical to accurate quantitative analysis of PET imaging. Experiments relating to arterial input function corrections revealed rapid tracer metabolism in pig plasma. At 5 min after tracer administration, the parent compound was reduced to $\sim$ 68%, then to $\sim$ 17% of the radioactive signal at 10 min in pig plasma. Rapid metabolism of the parent tracer results in a reduced quantity available for tissue and in specific binding to AT_1Rs, but can be accounted for in the quantitative evaluation by applying the fitted correction function (section 4.3.2.2.) over the duration of the scan. However, following metabolite correction, the Logan DV model did not seem to fit the data. This suggests that some labeled metabolites may be entering the tissue and binding to something unknown, that is, other than AT_1Rs. If this were the case, a "dual-input" compartmental model (Kuwabara et al., 1993) could be applied rather than Logan graphical analysis. A dual-input compartmental model requires two plasma inputs:

parent tracer and metabolite. Two parallel tissue compartments are attached to the first tissue compartment, that is, for the parent tracer, and one tissue compartment for the metabolite. If the compartments for the two inputs were independent, then the model could be simulated separately for each input and the resulting tissue curves could be simply summed. Previous work from my colleague Natasha Arksey in our lab exhibited the presence of hydrophilic labeled metabolites in rat kidney extracts (see Figure 12 and section 5.5.) that were not blocked by saturating doses of Candesartan. This could explain the "dual-input" function observed in pigs. Nonetheless, kinetic modeling is beyond the scope of this thesis, so correction for metabolites was not performed. With results expressed as SUVs, such corrections are not necessary. SUVs are commonly used in PET especially when no arterial input function is available for detailed pharmacokinetic modeling (Lucignani et al., 2004).

The second factor typically complicating the accurate determination of arterial input is the possible changes of whole blood and plasma ratios over time. This wasn't problematic in our case. The measured plasma to whole blood ratio was unchanged over time, which facilitated this part of the corrections. This is in contrast to most other tracers such as (R)-[^{11}C]rolipram, which showed a shift in radioactivity from whole blood to plasma over time, and thus required applying an equation fit to the ratio data to provide a whole blood correction for radioactivity plasma over time (Thomas et al., 2011).

[^{18}F]FPyKYNE-Losartan in blood is not bound to RBCs, it is carried by plasma proteins (albumin) as shown from rat plasma protein binding assessment where 97% of injected tracer was bound to plasma proteins (section 5.4.). This could also explain why the plasma\ whole blood radioactivity ratio is greater than 1 in pig plasma.

Tracer DVs are also affected by the vascular fraction (V_B) of the tissue. Including the vascular fraction in the calculation of the DV would compensate for the possible radioactivity lost in the blood vessels surrounding the target tissue. For example, V_B in the heart is 40% while it is 5% in the brain (Smith et al., 2001; St. Lawrence et al., 2012; Rizzo et al., 2014): the heart has a blood pool/cavity along the heart

muscle, so spill over is known to take place. The vascular fraction for heart tissue is thus high to compensate for vascular radioactivity. Whereas, this fraction is much lower in the brain that, unlike the heart, lacks any blood pool and is directly perfused with blood vessels such that no loss of radioactivity occurs. As for the kidney, which is considered a "vascular organ", vessels are close to the tissue with no blood cavities or spill over, so its V_B is expected to be less than that of the heart yet larger than that of the brain. A study reported that the vascular fraction in kidney cortex is 33% on average (Smith et al., 2001). In our pig PET analysis, kidney vascular fraction was negligible (V_B was set to be zero in the Logan parameters section), however, it should be accounted for when determining DVs to obtain more accurate values.

5.4. High plasma protein binding

The binding of the drug to plasma (and tissue) proteins is a major determinant of drug disposition (distribution). It has a very important effect on drug dynamics since only the free (unbound) drug interacts with receptors (Benet et al., 2002). Thus, assessing plasma protein binding is important for the characterization of a novel tracer.

Proteins are very large, very complex molecules consisting of chains of amino acids joined by peptide bonds often forming compartments into which other molecules could neatly fit. These sites are called binding sites. Knowing that the tissue can only access drug available in plasma, the degree to which the drug binds to plasma proteins may affect its efficiency. The less bound the drug or the more "free" it is, the more efficiently it can traverse cell membranes or diffuse. Most commonly, a loose and rapidly reversible interaction (lipophilic or hydrogen binding) takes place between the ligand and plasma proteins. Then, a chemical equilibrium will exist between the bound and unbound states such that: Protein + Drug ↔ Protein-Drug Complex. If a drug is displaced from plasma proteins it would increase the unbound drug concentration and increase the drug effect. Notably, it is the unbound fraction that exhibits

pharmacological effect by accessing the receptor. It is also the fraction that may be metabolized and eliminated. Changes in the levels of free drug changes the volume of distribution because free drug may distribute into the tissues leading to a decrease in plasma concentration profile. Generally, when plasma protein binding is greater than 90%, the drug is considered highly bound (Benet et al., 2002).

The ultrafiltration device utilized to assess plasma protein binding has a membrane cutoff MW of 30000 Da. It retains 99.9% of serum proteins. Albumin is responsible for the majority of drug-protein interactions, due to its abundance (60% of total plasma proteins) and its molecular structure that allows it to reversibly bind to various ligands. Knowing that rat serum albumin has a MW of 64.6 kDa (MW of human serum albumin= 67 kDa), [^{18}F]FPyKYNE-Losartan (MW= 627.11 g/mol) bound to albumin would be unable to pass through the membrane into the lower chamber.

[^{18}F]FPyKYNE-Losartan displayed high plasma protein binding with only 3% of it freely available for uptake by tissue and metabolism, while 97% is bound to plasma proteins (primarily albumin). One would think that this decreases the efficiency of the tracer as only a very small percentage could access the receptors. However, as reported by Smith et al. (2010), many of the top 100 most prescribed drugs have greater than 98% plasma protein binding. This highlights that plasma protein binding has no effect on the success of drug candidates; drugs with high plasma protein binding are used in a wide variety of therapeutic areas, such as cardiovascular disease (Losartan, Warfarin and Furosemide); pain (Diclofenac and Naproxen); metabolic diseases (Rosiglitazone, Glyburide and Pioglitazone); allergy and respiratory conditions (Cetirizine and Montelukast); and central nervous system disorders (Sertraline) (Smith et al., 2010). Moreover, not often does plasma protein binding and displacement have clinical relevance since the free drug concentration is controlled by the free drug clearance which is independent of plasma binding (Benet et al., 2002). With respect to PET radioligands specifically, it is expected that when equilibrium between the free and plasma protein bound tracer is rapidly reached, most of the bound tracer would become available for tissue during the typical PET scan (Berridge, 2009).

Losartan, the parent compound of our tracer, is 98% bound to plasma proteins (Christ, 1995). It is transformed into seven different metabolites, and the relative abundance of these compounds differs between humans and rats. Rats primarily transform Losartan into EXP3174 (the active metabolite of Losartan) that was shown to exhibit at least 10 times the affinity of Losartan for the AT_1R ($IC_{50} \cong 4 \times 10^{-9}$ nM; Michel et al., 2013) (Stearns et al., 1992; Krovat and Langer, 2003). EXP3174 is 99% bound. Thus, the AT_1R antagonists Losartan and EXP3174 are highly bound to plasma albumin in humans (Christ, 1995). Similar plasma protein binding results are observed between Losartan and [^{18}F]FPyKYNE-Losartan, confirming our hypothesis.

5.5. Favorable Metabolism Profile

Drug metabolism, also known as xenobiotic metabolism, is the biochemical modification of pharmaceutical substances or xenobiotics through specialized enzymatic systems of a living organism. Drug metabolism often converts lipophilic compounds into more readily excreted hydrophilic products. Generally, the rate of metabolism determines the duration and intensity of a drug's pharmacological action. So when a drug or compound is injected into the body it is metabolized into smaller molecules called metabolites. The metabolism of [^{18}F]FPyKYNE-Losartan was shown to be different between rats and pigs, possibly due to the involvement of different enzymes in the metabolism pathway. [^{18}F]FPyKYNE-Losartan is broken down into 2 types of metabolites in rats: hydrophilic and hydrophobic, yet only hydrophilic labeled metabolite(s) appear in pigs.

The nature of the labeled metabolites is determined through reverse-phase HPLC which separates molecules based on their polarity, that is, the earlier they are eluted the more polar (hydrophilic) they are. However, it is important to note that determining the identity of these metabolites was not pursued in the course of this thesis, as it requires further studies and syntheses. Not to mention that large animals (i.e. pigs) and rats exhibit different metabolism profiles, which is also to be expected different in humans.

Our primary objective concerning metabolism studies is to determine if the presence of labeled metabolites in plasma and kidney will "confound" AT_1R density measurements (via [^{18}F]FPyKYNE-Losartan and PET), so identifying the chemical "nature" of the metabolites was sufficient for the purpose of this thesis.

By definition, hydrophilic molecules are polar molecules that have a tendency to interact with or be dissolved by water and other polar substances. Hydrophobic molecules are nonpolar, and thus, prefer other neutral molecules and nonpolar solvents. Examples of hydrophobic molecules include the alkanes, oils, fats, and greasy substances in general (IUPAC 1997; Akhavan et al., 2013). FPyKYNE-Losartan is a lipophilic/hydrophobic molecule (MW= 627.11 g/mol) which has been shown to bind specifically to AT_1Rs in vivo (Arksey et al., 2014). Conversely, more hydrophilic molecules are less likely to bind to AT_1Rs. Labeled metabolite peaks detected early from the HPLC chromatograms (before the column switch) are hydrophilic/polar because they leaked through the capture column and did not stick to the HLB sorbent; these molecules will very likely display different structures than Losartan. They are referred to as "unretained metabolites". Hydrophobic labeled metabolites and unchanged [^{18}F]FPyKYNE-Losartan are detected later after the switch. The peak of [^{18}F]FPyKYNE-Losartan in every run was confirmed by the control samples which indicate the retention time of authentic tracer only. In rats, HPLC metabolite analysis revealed that only a very small proportion of the authentic tracer is metabolized into a hydrophobic metabolite (less than 6% at all time points studied), thus, no or very slight interference is expected with the binding signal of [^{18}F]FPyKYNE-Losartan. In pigs, the PET signal is expected to be solely from unchanged [^{18}F]FPyKYNE-Losartan as the only other labeled molecules present are of hydrophilic nature. This avoids the problem of signal interference by radioactive metabolites and facilitates kinetic modeling of the tracer, which is normally a characteristic of a tracer that can be quantified.

One limitation of the procedure is that the total injected activity is not completely retained by the capture column in control samples. Ideally, the capture cartridge should retain close to 100% of the

activity injected and be easily removed by the analytical column solvent. However, the reason why spiked samples get unretained is that plasma protein binding and interaction of macromolecules prevent the sample from being "free" and thus captured. Urea is added to disrupt protein-product interactions and plasma protein binding (Hilton et al., 2000). Since at the time of performing this study the plasma protein binding of our tracer was unknown but that of the parent compound, Losartan, was known as being high (98%) (Christ, 1995), adding urea was accomplished. With urea, the unretained percentage of authentic [^{18}F]FPyKYNE-Losartan was only 6% in rat and pig plasma, and 4% in rat kidney tissue. As noted previously (sections 3.7. and 4.6.), this proportion of tracer unretained by the capture cartridge during control studies was used to correct the areas of peak 1 (unretained metabolites) and unchanged tracer in the sample runs. As a result, if the amount of unretained activity was misleadingly high in the control samples, then the amount of unretained activity in a sample after correction would be underestimated, while the amount of tracer would be overestimated. This is a factor that could have potentially affected the reproducibility of our results. Other factors might be the amount of tissues run per cartridge, and the amount of activity injected.

Tracer metabolism in rat kidneys reflected more stability of the tracer than in plasma, since 58 $\pm$ 19% of total radioactivity refers to unchanged [^{18}F]FPyKYNE-Losartan at 30 min. The greater tissue retention of the tracer could be related to the dissociation time ($t_{1/2}$) of Losartan, which is reported in pharmacokinetic studies to be 67 min (Kakuta et al., 2005; Michel et al., 2013). Thus, a longer residence time at the receptor, and greater tissue retention over time could be expected. These results were correlated with PET TACs in rats which revealed that radioactivity is not cleared from kidneys before 60 min. Although hydrophobic metabolites are present, their presence in very minor proportions suggests minimal interference of ^{18}F- labeled metabolites to AT_1Rs in rats.

Previous work on [^{18}F]FPyKYNE-Losartan in rats (Arksey; 2012) has shown that blocking AT_1Rs with Candesartan caused an increase in the proportions of hydrophilic metabolites in kidney tissue, whereas

hydrophobic metabolites and unchanged tracer were reduced (see Figure 12 in section 1.11.). This confirms the specificity of the tracer to AT_1Rs since its proportion decreases when its binding site is unavailable. The proportion of labeled hydrophilic metabolites (compared to parent tracer) was increased in rat kidneys indicating absence of binding to AT_1Rs of labeled metabolites. This suggests that the signal corresponding to labeled metabolites can be "added" to the nonspecific binding compartment in the quantification process using PET. Despite the slight decrease of labeled hydrophobic metabolite proportions upon blocking, their interference with the overall binding signal in rat kidney is considered negligible as they are present in very small percentages (< 5%).

Normal pig plasma depicted more rapid metabolism of [^{18}F]FPyKYNE-Losartan than that of rats, for 23 ± 10% of the tracer was present in rat plasma at 30 min while being cleared out by that time in pigs (0% at 30 min). Although a 30 min time-point was not performed for pig metabolism studies, it is obvious from a curve fit that the fraction of unmetabolized tracer at 30 min is 0 (see Figure 47). In pigs, results suggest rapid excretion of [^{18}F]FPyKYNE-Losartan when administered intravenously.

When the AT_1Rs were blocked with Candesartan (10 mg/Kg) in pigs, plasma HPLC analysis displayed similar radioactive peaks as in baseline studies (peaks 1 and 2), yet with a faster clearance of [^{18}F]FPyKYNE-Losartan (Figure 65). This suggests that blocking the receptors renders the tracer more available in plasma, thus, more subject to metabolism into the hydrophilic metabolites. At 10 min, a significant difference in the proportion of unchanged [^{18}F]FPyKYNE-Losartan between normal and blocking conditions was detected (p-value= 0.002).

It is obvious from pig metabolism that the tracer is cleared rapidly from the circulation, which is a desirable property of a radiotracer (rapid clearance from plasma and nonspecific regions: see section 1.8.). Another advantage is the absence of hydrophobic metabolites of the tracer in pigs which facilitates renal AT_1R uptake quantification of [^{18}F]FPyKYNE-Losartan. However, a limitation of the pig studies is that

kidney tissue was not analyzed, as sacrificing large animals in big numbers for every experiment is not done routinely.

5.6. Dosimetry Profile

Most tissues demonstrated a rapid uptake of [^{18}F]FPyKYNE-Losartan, with levels gradually decreasing 5 min following radiotracer injection, except gastrointestinal contents and urine which increased over time. Liver showed highest uptake (~80% at 5 min and 60-70% by 60 min) and accounted for more than 36% of the ED in both sexes, with residence times also similar between the sexes. This result suggests that the hepatobiliary system (liver, gall bladder and bile ducts) is primarily responsible for eliminating [^{18}F]FPyKYNE-Losartan from the body, while the kidneys are the secondary route of excretion (through urine). This goes in line with the expected excretion pathways of the radioligand from previous studies on the parent compound Losartan, which reported that its primary elimination pathway is via the liver and specifically the cytochromes (Diez, 2006). More precisely, Losartan is rapidly converted in the liver to a more potent metabolite (EXP3174) via oxidation with an affinity 20 to 30 times higher for AT_1R, and is then eliminated via renal and hepatic routes (Dickstein et al., 1998). So, given the similarity in structures between Losartan and FPyKYNE-Losartan, it is expected that they will exhibit similar pharmacokinetic profiles.

There are two routes of excretion: renal and hepatobiliary. Usually, smaller hydrophilic compounds are excreted by the kidney and eliminated from the body in urine following glomerular filtration. Hydrophilic or water-soluble substances are more easily eliminated through this route (Prokop et al., 2008; Chen, 2012). Whereas, larger more hydrophobic molecules are excreted via the hepatobiliary route. Increased lipophilicity/hydrophobicity has been correlated with higher liver uptake and higher affinity to many metabolic enzymes such as P450 complex. Through this route, the drug enters the liver from blood then into the gastrointestinal tract (GIT) via bile ducts. Bile producing cells or hepatocytes produce bile stored in the gallbladder and enters the small intestine through bile ducts to aid in digestion (Erwin, 2008;

Diwan, 2012). The drug is transited through the duodenum, jejunum and ileum of the small intestine, then enters the large intestine where wastes are formed, and finally leaves the body through the feces. The liver is a major site for drug metabolism that aids in the elimination process by converting lipid-soluble substances into more hydrophilic compounds more easily excreted by the kidney (Prokop et al., 2008). Hence, for hydrophobic compounds as our tracer, the hepatobiliary pathway is the main elimination route explaining our results.

A noteworthy observation was the difference in radioactive uptake of the small intestine and large intestine between male and female rats. The small intestine displayed less retention in males than in females, while upper and lower large intestine exhibited higher uptake in males than in females at all time points. This could be explained by the difference in bowel movement between the sexes. Chen et al. (1995) reported that male rats have faster gastric voiding and intestinal transit than females.

A mean of 85% of the total ID was recovered in the organs and carcass at the time points studied. Gender averaged ED calculated using ICRP 60 and 103 was 2.97E-02 (mSv/MBq) and 3.06E-02 (mSv/MBq), respectively, which is comparable to other ^{18}F-tracers such as 2-[^{18}F]-fluoro-A-85380 (ED= 2.78E-02 mSv/MBq), O-(2-[^{18}F]fluoroethyl)-L-tyrosine (ED= 1.65E-02 mSv/MBq), and [^{18}F]FDG (ED= 2.4E-02 mSv/MBq) (Mejia et al., 1991; Pauleit et al., 2003; Obrzut et al., 2005). According to ICRP 80 which published dose estimates of other F-18 tracers currently in use, [^{18}F]FPyKYNE-Losartan's ED is 20% higher than fluorine (ED= 2.4E-02 mSv/MBq) and 38% higher than FDG (ED= 1.9E-02 mSv/MBq) (ICRP Publication 80: 113-120). However, most rat extrapolations tend to overestimate the results.

The EDs calculated for [^{18}F]FPyKYNE-Losartan are within the range of those reported in the literature for other ^{18}F labeled PET tracers and are well below the regulatory limits reported by the Radioactive Drug Research Committee guidelines (ICRP Publication 80: 113-120). Additionally, all tissue and whole body dose values are below the 3-5 rem safety limits recommended by the FDA. Therefore,

[^{18}F]FPyKYNE-Losartan has an acceptable dosimetry profile and is within safe limits for use in human studies. These findings further support its potential application as an AT_1R PET tracer.

5.7. Tables and Figures

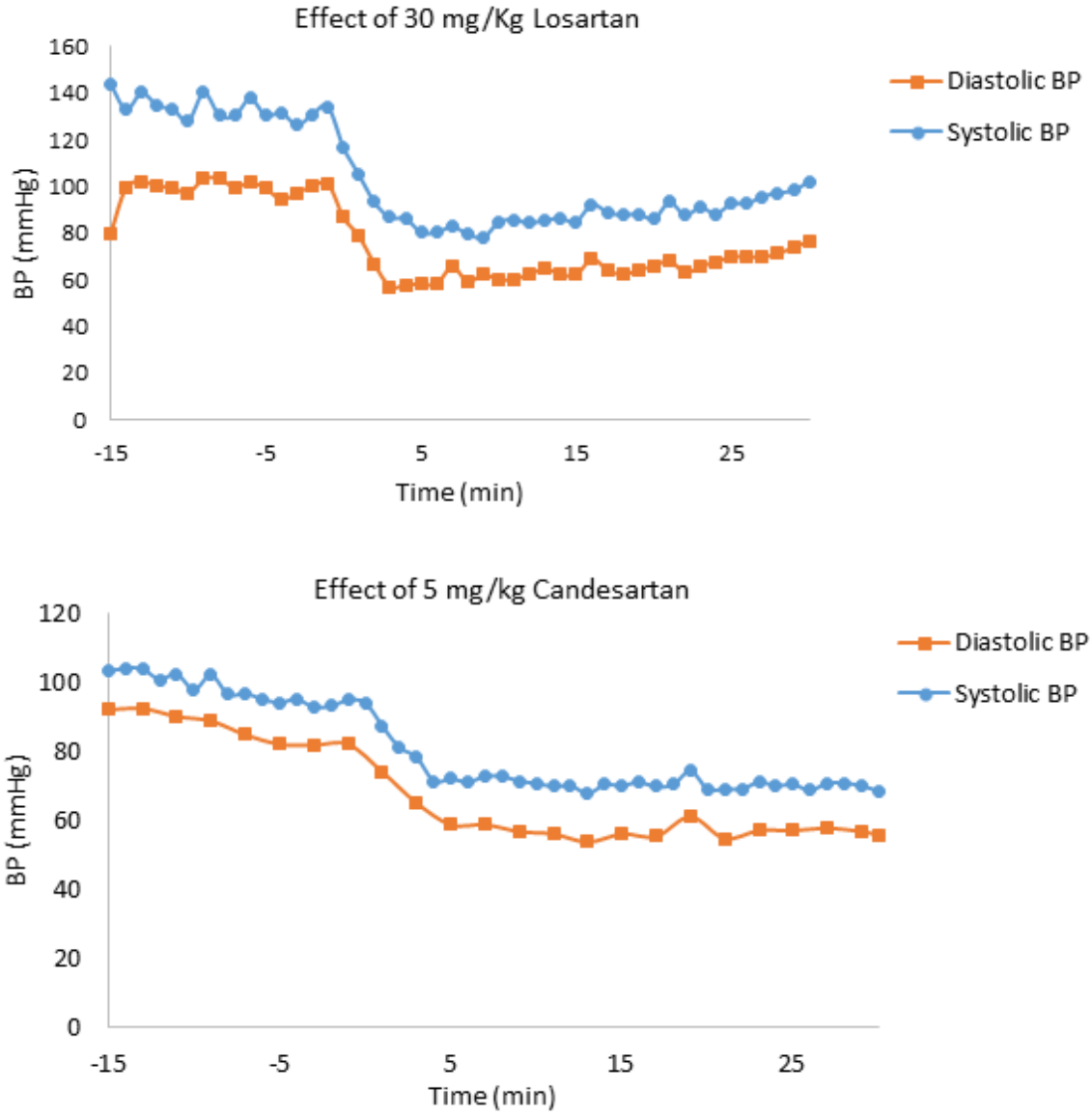

FIGURE 62- SAMPLE GRAPHS DISPLAYING VARIATION IN BOTH SYSTOLIC AND DIASTOLIC BLOOD PRESSURE UPON ARB ADMINISTRATION. A SIMILAR VARIATION IS OBSERVED IN BOTH BLOOD PRESSURES SUGGESTING THAT EITHER ONE COULD BE USED FOR DATA ANALYSIS.

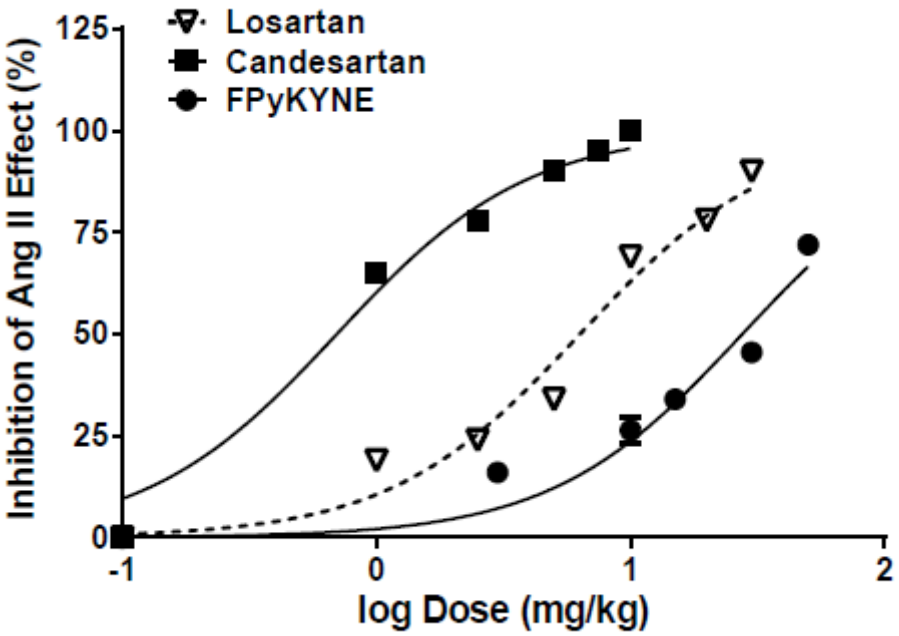

FIGURE 63- NONLINEAR CURVE FITTING USING FOUR-PARAMETER LOGISTIC EQUATION GRAPHPAD PRISM 6.02 (BOTTOM SET TO A CONSTANT VALUE OF 0 AND TOP SET TO VALUE EQUAL TO OR LOWER THAN 100). THIS GRAPH REPRESENTS THE SECOND MODEL USED FOR CURVE FITTING OF THE ANTAGONISTIC STUDIES, WHERE THE INHIBITION OF ANG II EFFECT (%) WAS FIT AGAINST LOG OF THE DOSE (MG/KG) FOR LOSARTAN, CANDESARTAN AND FPYKYNE-LOSARTAN.

TABLE 16- RESULTS OBTAINED USING THE SECOND MODEL OF CURVE FITTING FOR THE ANTAGONISTIC STUDIES. FOR THE FITTING EQUATION USED, THE BASAL POINT WAS CONSTRAINED TO A VALUE OF "0" AND THE TOP VALUES (MAXIMAL INHIBITORY EFFECT) FOR LOSARTAN, CANDESARTAN AND FPYKYNE-LOSARTAN WERE UNCONSTRAINED. HOWEVER, THIS WAS NOT THE PREFERRED MODEL FOR DATA ANALYSIS.

	Losartan	Candesartan	FPyKYNE
Best-fit values			
Bottom	= 0.0	= 0.0	= 0.0
Top	~ 100.0	~ 100.0	~ 100.0
LogID50	0.8014	-0.1556	1.440
HillSlope	1.156	1.156	1.156
ID50	6.3	0.7	27.6

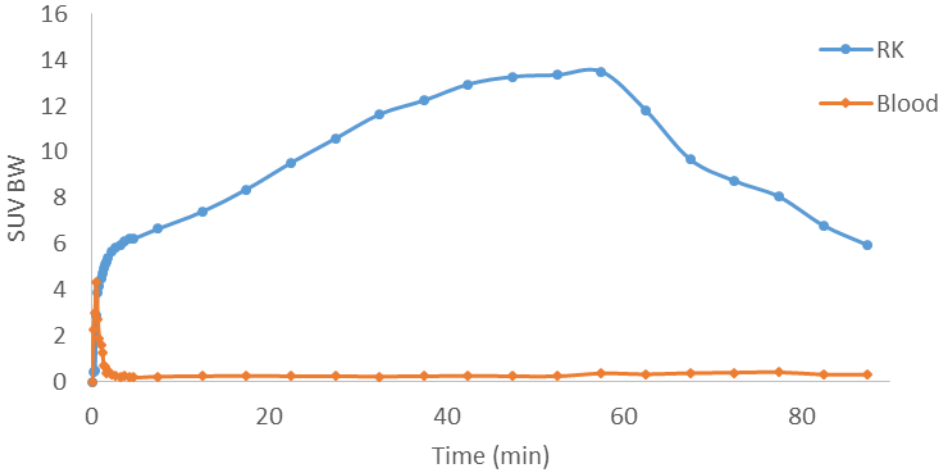

FIGURE 64- BLOCKING SCAN OF PIG 1. FOR THIS SCAN CANDESARTAN (10 MG/KG) WAS CO-INJECTED WITH THE TRACER INTRAVENOUSLY. AS SHOWN BY THE TAC, RIGHT KIDNEY (RK) UPTAKE INCREASES WITH TIME, SO AT_1RS WERE NOT PROPERLY BLOCKED WITH THIS PROTOCOL. CANDESARTAN HAS TO BE ADMINISTERED PRIOR TO THE TRACER TO ENSURE BLOCKAGE OF AT_1RS AND PREVENT TRACER SPECIFIC BINDING.

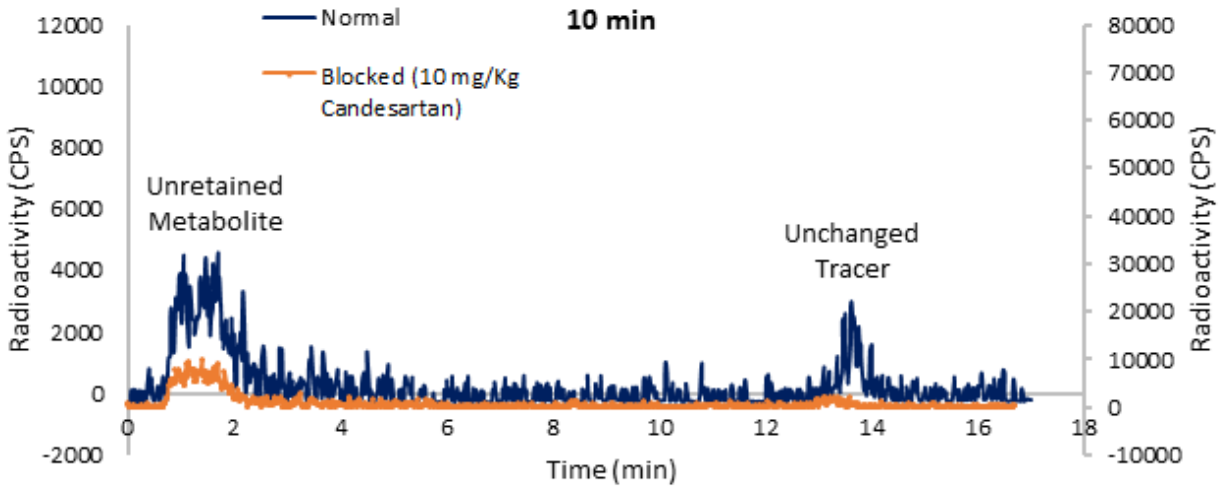

FIGURE 65- A COMPARISON BETWEEN UNRETAINED METABOLITE(S) (HYDROPHILIC METABOLITE(S)) AND UNCHANGED [^{18}F]FPYKYNE-LOSARTAN PROPORTIONS IN PIG PLASMA AT 10 MIN, IN NORMAL AND BLOCKING CONDITIONS. BLOCKING AT_1RS WITH CANDESARTAN RESULTS IN A FASTER METABOLISM OF THE TRACER BY WHICH ITS PROPORTION DECREASES FROM 17% TO 4% AT 10 MIN.

6. Conclusion

Several conclusions can be drawn from the results of the studies in this thesis. In vitro binding studies demonstrated that [^{18}F]FPyKYNE-Losartan binds to the renal cortex and medulla with high affinity (pK_d= 6.93-7.68). This result correlates with known AT_1R densities. Upon binding to AT_1Rs in rats, FPyKYNE-Losartan exhibits full antagonism of Ang II effects in vivo similarly to its parent compound Losartan, however with four times less potency. In vivo microPET and PET imaging revealed high uptake, good contrast and specific binding to AT_1Rs in the rat and pig kidney cortex. Reproducible imaging procedure and results in rats and pigs provide evidence that the quantification of tracer uptake using SUVs is reliable. Metabolism studies revealed the presence of labeled hydrophilic metabolite(s) and a hydrophobic metabolite in the plasma and kidney of rats, while only labeled hydrophilic metabolite(s) in pig plasma. Blocking AT_1Rs with Candesartan in pigs causes a faster metabolism for the tracer in plasma and reduced tracer retention in the kidney, suggesting that [^{18}F]FPyKYNE-Losartan binds specifically to renal AT_1Rs, and that only authentic radiotracer is binding to AT_1Rs. Dosimetry studies in rats demonstrated that effective doses are well below the safe limits reported for clinically used radioligands. Collectively, these findings suggest that [^{18}F]FPyKYNE-Losartan is a suitable radioligand for translational research, and support its potential use to image human renal AT_1Rs via PET imaging. Having a parent compound approved for clinical use will facilitate Health Canada approval for such novel research in humans.

7. Future Directions

Additional in vitro experiments could be done to provide further data about [^{18}F]FPyKYNE-Losartan. For instance, to study the reversibility of this radioligand, displacement studies may be performed through three sets of experiments: Blocking AT_1Rs with a saturating dose of an AT_1R blocker (Candesartan, Losartan) added to the incubation 15 min after tracer addition, co-incubating with the tracer and the saturating dose of the AT_1R blocker, and incubating with the AT_1R blocker 15 min prior to tracer addition.

The three assays are complementary to assess binding reversibility to AT_1Rs. If [^{18}F]FPyKYNE-Losartan binds irreversibly, then it would not be displaced by the AT_1R blocker. The results of the second and third assays are dependent on the type of the blockers used (insurmountable/surmountable) and their potencies compared to the tracer. Additionally, determining the ability of [**^{18}F**]FPyKYNE-Losartan to image AT_1Rs in disease states is also necessary, as it represents an important development in understanding the role of the AT_1R in pathological conditions with altered receptor expression, such as MI, hypertension, diabetes and many others. Henceforth, future goals should include developing small or large animal models of disease to assess the ability of [^{18}F]FPyKYNE-Losartan in detecting AT_1R density changes in vivo. Current work is underway to evaluate the changes in AT_1Rs in 5/6 nephrectomy models, and the ability of [^{18}F]FPyKYNE-Losartan to detect these changes.

Most characterization steps crucial for developing a useful clinical radiotracer have been done. Initial human PET studies are proposed to be started in 2015. Further studies are required to evaluate the presence or absence of [**^{18}F**]FPyKYNE-Losartan metabolites in humans, and if present, the contribution of these metabolites over time, as well as binding of the tracer to plasma proteins and plasma-to-whole blood radioactivity, all of which are needed for arterial input function corrections. Data from dosimetry, pharmacology, metabolism and small animal PET experiments in rats as well as PET imaging in pigs indicate that [**^{18}F**]FPyKYNE-Losartan is a promising radioligand for further use in human PET scans.

Ultimately, the outcome of our and other's work is clinical imaging. So the target is establishing [^{18}F]FPyKYNE-Losartan as a clinically reliable tool that allows non-invasive imaging of the AT_1R in patients with disease. With this becoming possible, not only will researchers get a better understanding of disease, but will also make use of this information to guide therapy and provide better patient outcome. More specifically, molecular imaging may be used for disease diagnosis, monitoring disease progression and individual optimization of AT_1R blockade, based on the level of receptor occupancy in target tissue. The

presented data from the studies altogether provide potential for [^{18}F]FPyKYNE-Losartan to be used as a radiotracer for PET imaging of the AT_1R.

8. References

Akhavan B, Jarvis K, Majewski P. Hydrophobic Plasma Polymer Coated Silica Particles for Petroleum Hydrocarbon Removal. *ACS Appl Mater Interfaces*. 5 (2013): 8563-8571.

Allen AM, Zhuo J, Mendelsohn FA. Localization of angiotensin AT1 and AT2 receptors. *J Am Soc Nephrol*. 10 (1999): S23-9.

Almansa C, Gomez LA, Cavalcanti FL, de Arriba AF, Garcia-Rafanell J, Forn J. Synthesis and structure-activity relationship of a new series of potent AT1 selective angiotensin II receptor antagonists: 5-(biphenyl-4-ylmethyl) pyrazoles. *J Med Chem*. 40 (1997): 547-558.

Almansa C, Gomez LA, Cavalcanti FL, de Arriba AF, Rodriguez R, Carceller E, Garcia-Rafanell J, Forn J. Diphenylpropionic Acids as New AT1 Selective Angiotensin II Antagonists. *J Med Chem*. 39 (1996): 2197-2206.

Almuhaideb A, Papathanasiou N, Bomanji J. 18F-FDG PET/CT Imaging In Oncology. *Ann Saudi Med*. 31 (2011): 3-13.

Amiri F, Garcia R. Renal Angiotensin II Receptor Regulation in Two-Kidney, One Clip Hypertensic Rats. *Hypertension.* 30 (1997): 337-344.

Arksey N, Hadizad T, Ismail B, Hachem M, Valdivia AC, Beanlands RS, deKemp RA, DaSilva JN. Synthesis and evaluation of the novel 2-[18F]fluoro-3-propoxy-triazole-pyridine-substituted losartan for imaging AT1 receptors. *Bioorg Med Chem*. 22 (2014): 3931-3937.

ASTM E177 Standard Guide for Conducting a Repeatability and Reproducibility Study on Test Equipment for Nondestructive Testing.

ASTM F1469 Standard Guide for Conducting a Repeatability and Reproducibility Study on Test Equipment for Nondestructive Testing.

Bader M. Tissue renin-angiotensin-aldosterone systems: Targets for pharmacological therapy. *Annu Rev Pharmacol Toxicol*. 50 (2010): 439-65.

Baker KM, Booz GW, Dostal DE. Cardiac Actions of Angiotensin II: Role of an Intracardiac Renin-Angiotensin System. *Annu Rev Physiol*. 54 (1992): 227-41.

Barra S, Vitagliano A, Cuomo V, Vitagliano G, Gaeta G. Vascular and metabolic effects of angiotensin II receptor blockers. *Expert Opin Pharmacother*. 10 (2009): 173-189.

Beaulieu S, Kinahan P, Tseng J, Dunnwald LK, Schubert EK, Pham P, Lewellen B, Mankoff D.A. SUV varies with time after injection in (18)F-FDG PET of breast cancer: characterization and method to adjust for time differences. *J Nucl Med*. 44 (2003): 1044-50.

Benet LZ, Hoener BA. Changes in plasma protein binding have little clinical relevance. *Clin Pharmacol Ther*. 71 (2002): 115-21.

Berger A. Positron Emission Tomography. *BMJ*. 326 (2003): 1449.

Bernhart CA, Perreaut PM, Ferrari BP, Muneaux YA, Assens JL, Clement J, Haudricourt F, Muneaux CF, Taillades JE, Vignal MA. A new series of imidazolones: highly specific and potent nonpeptide AT1 angiotensin II receptor antagonists. *J Med Chem*. 36 (1993): 3371-80.

Bernstein KE, Merrero MB. The Importance of Tyrosine Phosphorylation in Angiotensin II Signaling. *Trends Cardiovasc Med*. 6 (1996): 179-87.

Berridge MS. The importance of kinetic enhancement. *J Nucl Med.* 50 (2009): 1203-1204.

Bhuiyan MA, Ishiguro M, Hossain M, Nakamura T, Ozaki M, Miura S, Nagatomo T. Binding sites of valsartan candesartan and losartan with angiotensin II receptor 1 subtype by molecular modeling. *Life Sciences.* 85 (2009): 136-140.

Billet S, Aguilar F, Baudry C, Clauser E. Role of angiotensin II AT1 receptor activation in cardiovascular diseases. *Kidney Intern*. 74 (2008): 1379-1384.

Bland JM, Altman DG. Statistical methods for assessing agreement between two methods of clinical measurement. *Lancet*. (1986): 307-310.

Bottari SP, de Gasparo M, Steckelings UM, Levens NR. Angiotensin II receptor subtypes: Characterization, signalling mechanisms, and possible physiological implications. *Front Neuroendocrinol*. 14 (1993): 123-71.

Brewster UC, Perazella MA. The renin-angiotensin-aldosterone system and the kidney: effects on kidney disease. *Am J Med*. 116 (2004): 263-72.

Buchanan JW, Wahl RL (editor). Principles and Practices of Positron Emission Tomography. *Lippincott Williams & Wilkins* (2002).

Burson JM, Aguilera G, Gross KW, Sigmund CD. Differential expression of angiotensin receptor 1A and 1B in mouse. *Am J Physiol*. 276 (1994): E260-7.

Carini DJ, Duncia JV, Aldrich PE, Chiu AT, Johnson AL, Pierce ME, Price WA, Santella JB 3rd, Wells GJ, Wexler RR. Nonpeptide angiotensin II receptor antagonists: the discovery of a series of N-(biphenylylmethyl)imidazoles as potent, orally active antihypertensives. *J Med Chem*. 34 (1991): 2525-2547.

Champion HC, Czapla MA, Kadowitz PJ. Responses to angiotensin peptides are mediated by AT1 receptors in the rat. *Am J Physiol*. 274 (1998): E115-23.

Chang RS, Lotti VJ. Angiotensin receptor subtypes in rat, rabbit and monkey tissues: relative distribution and species dependency. *Life Sci*. 49 (1991): 1485 1490.

Chen CH. *Activation and Detoxification Enzymes*. Chapter 2. New York, USA. (2012): 7-16.

Chen TS, Doong ML, Chang FY, Lee SD, Wang PS. Effects of sex steroid hormones on gastric emptying and gastrointestinal transit in rats. *Am J Physiol*. 268 (1995): G171-6.

Cheng HF, Burns KD, Harris RC. Reduced proximal tubule angiotensin II receptor expression in streptozotocin-induced diabetes mellitus. *Kidney Int*. 46 (1994): 1603-10.

Cherry SR, Gambhir SS. Use of Positron Emission Tomography in Animal Research. *ILAR J*. 42 (2001): 219-32.

Chiu AT, Dunscomb J, Kosierowski J, Burton CR, Santumenna LD, Corjay MH, Benfield P. The Ligand Binding Signatures of the Rat AT1A, AT1B and the Human AT1 Receptors Are Essentially Identical. *Biochem Biophys Res Commun*. 197 (1993): 440-449.Christ DD. Human plasma protein binding of the angiotensin II receptor antagonist losartan potassium (DuP 753/MK 954) and its pharmacologically active metabolite EXP3174. *J Clin Pharmacol*. 35 (1995): 515-20.

Christensen GL, Kelstrup CD, Lyngsø C, Sarwar U, Bøgebo R, Sheikh SP, Gammeltoft S, Olsen JV, Hansen JL. Quantitative phosphoproteomics dissection of seven-transmembrane receptor signaling using full and biased agonists. *Mol Cell Proteomics*. 9 (2010): 1540-53.

Christophe B, Libon R, Cazaubon C, Nisato D, Manning A, Chatelain P. Effects of irbesartan (SR 47436/BMS-186295) on angiotensin II-induced pressor responses in the pithed rat: potential mechanisms of action. *Eur J Pharmacol*. 281 (1995): 161-171.

Cohn JN. Rationale for angiotensin II receptor blocker therapy in chronic heart failure. *J Renin Angiotensin Syst*. 1 (2000): S38-40.

Dasgupta C, Zhang L. Angiotensin II receptors and drug discovery in cardiovascular disease. *Drug Discov Today.* 16 (2011): 22-34.

Davenport AP, Russel FD. Radioligand binding assays: Theory and Practice. *Current Directions in Radiopharmaceutical Research and Development*. 30 (1996): 169-179.

de Gasparo M, Catt KJ, Inagami T, Wright JW, Unger T. International union of pharmacology. XXIII. The angiotensin II receptors. *Pharmacol Rev*. 52 (2000): 415-72.

de Gasparo M, Levens NR. Pharmacology of angiotensin II receptors in the kidney. *Kidney Int*. 46 (1994): 1486-91.

Di Carli MF, Dorbala S, Meserve J, El Fakhri G, Sitek A, Moore SC. Clinical myocardial perfusion PET/CT. *J Nucl Med*. 48 (2007): 783-93.

Dickstein K, Timmermans P, Segal R. Losartan: a selective angiotensin II type 1 (AT1) receptor antagonist for the treatment of heart failure. *Expert Opin Investig Drugs*. 7 (1998): 1897-914.

Diez J. Review of the molecular pharmacology of Losartan and its possible relevance to stroke prevention in patients with hypertension. *Clin Ther*. 28 (2006): 832-848.

Dinh DT, Frauman AG, Johnston CI, Fabiani ME. Angiotensin receptors: distribution, signalling and function. *Clinical Science*. 100 (2001): 481-492.

Diwan JJ. Lipoproteins: Lipid Digestion & Transport. Rensselaer Polytechnic Institute. Retrieved. (2012).

Dostal D, Baker K. The Cardiac Renin-Angiotensin System: Conceptual, or a Regulator of Cardiac Function? *Circ Res*. 85 (1999): 643-650.

Elton TS, Stephan CC, Taylor GR, Kimball MG, Martin MM, Durand JN, Oparil S. Isolation of two distinct type I angiotensin II receptor genes. *Biochem Biophys Res Commun*. 184 (1992): 1067-1073.

Erwin K. Hepatology: Textbook and Atlas. Germany: Springer (2008): 38.

Fabiani ME, Dinh DT, Nassis L, Casley DJ, Johnston CI. In Vivo Inhibition of Angiotensin Receptors in the Rat Kidney by Candesartan Cilexetil: A Comparison with Losartan. *Am J Hypertens*. 13 (2000): 1005-1013.

Fabiilli ML, Piert MR, Koeppe RA, Sherman PS, Quesada CA, Kripfgans OD. Assessment of the biodistribution of an [18F]FDG-loaded perfluorocarbon double emulsion using dynamic micro-PET in rats. *Contrast Media Mol Imaging*. 8 (2013): 366-374.

Farkas S, Nagy K, Jia Z, Harkany T, Palkovits M, Donohou SR, Pike VW, Halldin C, Máthé D, Csiba L, Gulyás B. The decrease of dopamine D_2/D_3 receptor densities in the putamen and nucleus caudatus goes parallel with maintained levels of CB_1 cannabinoid receptors in Parkinson's disease: a preliminary autoradiographic study with the selective dopamine D_2/D_3 antagonist [^{3}H]raclopride and the novel CB_1 inverse agonist [^{125}I]SD7015. *Brain Res Bull*. 87 (2012): 504-10.

Feller PA, Sodd VJ. Dosimetry of four heart-imaging radionucleotides: 43 K, 81 Rb, 129 Cs, and 201 Ti. *J Nucl Med*. 16 (1975): 1070-1075.

Foreman JC, Johansen T. Textbook of Receptor Pharmacology (Second ed.). Boca Raton, Florida: CRC L.L.C. 2003: 153-180.

Fukushima K, Bravo PE, Higuchi T, Schuleri KH, Lin X, Abraham MR, Xia J, Mathews WB, Dannals RF, Lardo AC, Szabo Z, Bengel FM. Molecular PET/CT Imaging of Cardiac Angiotensin II Type 1 Receptors. *J Am Coll Cardiol*. 60 (2012): 2527-2534.

Fumita M, Innis RB. Neuropsychopharmacology: The Fifth Generation of Progress. Chapter 31: In Vivo Molecular Imaging. 2002: 412-425.

Fyhrquist F, Saijonmaa O. Renin-angiotensin system revisited. *J Intern Med*. 264 (2008): 224-236.

Gabathuler R. Approaches to transport therapeutic drugs across the blood–brain barrier to treat brain diseases. Neurobiology of Disease. 37 (2010): 48-57.

Gad SC. Ed. *Pharmaceutical Manufacturing Handbook: Production and Process*. Wiley, New Jersey, 2008.

Gallo-Payet N, Guimond MO, Bilodeau L, Wallinder C, Alterman M, Hallberg A. Angiotensin II, a Neuropeptide at the Frontier between Endocrinology and Neuroscience: Is There a Link between the Angiotensin II Type 2 Receptor and Alzheimer's Disease? *Front Endocrinol (Lausanne).* 2 (2011): 2:17.

Gambhir SS. Molecular imaging of cancer with positron emission tomography. *Nat Rev Cancer*. (2002): 683-693.

Givertz MM. Manipulation of the Renin-Angiotensin System. *Circulation*. 104 (2001): 14-18.

Godin CM, Ferguson SS. Biased agonism of the angiotensin II type 1 receptor. *Mini Rev Med Chem*. 12 (2012): 812-6.

Gousias IS, Reuckert D, Heckemann RA, Dyct LE, Boardman JP, Edwards AD, Hammers A. Auotomatic segmentation of brain MRIs of 2-years-old into 83 regions of interest. *Neuroimage*. 40 (2008): 672-84.

Grant TL, McGrath JC. Interactions between angiotensin II and a-adrenoceptor agonists mediating pressor responses in the pithed rat. *Br J Pharmacol*. 95 (1988): 1229-1240.

Grant TL, McGrath JC. Interactions between angiotensin II, sympathetic nerve-mediated pressor response and cyclo-oxygenase products in the pithed rat. *Br J Pharmacol*. 95 (1988): 1220-8.

Greindling KK, Lassègue B, Alexander RW. Angiotensin receptors and their therapeutic implications. *Annu Rev Pharmacol Toxicol*. 36 (1996): 281-306.

Griendling KK, Delafontaine P, Rittenhouse SE, Gimbrone MA Jr, Alexander RW. Correlation of receptor sequestration with sustained diacylglycerol accumulation in angiotensin II-stimulated cultured vascular smooth muscle cells. *J Biol Chem*. 262 (1987): 14555-14562.

Guimaraes S, Pinheiro H. Functional evidence that in the cardiovascular system AT1 angiotensin II receptors are AT1B prejuntionally and AT1A postjunctionally. *Cardiovasc Res*. 67 (2005): 208-215.

Gunn RN, Gunn SR, Cunningham VJ. Positron emission tomography compartmental models. *J Cereb Blood Flow Metab.* 21 (2001): 635-652.

Hadizad T, Collins J, Beanlands RS, DaSilva JN. Radiosynthesis of [11C]methyl-EXP31174, a potential imaging agent for angiotensin AT1 receptors. Abstract. *World Molecular Imaging Congress*. Kyoto, Japan. (2010).

Hadizad T, Kirkpatrick SA, Mason S, Burns K, Beanlands RS, Dasilva JN. Novel O-[(11)C]methylated derivatives of candesartan as angiotensin II AT(1) receptor imaging ligands: radiosynthesis and ex vivo evaluation in rats. *Bioorg Med Chem*. 17 (2009a): 7971-7977.

Hadizad T, Mason S, Collins J, Kirkpatrick S, Beanlands RS, DaSilva JN. Radiosynthesis of [11C]-methyl-losartan, a potential imaging agent for angiotensin AT1 receptors. Abstract. *J Labelled Comp Radiopharm.* 92 (2009b): S426.

Hammers A, Allon R, Koepp MJ, Free SL, Myers R, Lemieux L, Mitchell TN, Brooks DJ, Ducan JS. Three-dimensional maximum probability atlas of the human brain, with particular reference to the temporal lobe. *Hum Brain Mapp*. 19 (2003): 224-47.

Higuchi T, Fukushima K, Xia J, Mathews WB, Lautamäki R, Bravo PE, Javadi MS, Dannals RF, Szabo Z, Bengel FM. Radionuclide Imaging of Angiotensin II Type 1 Receptor Upregulation After Myocardial Ischemia-Reperfusion Injury. *J Nucl Med*. 51 (2001): 1956-1961.

Hilton J, Yokoi F, Dannals RF, Ravert HT, Szabo Z, Wong DF. Column-switching HPLC for the analysis of plasma in PET imaging studies. *Nucl Med Biol*. 27 (2000): 627-30.

Hume SP, Gunn RN, Jones T. Pharmacological constraints associated with positron emission tomographic scanning of small laboratory animals. *Eur J Nucl Med*. 25 (1998): 173-176.

Hutchins G, Miller M, Soon V, Receveur T. Small animal PET imaging. *ILAR J*. 49 (2008): 54-65.

ICRP. Radiation dose of patients from radiopharmaceuticals (addendum 2 to ICRP publication 53). *Ann ICRP*. 28 (1998): 1-126.

ICRP. Radiation dose of patients from radiopharmaceuticals. A report of a Task Group of Committee 2 of the International Commission of Radiological Protection. *Ann ICRP.* 18 (1987): 1-377.

Inagami T, Iwai N, Sasaki K, Yamamo Y, Bardhan S, Chaki S, Guo DF, Furuta H. Cloning, expression and regulation of angiotensin II receptors. *J Hypertens*. 10 (1992): 713-6.

Inagami T. The renin-angiotensin system. *Essays Biochem*. 28 (1994): 147-64.

IUPAC. *Compendium of Chemical Terminology*. 2nd ed. (the "Gold Book") (1997). Online corrected version (2006).

Jagoda EM, Vaquero JJ, Seidel J, Green MV, Eckelman WC. Experiment assessment of mass effects in the rat: implications for small animal PET imaging. *Nucl Med Biol*. 31 (2004): 771-779.

Johnström P, Bird JL, Davenport AP. Chapter 10: Quantitative Phosphor Imaging Autoradiography of Radioligands for Positron Emission Tomography. *Receptor Binding Techniques, Methods in Molecular Biology*. 897 (2012).

Jong A, Huang SH. Blood-brain barrier drug discovery for central nervous system infections. *Curr Drug Targets Infect Disord*. 5 (2005): 65-72.

Kakinuma Y, Fogo A, Inagami T, Ichikawa I. Intrarenal localization of angiotensin II type I receptor mRNA in the rat. *Kindey Int*. 43 (1993): 1229-1235.

Kakuta H, Sudoh K, Sasamata M, Yamagishi S. Telmisartan has the strongest binding affinity to angiotensin II type 1 receptor: comparison with other angiotensin II type 1 receptor blockers. *Int J Clin Pharmacol Res*. 25 (2005): 41-46.

Kelloff GJ, Hoffman JM, Johnson B, Scher HI, Siegel BA, Cheng EY, Cheson BD, O'shaughnessy J, Guyton KZ, Mankoff DA, Shankar L, Larson SM, Sigman CC, Schilsky RL, Sullivan DC. Progress and promise of FDG-PET imaging for cancer patient management and oncologic drug development. *Clin Cancer Res*. 11 (2005): 2785-808.

Kenk M, Greene M, Lortie M, Dekemp RA, Beanlands RS, Dasilva JN. Use of a column-switching high-performance liquid chromatography method to assess the presence of specific binding of (R)- and (S)-[(11)C]rolipram and their labeled metabolites to the phosphodiesterase-4 enzyme in rat plasma and tissues. *Nucl Med Biol*. 35 (2008): 515-521.

Kimura Y, Naganawa M, Shidahara M, Ikoma Y, Watabe H. Pet kinetic analysis—pitfalls and a solution for the Logan plot. *Ann Nuclear Med*. 21 (2007): 1-8.

Kinahan PE, Fletcher JW. PET/CT Standardized Uptake Values (SUVs) in Clinical Practice and Assessing Response to Therapy. *Semin Ultrasound CT MR*. 31 (2010): 496-505.

Kinahan PE, Fletcher JW. PET/CT Standardized Uptake Values (SUVs) in Clinical Practice and Assessing Response to Therapy. *Semin Ultrasound CT MR*. 31 (2010): 496-505.

Kobori H, Nangakv M, Navar LG, Nishiyama A. The intrarenal renin-angiotensin system: from physiology to the pathobiology of hypertension and kidney disease. *Pharmacol Rev*. 59 (2007): 251-87.

Kolb HC, Finn MG, Sharpless KB. Click Chemsitry: Diverse Chemical Function from a Few Good Reactions. *Angew Chem Int Ed Engl*. 40 (2001): 2004-2021.

Krovat EM, Langer T. Non-peptide angiotensin II receptor antagonists: chemical feature based pharmacophore identification. *J Med Chem*. 46 (2003): 716-726.

Kubo K, Kohara Y, Imamiya E, Sugiura Y, Inada Y, Furukawa Y, Nishikawa K, Naka T. Nonpeptide angiotensin II receptor antagonists. Synthesis and biological activity of benzimidazolecarboxylic acids. *J Med Chem*. 36 (1993): 2182-95.

Kumar D, Luan L, Pathak S, Salhan D, Magoon S, Singhal PC. Ang II enhances tubular cell Ets-1 expression and associated down stream signaling is mediated through AT1 receptors. *Ren Fail*. 32 (2010): 986-991.

Kuwabara H, Cumming P, Reith J, Léger G, Diksic M, Evans AC, Gjedde A. Human striatal L-DOPA decarboxylase activity estimated in vivo using 6- [^{18}F]fluoro-DOPA and positron emission tomography: error analysis and application to normal subjects. *J Cereb Blood Flow Metab.* 13 (1993): 43-56.

Lammertsma AA. Radioligand studies: imaging and quantitative analysis. *Eur Neuropsychopharmacol.* 12 (2002): 513-516.

Laruelle M, Slifstein M, Huang Y. Relationships between radiotracer properties and image quality in molecular imaging of the brain with positron emission tomography. *Mol Imaging Biol.* 5 (2003): 363-375.

Lenkei Z, Corvol P, Llorens-Cortes C. The angiotensin receptor subtype AT1a predominates in rat forebrain areas involved in blood pressure, body fluid homeostasis and neuroendocrine control. *Mol Brain Res*. 30 (1995): 53-60.

Leung PS, Carlsson PO. Tissue renin-angiotensin system: its expression, localization, regulation and potential role in the pancreas. *J Mol Endocrinol*. 26 (2001): 155-164.

Loevinger B, Budinger T, Watson E. Mird primer for absorbed dose calculations. *Soc Nucl Med*. New York (1988).

Logan J, Fowler JS, Volkow ND, Wang GJ, Ding YS, Alexoff DL. Distribution volume ratios without blood sampling from graphical analysis of PET data. *J Cereb Blood Flow Metab*. 16 (1996): 834-840.

Logan J, Fowler JS, Volkow ND, Wolt AP, Dewey SL, Schlyer DJ, MacGregor RR, Hitzemann R, Bendriem B, Gatley SJ, Christman DR. Graphical Analysis of Reversible Radioligand Binding from Time-Activity Measurements Applied to [N-{+11}C-methyl]-(-)-Cocain PET Studies in Human Subjects. *J Cereb Blood Flow Metab*. 10 (1990): 740-747.

Logan J. Graphical analysis of PET data applied to reversible and irreversible tracers. *Nucl Med Biol*. 27 (2000): 661-670.

Lortie M, DaSilva JN, Kirkpatrick SA, Hadizad T, Ismail BA, Beanlands RS, deKemp RA. Analysis of [11C]methyl-candesartan kinetics in the rat kidney for the assessment of angiotensin II type 1 receptor density in vivo with PET. *Nucl Med Biol*. 40 (2013): 252-261.

Lourenco CM, Houle S, Wilson AA, DaSilva JN. Characterization of r-[11C]rolipram for PET imaging of phosphodieterase-4: in vivo binding, metabolism, and dosimetry studies in rats. *Nucl Med Biol.* 28 (2001): 347-358.

Lucignani G, Paganelli G, Bombardieri E. The use of standardized uptake values for assessing FDG uptake with PET in oncology: a clinical perspective. *Nucl Med Commun*. 25 (2004): 651-6.

Macgregor GA, Markandu ND, Roulston JE, Jones JC, Morton JJ. Maintenance of blood pressure by the renin-angiotensin system in normal man. *Nature.* 291 (1981): 329-331.

Maggioni AP, Anand I, Gottlieb SO, Latini R, Tognoni G, Cohn JN. Effects of valsartan on morbidity and mortality in patients with heart failure not receiving angiotensin-converting enzyme inhibitors. *J Am Coll Cardiol*. 40 (2002): 1414-21.

Marrero MB, Fulton D, Stepp D, Stern DM. Angiotensin II-induced insulin resistance and protein tyrosine phosphatases. *Arterioscler Thromb Vasc Biol*. 24 (2004): 2009-2013.

McAlpine HM, Morton JJ, Leckie B, Rumley A, Gillen G, Dargie HJ. Neuroendocrine activation after acute myocardial infarct in rats. *Am J Physiol Heart Circ Physiol*. 286 (2004): H1665-71.

Meggs LG, Coupet J, Huang H, Cheng W, Li P, Capasso JM, Homcy CJ, Anversa P. Regulation of angiotensin II receptors on ventricular myocytes after myocardial infarction in rats. *Circ Res*. 72 (1993): 1149-62.

Mehta PK, Griendling KK. Angiotensin II cell signaling: physiological and pathophysiological effects in the cardiovascular system. *Am J Physiol Cell Physiol*. 292 (2007): C82-97.

Mejia AA, Nakamura T, Masatoshi I, Hatazawa J, Masaki M, Watanuki S. Estimation of Absorbed Doses in Humans Due to Intravenous Administration of Fluorine- 18- Fluorodeoxyglucose in PET Studies. *J Nucl Med*. 32 (1991): 699-706.

Mento PF, Pica ME, Hilepo J, Chang J, Hirsch L, Wilkes BM. Increased expression of glomerular AT1 receptors in rats with myocardial infarction. *Am J Physiol*. 275 (1998): H1247-53.

Meredith P. Comparative ARB pharmacology. *Br J Cardiol*. 17 (2010): s3-s5.

Michel MC, Foster C, Brunner HR, Liu L. A Systematic Comparison of the Properties of Clinically Used Angiotensin II Type 1 Receptor Antagonists. *Pharmacol Rev*. 65 (2013): 809-848.

Niu T, Chen X, Xu X. Drugs. Angiotensin converting enzyme gene insertion/deletion polymorphism and cardiovascular disease: therapeutic implications. 62 (2002): 977-93.

Nogueira EF, Xing Y, Morris CA, Rainey WE. Role of angiotensin II-induced rapid response genes in the regulation of enzymes needed for aldosterone synthesis. *J Mol Endocrinol*. 42 (2009): 319-30.

Obermüller N, Unger T, Culman J, Gohlke P, de Gasparo M, Bottari SP. Distribution of angiotensin II receptor subtypes in rat brain nuclei. *Neurosci Lett.* 132 (1991): 11-15.

Obrzut SL, Koren AO, Mandelkern MA, Brody AL, Hoh CK, London ED. Whole-body radiation dosimetry of 2-[F-18]fluoro-A-85380 in human PET imaging studies. *J Nucl Med Biol*. 32 (2005): 869-74.

Okazaki T, Watanabe T, Kikuchi K, Suga A, Shibasaki M, Fujimori A, Inagaki O, Yanagisawa I. Studies on nonpeptide angiotensin II receptor antagonists. IV. Synthesis and biological evaluation of 4-acrylamide-1H-imidazole derivatives. *Chem Pharm Bull*. 46 (1998): 973-81.

Parasuraman S, Raveendran R. Measurement of invasive blood pressure in rats. *J Pharmacol Pharmacother.* 3 (2012): 172-177.

Pardridge WM. BBB drug targeting: the future of brain drug development. *Mol Interv.* 3 (2003): 90-105.

Pardridge WM. Blood-brain barrier delivery. *Drug Discov Today*. 12 (2007c): 54-61.

Pardridge WM. CNS drug design based on principles of blood–brain barrier transport. *J Neurochem*. 70 (1998): 1781-1792.

Pardridge WM. Drug targeting to the brain. Pharma. Res. 24, 1733-1744.

Pardridge WM. The blood–brain barrier: bottleneck in brain drug development. *NeuroRx.* 2 (2005): 3-14.

Pardridge WM. Transport of small molecules through the blood–brain barrier: biology and methodology. *Adv Drug Deliv Rev.* 15 (1995): 5-36.

Pardridge, W.M., 2007b. shRNA and siRNA delivery to the brain. *Adv Drug Deliv Rev*. 59 (2007a): 141-152.

Paul M, Poyan Mehr A, Kreutz R. Physiology of local renin-angiotensin systems. *Physiol Rev*. 86 (2006): 747-803.

Pauleit D, Floeth F, Herzoq H, Hamacher K, Tellmann L, Muller HW, Coenen HH, Langen KJ. Whole-body distribution and dosimetry of O-(2-[18F]fluoroethyl)-L-tyrosine. *Eur J Nucl Med Mol Imaging*. 30 (2003): 519-24.

Pfeffer MA, Lamas GA, Vaughan DE, Parisi AF, Braunwald E. Effect of captopril on progressive ventricular dilatation after anterior myocardial infarction. *N Engl J Med*. 319 (1988): 80-6.

Pike VW. PET Radiotracers: crossing the blood-brain barrier and surviving metabolism. *Trends Pharmacol Sci.* 30 (2009): 431-440.

Prokop A, Davidson JM. Nanovehicular Intracellular Delivery Systems. *J Pharm Sci*. 97 (2008): 3518-3590.

Rahmim A, Zaidi H. PET versus SPECT: strengths, limitations and challenges. *Nucl Med Commun*. 29 (2008): 193-207.

Reiss K, Capasso JM, Huang HE, Meggs LG, Li P, Anversa P. ANG II receptors, c-myc, and c-jun in myocytes after myocardial infarction and ventricular failure. *Am J Physiol*. 294 (1993): H760-9.

Ribeiro-Oliveira A, Nogveira A, Pereira R, Boas W, dos Santos R, Silva A. The renin-angiotensin system and diabetes: An update. *Vasc Health Risk Manag.* 4 (2008): 787-803.

Rizzo G, Veronese M, Tonietto M, Zanotti-Fregonara P, Turkheimer FE, Bertoldo A. Kinetic modeling without accounting for the vascular component impairs the quantification of [11C]PBR28 brain PET data. *J Cereb Blood Flow Metab*. 34 (2014): 1060-1069.

Rockman HA, Koch WJ, Leftkowitz RJ. Seven-transmembrane-spanning receptors and heart function. *Nature*. 415 (2002): 206-12.

Roth BL. University of North Carolina at Chapel Hill. Assay Protocol Book.

Rousset OG, Ma Y, Evans AC. Correction for partial volume effects in PET: principle and validation. *J Nucl Med*. 39 (1998): 904-11.

Ruiz-Ortega M, Lorenzo O, Rupérez M, Esteban V, Suzuki Y, Mezzano S, Plaza JJ, Egido J. Role of the Renin-Angiotensin System in Vascular Diseases. *Hypertension*. 38 (2001): 1382-1387.

Sadoshima J. Versatility of the Angiotensin II Type 1 Receptor. *Circ Res.* 82 (1998): 1352-1355.

Sawada GA, Williams LR, Lutzke BS, Raub TJ. Novel, highly lipophilic antioxidants readily diffuse across the blood–brain barrier and access intracellular sites. *J Pharm Exp Ther*. 288 (1999): 1327-1333.

Schain M, Benjaminsson S, Varnäs K, Forsberg A, Halldin C, Lansner A, Farde L, Varrone A. Arterial input function derived from pairwise correlations between PET-image voxels. *J Cereb Blood Flow Metab.* 33(2013): 1058-1065.

Schmitz U, Ishida T, Ishida M, Surapisitchat J, Hasham MI, Pelech S, Berk BC. Angiotensin II stimulates p21-activated kinase in vascular smooth muscle cells: role in activation of JNK. *Circ Res*. 82 (1998): 1272-1278.

Shuttleworth G, Hunter MG, Broughton Pipkin F. Autoradiographic determination of angiotensin II receptors in prepubertal and postpubertal pig ovarian tissue. *Reproduction*. 122 (2001): 701-10.

Siragy H. Post-MI Repair and Remodeling: From Neurohormones to Cell Regulation. *Am J Cardiol*. 84 (1999): 3S-8S.

Smith AM, Materne R, Van Beers BE. Quantitative Measurement of Blood Perfusion, GFR and Arterial Vascular Fraction ion the Kidney Cortex. *Proc Intl Soc Mag Reson Med*. 9 (2001): 367.

Smith DA, Di L, Kerns EH. The effect of plasma protein binding on in vivo efficacy: misconceptions in drug discovery. *Nat Rev Drug Discov*. 9 (2010): 929-939.

Soret M, Bacharach SL, Buvant I. Partail-Volume effect in PET tumor imaging. *J Nucl Med*. 48 (2007): 932-45.

St Lawrence KS, Owen D, Wang DJ. A Two-Stage Approach for Measuring Vascular Water Exchange and Arterial Transit Time by Diffusion-Weighted Perfusion MRI. *Magn Reson Med*. 67 (2012): 1275-1284.

Stearns RA, Miller RR, Doss GA, Chakravarty PK, Rosegay A, Gatto GJ, Chiu SH. metabolism of DuP 753, a nonpeptide angiotensin II receptor antagonist, by rat, monkey, and human liver slices. *Drug Metab Dispos*. 20 (1992): 281-287.

Swindle MM, Makin A, Herron AJ, Clubb FJ Jr, Frazier KS. Swine as Models in Biomedical Research and Toxicology Testing. *Vet Pathol*. 49 (2012): 344-356.

Tai YC, Laforest R. Instrumental Aspects of Animal PET. *Annu Rev Biomed Eng*. 7 (2005): 255-285.

Takezako T, Gogonea C, Saad Y, Noda K, Karnik SS. "Network leaning" as a mechanism of insurmountable antagonism of the angiotensin II type 1 receptor by non-peptide antagonists. *J Biol Chem*. 15 (2004): 15248-57.

Tan J, Wang H, Leenen FHH. Increases in brain and cardiac AT1 receptor and ACE densities after myocardial infarct in rats. *Am J Physiol Heart Circ Physiol*. 286 (2004): H1665-H1671.

Taubman MB. Angiotensin II: A Vasoactive Hormone with Ever-Increasing Biological Roles. *Circ Res*. 92 (2003): 9-11.

Thackeray JT, Renaud JM, Kordos M, Klein R, Dekemp RA, Beanlands RS, DaSilva JN. Test-retest repeatability of quantitative cardiac 11C-meta-hydroxyephedrine measurements in rats by small animal positron emission tomography. *Nucl Med Biol*. 40 (2013): 676-81.

Thomas AJ, DaSilva JN, Lortie M, Renaud JM, Kenk M, Beanlands RS, deKemp RA. PET of (R)-11C-Rolipram Binding to Phosphodiesterase-4 Is Reproducible and Sensitive to Increased Norepinephrine in the Rat Heart. *J Nucl Med.* 52 (2011): 263-269.

Thomas AJ, DaSilva JN, Lortie M, Renaud JM, Kenk M, Beanlands RS, deKemp RA. PET of (R)-(11)C-Rolipram Binding to Phosphodiesterase-4 Is Reproducible and Sensitive to Increased Norepinephrine in the Rat Heart. *J Nucl Med.* 52 (2011): 263-269.

Thomas WG. Regulation of angiotensin II type 1 (AT1) receptor function. *Regul Pept*. 79 (1999): 9-23.

Thörn HA, Lundahl A, Schrickx JA, Dickinson PA, Lennernäs H. Drug metabolism of CYP3A4, CYP2C9 and CYP2D6 substrates in pigs and humans. *Eur J Pharm Sci*. 43 (2011): 89-98.

Thorn SL, deKemp RA, Dumouchel T, Klein R, Renaud JM, Wells RG, Gollob MH, Beanlands RS, DaSilva JN. Repeatable noninvasive measurement of mouse myocardial glucose uptake with 18F-FDG: evaluation of tracer kinetics in a type 1 diabetes model. *J Nucl Med*. 54 (2013): 1637-44.

Tilley DG. G protein-dependent and -independent signaling pathways and their impact on cardiac function. *Circ Res*. 109 (2011): 217-230.

Timmermans PB, Carini DJ, Chiu AT, Duncia JV, Price WA Jr, Wells GJ, Wong PC, Wexler RR, Johnson AL. Angiotensin II receptor antagonists. From discovery to antihypertensive drugs. *Hypertension*. 18 (1991): III 136-42.

Timmermans PB, Chiu AT, Herblin WF, Wong PC, Smith RD. Angiotensin II receptor subtypes. *Am J Hypertens*. 5 (1992): 406-10.

Unger T. The role of the renin-angiotensin system in the development of cardiovascular disease. *Am J Cardiol*. 89 (2002): 3A-9A.

Valdivia AC, Estrada M, Stewart D, Beanlands RS, DaSilva JN. A Fast, Simple and Reproducible Automated Synthesis of [18F]FPyKYNE-c(RGDyK) for PET Imaging αvβ3 Receptors. *J Label Compd Radiopharm*. 55 (2012): 57-60.

van der Veldt AA, Smit EF, Lammertsma AA. Positron Emission Tomography as a Method for Measuring Drug Delivery to Tumors in vivo: The Example of [(11)C]docetaxel. *Front Oncol*. 13 (2013): 3-208.

van Koppen CJ, Jakobs KH. Arrestin-independent internalization of G protein-coupled receptors. *Mol Pharmacol*. 66 (2004): 365-7.

Vanderheyden PM, Fierens FL, De Backer JP, Fraeyman N, Vauquelin G. Dintinction between surmountable and insurmountable selective AT1 receptor antagonists by use of cho-k1 cells expressing human angiotensin II at AT1 receptors. *Br J Pharmacol*. 126 (1999): 1057-1065.

Villemagne VL, Furumoto S, Fodero-Tavoletti M, Harada R, Mulligan RS, Kudo Y, Masters CL, Yanai K, Rowe CC, Okamura N. The Challenges of Tau Imaging. *Future Neurology.* 7 (2012): 409-421.

Vogt L, Kocks MJ, Laverman GD, Navis G. Renoprotection by blockade of the renin-angiotensin-aldosterone system in diabetic and non-diabetic chronic kidney disease. Specific involvement of intra-renal angiotensin-converting enzyme activity in therapy resistance? *Minerva Med*. 95 (2004): 395-409.

Wada T, Inada Y, Sanada T, Ojima M, Shibouta Y, Noda M, Nishikawa K. Effect of an angiotensin II receptor antagonist, CV-11974, and its prodrug, TCV-116, on production of aldosterone. *Eur J Pharmacol*. 253 (1994): 27-34.

Wang DH, Yao A, Zhao H, DiPette DJ. Distinct mechanisms of modulation of angiotensin II type I receptor gene expression in heart and aorta. *Hypertension*. 29 (1997): 1104-8.

Wassmann S, Nickenig G. Pathophysiological regulation of the AT1-receptor and implications for vascular disease. *J Hypertens Suppl*. 24 (2006): 515-21.

Weber KT. Aldosterone in congestive heart failure. *N Eng l J Med*. 345 (2001): 1689-97.

Weir MR, Dzav VJ. The renin-angiotensin-aldosterone system: a specific target for hypertension management. *Am J Hypertens*. 12 (1999): 205S-213S.

Wharton J, Morgan K, Rutherford RA, Catravas JD, Chester A, Whitehead BF, De Leval MR, Yacoub MH, Polak JM. Differential distribution of angiotensin 2 receptors in the normal and failing human heart. *J Pharmacol Exp Ther*. 284 (1998): 323-336.

Wong PC, Price WA, Chiu AT, Duncia JV, Carini DJ, Wexler RR, Johnson AL, Timmermans PB. Nonpeptide Angiotensin II Receptor Antagonists. VIII. Characterization of Functional Antagonism Displayed by DuP753, an Orally Active Antihypertensive Agent. *J Pharmacol Exp Ther*. 252 (1990): 719-25.

Xia J, Seckin E, Xiang Y, Vranesic M, Mathews WB, Hong K, Bluemke DA, Lerman LO, Szabo Z. Positron-emission tomography imaging of the angiotensin II subtype 1 receptor in swine renal artery stenosis. *Hypertension*. 51 (2008): 466-73.

Yang LX, Yang ZH, Guo RW, Ye JS, Liu H. Angiotensin II induces extracellular matrix metalloproteinase inducer expression via an AT1R dependent pathway in aortic atherosclerotic plaque in apolipoprotein E knockout mice. *J Renin Angiotensin Aldosterone Syst*. 13 (2012): 67-75.

Yoshimura Y, Tada N, Kubo K, Miyamoto M, Inada Y, Nishikawa K, Naka T. Evaluation and improvement of bioavailability of a new angiotensin II receptor antagonist, 2-butyl-1-[2'-(1H-tetrazol-5-yl)biphenyl-4-yl]methyl-1H-benzimidazole-7-carboxylic acid by making prodrug. *Int J Pharm*. 103 (1994): 1-7.

Yoshinaga K, Klein R, Tamaki N. Generator-produced rubidium-82 positron emission tomography myocardial perfusion imaging-From basic aspects to clinical applications. *J Cardiol.* 55 (2010): 163-73.

Yusuf S, Sleight P, Pogue J, Bosch J, Davies R, Dagenais G. Effects of an angiotensin-converting enzyme inhibitor, ramipril, on cardiovascular events in high-risk patients. The Heart Outcomes Prevention Evaluation Study Investigator. *N Engl J Med*. 342 (2000): 145-53.

Zaman MA, Oparil S, Calhoum DA. Drugs targeting the renin-angiotensin aldosterone system. *Nature*. 1 (2002): 621-36.

Zober TG, Mathews WB, Seckin E, Yoo SE, Hilton J, Xia J, Sandberg K, Ravert HT, Dannals RF, Szabo Z. PET Imaging of the AT1 receptor with [11C]KR31173. *Nucl Med Biol*. 33 (2006): 5-13.